Volume 2

Chapter 3

Late Triassic to Jurassic Magmatism in Colombia: Implications for the Evolution of the Northern Margin of South America

https://doi.org/10.32685/pub.esp.36.2019.03
Published online 16 October 2020

Julián Andrés LÓPEZ–ISAZA[1]* and Carlos Augusto ZULUAGA[2]

1 jlopez@sgc.gov.co, jalopezi@unal.edu.co
Servicio Geológico Colombiano
Diagonal 53 n.° 34–53
Bogotá, Colombia
Universidad Nacional de Colombia
Sede Bogotá
Carrera 30 n.° 45–03
Bogotá, Colombia

2 cazuluagacas@unal.edu.co
Universidad Nacional de Colombia
Sede Bogotá
Carrera 30 n.° 45–03
Bogotá, Colombia

* Corresponding author

Supplementary Information:

S: https://www2.sgc.gov.co/LibroGeologiaColombia/tgc/sgcpubesp36201903s.pdf

Abstract Volcanic and plutonic rocks that compose the Late Triassic to Jurassic magmatic belt in Colombia result from partial melting of lower crustal rocks mixed with mantle melts in a continental margin setting. Lithologies include quartz monzonites, monzogranites, syenogranites (locally leucocratic), granodiorites, tonalites, diorites, gabbros, and volcaniclastic successions intersected by porphyritic hypabyssal rocks of andesitic, dacitic, and latitic compositions. The elongated geometry of plutons suggests that the accommodation spaces of magmatic pulses were related to transtensional environments in a supra–subduction tectonic framework with mantle interaction, melting of slab sediments, and crustal contamination. The nature of magmatism resulted from interactions between crustal and mantle–derived magmas in a continental margin setting that progressively changed from Late Triassic postcollisional extension (associated with orogenic collapse?) to a predominantly Late Jurassic volcanic arc developed in a supra–subduction regime; the evolution of the magmatic belt is marked spatially from east to west and temporally over a time span of approximately 60 my. The sources of the Late Triassic to Jurassic magmatic belt are varied and associated with melting of the supra–subduction mantle wedge and differentiation of tholeiitic or mildly calc–alkaline basalts and intermediate rocks and include partial melting of pelitic rocks, tonalites, granodiorites, tholeiites, and high–aluminum basalts or andesites.

Keywords: *high–potassium calc–alkaline rocks, shoshonitic magmatism, active continental margin, postcollisional magmatism, oblique subduction.*

Resumen Las rocas volcánicas y plutónicas que conforman el cinturón magmático del Triásico Tardío–Jurásico en Colombia son el resultado de la fusión parcial de rocas de la corteza inferior mezcladas con fundidos provenientes del manto en un ambiente de margen continental. Las litologías corresponden a cuarzomonzonitas, monzogranitos, sienogranitos (localmente leucocráticos), granodioritas, tonalitas, dioritas, gabros y sucesiones volcanosedimentarias cortadas por rocas hipoabisales porfídicas de composición andesítica, dacítica y latítica. La geometría alargada de los plutones sugiere que los espacios para la acomodación de los pulsos magmáticos se relacionaron con ambientes estructurales transtensivos en un marco tectónico de suprasubducción con interacción del manto, fusión de los sedimentos de la placa subductante y contaminación cortical. La naturaleza del magmatismo es resultado de interacciones entre magmas derivados de la corteza y magmas derivados del manto en un margen continental

Citation: López–Isaza, J.A. & Zuluaga, C.A. 2020. Late Triassic to Jurassic magmatism in Colombia: Implications for the evolution of the northern margin of South America. In: Gómez, J. & Pinilla–Pachon, A.O. (editors), The Geology of Colombia, Volume 2 Mesozoic. Servicio Geológico Colombiano, Publicaciones Geológicas Especiales 36, p. 77–116. Bogotá. https://doi.org/10.32685/pub.esp.36.2019.03

que cambió progresivamente de extensional poscolisional (¿asociado con colapso orogénico?) durante el Triásico Tardío a un arco volcánico desarrollado en un régimen de suprasubducción durante el Jurásico Tardío predominantemente; la evolución del cinturón magmático se marca espacialmente de este a oeste y temporalmente sobre un lapso de aproximadamente 60 millones de años. Las fuentes del arco magmático del Triásico Tardío–Jurásico son variadas y están asociadas con la fusión de la cuña mantélica de suprasubducción y diferenciación de basaltos y rocas intermedias toleíticas o ligeramente calcoalcalinas e incluye fusión parcial de rocas pelíticas, tonalitas, granodioritas, toleítas y basaltos o andesitas ricas en aluminio.

Palabras clave: *rocas calcoalcalinas con alto potasio, magmatismo shoshonítico, margen continental activa, magmatismo poscolisional, subducción oblicua.*

1. Introduction

Igneous rocks, both volcanic and plutonic, develop in different tectonic settings, all of which are linked to the Wilson cycle and therefore to the supercontinent cycle (see, e.g., Nance et al., 2014; Frost et al., 2016; Chen & Zhao, 2017; and references therein). The Pangaea supercontinent reached its configuration during the Triassic, amalgamating continental blocks and terranes (ribbon continents) of different origins (Pindell, 1985; Jaillard et al., 1990; Stampfli et al., 2013; Scotese, 2014a; Belica et al., 2017; Riel et al., 2018). Paleogeographic reconstructions suggest that during late Paleozoic to early Mesozoic times, the northwestern margin of South America (Gondwana) was dominated by the convergence of the Farallón oceanic plate, also defined as the Panthalassa subduction zone along the western margin of Pangaea (Mišković et al., 2009; Muttoni et al., 2009; Belica et al., 2017; Riel et al., 2018). In this paper, we review the significance of Late Triassic and Jurassic magmatism in Colombia and its implications for the evolution of the northwestern margin of Gondwana.

During the Pangaea supercontinent agglomeration, the Alleghanian orogen recorded the closure of the Rheic Ocean and subsequent collision between Laurasia and Gondwana (Craddock et al., 2017). This tectonic framework allowed dextral transcurrent plate motion and the emplacement of Permian – Triassic syntectonic granitoids (e.g., Vinasco et al., 2006; López et al., 2007; Muttoni et al., 2009; Cardona et al., 2010; Cochrane et al., 2014a). On the other hand, the circum–Pacific orogenic system recorded the subduction of Panthalassa (van der Meer et al., 2012; Ganne et al., 2017; Ganne & Feng, 2018).

Later, during the Jurassic, the Pangaea supercontinent breakup marked the progressive opening of ocean basins and the drifting of Gondwana and Laurasia (Scotese, 2014b; Dera et al., 2015; Matthews et al., 2016; Martini & Ortega–Gutiérrez, 2018). In this context, prior to the Atlantic Ocean opening, the separation between the Yucatán Block and the passive margin of Gondwana to the north (today Venezuela) favored the development of the proto–Caribbean seaway (Pindell & Kennan, 2009; Noguera et al., 2011; Martini & Ortega–Gutiérrez, 2018). The Pacific margin of South America, during Mesozoic times, was also experiencing an extensional tectonic regime associated with block faulting and extension above a retreating slab (Pitcher, 1988, 1997). According to Pitcher (1997), this extensional regime started as early as the Permian – Triassic with the development of a graben in the eastern Andes of Perú and Bolivia, which led to crustal thinning and the formation of fault–bounded marginal basins to the west from mid–Ecuador to Patagonia. The northwestern corner of South America is also characterized by Late Triassic to Jurassic extensional marginal basins infilled with deposits produced from erosion, red beds and volcanic products (Cediel et al., 2003).

The modern Andes form a continuous mountain range along the western margin of South America and include fragments of several orogens that partly represent long–lived subduction. Magmatic arc assemblages were emplaced in a continental margin by persistent convergence and interaction between the "Pacific oceanic crust" and the continental "South American Plate" since the Paleozoic (Kirsch et al., 2016; Paul et al., 2018). In particular, a Late Triassic to Jurassic magmatic belt is recognized along the northern Andes from the Gulf of Guayaquil (southern Ecuador) to northern Colombia and Venezuela (Gansser, 1973; Pennington, 1981; Aggarwal, 1983; Aspden et al., 1992; Litherland et al., 1994; Ramos, 1999, 2009; Cediel et al., 2003; Leal–Mejía, 2011; Maloney et al., 2013; Cochrane et al., 2014a, 2014b; Spikings et al., 2015; van der Lelij et al., 2016). Across the Colombian Andes (Figure 1), the belt intersects crystalline basements composed of schists, amphibolites, gneisses, local granulites, and granitoids, with Proterozoic, Paleozoic, and Triassic ages (Aspden et al., 1987; 1992; Bayona et al., 1994; Litherland et al., 1994; Bustamante et al., 2010; Leal–

→

Figure 1. Distribution of Late Triassic to Jurassic magmatism in Colombia; plutonic, hypabyssal, and volcanic rocks representative of each zone are shown with the U/Pb zircon age ranges. Northern Zone: Guajira and Sierra Nevada de Santa Marta, Eastern Central Zone: Santander Massif, Western Central Zone: serranía de San Lucas and Central Cordillera north of 5° N, and Southern Zone: Upper Magdalena Valley.

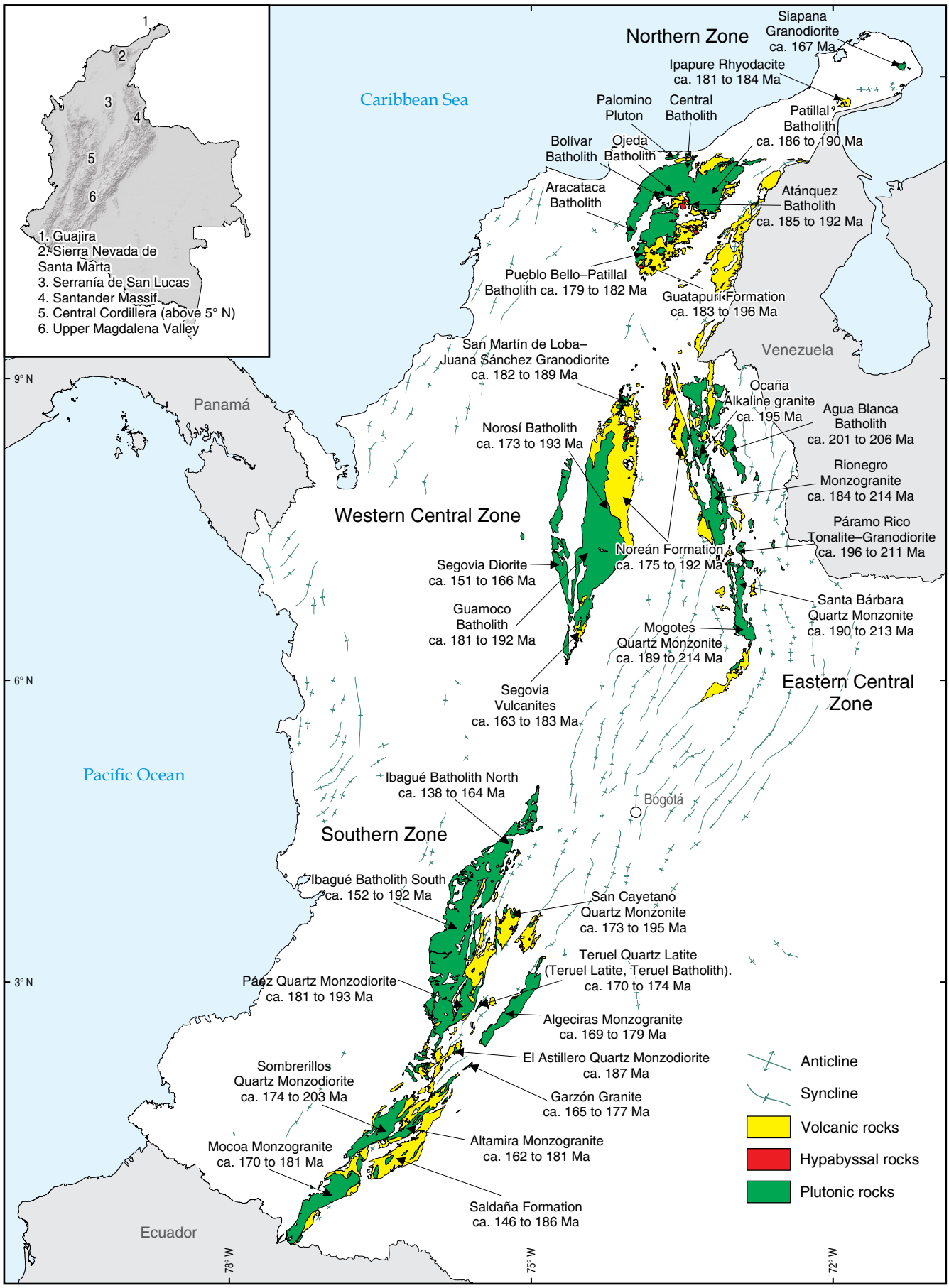
1
2
3
4
5
6
1. Guajira
2. Sierra Nevada de Santa Marta
3. Serranía de San Lucas
4. Santander Massif
5. Central Cordillera (above 5° N)
6. Upper Magdalena Valley
Northern Zone
Siapana Granodiorite ca. 167 Ma
Ipapure Rhyodacite ca. 181 to 184 Ma
Caribbean Sea
Palomino Pluton
Central Batholith
Patillal Batholith ca. 186 to 190 Ma
Bolívar Batholith
Ojeda Batholith
Aracataca Batholith
Atánquez Batholith ca. 185 to 192 Ma
Pueblo Bello–Patillal Batholith ca. 179 to 182 Ma
Guatapurí Formation ca. 183 to 196 Ma
Venezuela
San Martín de Loba–Juana Sánchez Granodiorite ca. 182 to 189 Ma
Ocaña Alkaline granite ca. 195 Ma
Agua Blanca Batholith ca. 201 to 206 Ma
Norosí Batholith ca. 173 to 193 Ma
Rionegro Monzogranite ca. 184 to 214 Ma
Panamá
Western Central Zone
Páramo Rico Tonalite–Granodiorite ca. 196 to 211 Ma
Noreán Formation ca. 175 to 192 Ma
Segovia Diorite ca. 151 to 166 Ma
Santa Bárbara Quartz Monzonite ca. 190 to 213 Ma
Guamoco Batholith ca. 181 to 192 Ma
Mogotes Quartz Monzonite ca. 189 to 214 Ma
Eastern Central Zone
Segovia Vulcanites ca. 163 to 183 Ma
Pacific Ocean
Ibagué Batholith North ca. 138 to 164 Ma
Bogotá
Southern Zone
Ibagué Batholith South ca. 152 to 192 Ma
San Cayetano Quartz Monzonite ca. 173 to 195 Ma
Teruel Quartz Latite (Teruel Latite, Teruel Batholith). ca. 170 to 174 Ma
Páez Quartz Monzodiorite ca. 181 to 193 Ma
Algeciras Monzogranite ca. 169 to 179 Ma
El Astillero Quartz Monzodiorite ca. 187 Ma
Sombrerillos Quartz Monzodiorite ca. 174 to 203 Ma
Garzón Granite ca. 165 to 177 Ma
Mocoa Monzogranite ca. 170 to 181 Ma
Altamira Monzogranite ca. 162 to 181 Ma
Saldaña Formation ca. 146 to 186 Ma
Ecuador
9° N
6° N
3° N
78° W
75° W
72° W
Anticline
Syncline
Volcanic rocks
Hypabyssal rocks
Plutonic rocks

Mejía, 2011; Leal–Mejía et al., 2011; Cochrane et al., 2014a, 2014b; Gómez et al., 2015; Spikings et al., 2015; Zuluaga et al., 2015; van der Lelij et al., 2016).

Models explaining this Late Triassic to Jurassic magmatic belt range from intracontinental extension to continental arc magmatism. Some models suggest the presence of bimodal magmatism that developed during intracontinental extension related to rifting and drifting of the Pangaea supercontinent (Pindell & Dewey, 1982; Clavijo, 1995a; Mojica & Kammer, 1996; Sarmiento–Rojas, 2001; Rolon, 2004; Sarmiento–Rojas et al., 2006; Bayona et al., 2012; Zapata et al., 2012). However, most commonly accepted models involve continental arc magmatism either in a back–arc extension tectonic setting (Leal–Mejía, 2011; Cochrane et al., 2014a, 2014b; Spikings et al., 2015) or along intra–arc extensional basins (Zuluaga et al., 2015). In either case, the geodynamic context is interpreted to have been dominated by subduction–related magmatism followed by the development of transtensional basins from the Late Jurassic to the Early Cretaceous.

The aim of this review is to document the interactions between crustal and mantle–derived magmas in a continental margin that progressively changed from a Late Triassic postcollisional extensional setting (associated with orogenic collapse?) to a predominantly Late Jurassic volcanic arc setting developed in a supra–subduction regime. To support this review, we present an analysis and interpretation of published and unpublished field relations, petrographic descriptions, whole–rock geochemical data, and U/Pb zircon ages. The data set is divided into four zones: (1) Northern Zone (Guajira and Sierra Nevada de Santa Marta); (2) Eastern Central Zone (Santander Massif); (3) Western Central Zone (north of 5° N latitude in the Central Cordillera and serranía de San Lucas); and (4) Southern Zone (Upper Magdalena Valley). This division takes into account both the distribution of igneous rocks along massifs and mountain ranges and the temporality of the magmatism. We argue that the dataset indicates (i) a supra–subduction regime and (ii) a northwestern South America Late Triassic to Jurassic flare–up over a time span of approximately 60 my. This model is supported mostly by an interpretation of variations in magmatic activity based on the relative abundance of known U/Pb zircon ages.

Tectonic interpretations presented here follow the collision concept of Bonin et al. (1998) and Song et al. (2015); e.g., collision is the "welding of at least two terranes into a new continental land", and from this concept, postcollision (or 'late orogenic') is defined as the "episode occurring after the major collision", postorogenic as the "subsequent episodes when the geodynamic context becomes entirely intraplate, with the welded terranes moving according to same pole of rotation", and anorogenic as "later episodes characterized by the presence of alkaline magmatic suites emplaced in intraplate rifts and not associated with local plate convergence". In this context, the magmatic events that accompany the postcollision state are characterized by the presence of peraluminous S–type granite suites and high–K calc–alkaline suites. Pearce et al. (1984) also note that granitic rocks are the most significant magmatic products of collisional belts and can be geochemically discriminated according to the type of collision (continent–continent, continent–arc, arc–arc) and the timing of the main deformation event (syncollisional, postcollisional). Chemically, peraluminous granites are approximately equivalent to S–type granites, and metaluminous granites are approximately equivalent to I–type granites (Chappell & White, 1974; Clarke, 1981; Nédélec & Bouchez, 2015), although I–type granites include Al–poor granites or weakly peraluminous granites (Miller, 1985; Nédélec & Bouchez, 2015). Peraluminous rocks are composed of muscovite, biotite, ilmenite, monazite, aluminosilicates, cordierite, garnet, topaz, tourmaline, spinel, and corundum and are related to continent–continent collision tectonics involving thickened continental crust (Clarke, 1992). Metaluminous rocks consist of biotite, minor muscovite, magnetite, titanite, allanite, orthopyroxene, clinopyroxene, hornblende, and epidote and are associated with subduction–related continental and island arcs (Clarke, 1992). Syncollisional granites are peraluminous S–type granites, and postcollisional granites commonly are calc–alkaline, weakly peraluminous to metaluminous I–type granites, although S– and A–type granites may also be found in this type of environment (Pearce et al., 1984).

The elements Zr, Nb, Y, Yb, La, Ta, Th, Hf, and Co are considered immobile in different geological environments. Therefore, they are used to discriminate tectonic settings and to differentiate magmatic processes and magma sources (Pearce, 1982, 1983; Pearce et al., 1984; Harris et al., 1986; Müller et al., 1992; Thiéblemont & Tégyey, 1994; Gorton & Schandl, 2000; Schandl & Gorton, 2002; Elliott, 2003; Pearce, 2008; Moreno et al., 2014). Additionally, the presence of high–potassium rocks is used to complement interpretations since the K_2O enrichments in granites from the high–potassium calc–alkaline and shoshonitic fields are features that can be generated by different mechanisms, including mantle–derived magma differentiation, reworking of sedimentary materials induced by mantle–derived magmas, or lower continental crust melting (Zhao et al., 2013; Bao et al., 2018).

2. Late Triassic to Jurassic Magmatic Belt in Colombia

The magmatic belt has a longitudinal axis that is parallel to the axes of the mountain ranges and intersects the crystalline cores. In this belt, a magma productivity of ca. 675 000 to 2 362 500 km^3 over a length of ca. 1500 km is estimated by Cochrane et al. (2014b). Most intrusive bodies are nested plutons with mainly sharp faulted contacts and local evidence of injection processes. Common compositional varieties in plutons include quartz monzonites, monzogranites, syenogranites, granodi-

orites, tonalites, diorites, and gabbros (Ordóñez–Carmona et al., 2006; Mantilla–Figueroa et al., 2013; van der Lelij, 2013; Cochrane et al., 2014b; Spikings et al., 2015; van der Lelij et al., 2016). These intrusive rocks usually contain quartz, alkali feldspar, and plagioclase and locally contain pyroxenes, some with muscovite and garnet (typical of S–type peraluminous granitoids) and others with biotite, hornblende, epidote (allanite), and titanite (typical of I–type metaluminous granitoids). In many cases, it is possible to identify intrusive relations with adjacent units due to the development of local injection fabrics and contact zones with hornfels (Figure 2). Plutons commonly have associated aplitic and pegmatitic dikes with compositions ranging from tonalite to gabbro; they are also cut by hypabyssal rhyolite to basalt dikes.

Within the belt, it is common to see volcanic rocks, including tuffs, ignimbrites, lavas, and hypabyssal rocks of different compositions. Volcanic rocks are found in volcanic–sedimentary successions that generally include poorly sorted, matrix–supported to clast–supported coarse tuffaceous deposits. Other commonly observed lithologies include lavas and hypabyssal rocks of dacitic to rhyolitic compositions (Tschanz et al., 1969, 1974; Jaillard et al., 1990; Bayona et al., 1994; Clavijo, 1995a, 1995b; Núñez et al., 1996; Ingeominas & Universidad Industrial de Santander, 2006a, 2006b, 2006c, 2006d; Colmenares et al., 2007; Pinilla–Ocampo, 2013; González et al., 2015a, 2015b, 2015c, 2015d, 2015e, 2015f; Zuluaga et al., 2015; Rodríguez et al., 2016a, 2016b, 2018a, 2018b, 2018c). Lavas are generally porphyritic with phenocrysts of feldspar, quartz, biotite, hornblende, and pyroxenes in a hyalocrystalline to microcrystalline matrix.

The petrographic characteristics for each zone are summarized in the following sections.

2.1. Northern Zone (Guajira and Sierra Nevada de Santa Marta, Table 1)

2.1.1. Guajira

In the Guajira region of Colombia, metaluminous and peraluminous granitoids and volcanic rocks of the high–potassium calc–alkaline series have been related to volcanic arcs that developed in a collisional setting along an active continental margin in the Jurassic (Zuluaga et al., 2015). Plutonic rocks belong to three main large bodies (Ipapure Granodiorite, Siapana Granodiorite, and Cosinas Tonalite) and include granodiorites, monzodiorites, diorites, and tonalites; the estimated ages of these rocks (Rb/Sr whole–rock and U/Pb zircon dating) range from 167 to 184 Ma (MacDonald, 1964; Cardona et al., 2006; Zuluaga et al., 2015; Ríos–Blandón, 2016). The volcanic rocks include andesites, dacites, rhyodacites, and tuffs, which are collectively termed the Ipapure Rhyodacite (Pinilla–Ocampo, 2013; Zuluaga et al., 2015).

2.1.2. Sierra Nevada de Santa Marta

The plutons in Sierra Nevada de Santa Marta consist of diorites, tonalites, granodiorites, and granites of Early Jurassic age that have been grouped into the Socorro Stock, the Nueva Lucha Pluton, and the Central, Bolívar, Ojeda, Aracataca, Atánquez, Pueblo Bello, and Patillal Batholiths (Tschanz et al., 1969, 1974; Colmenares et al., 2007; Quandt, 2013). These rocks have been classified as metaluminous, I–type calc–alkaline rocks of the medium to high–potassium series, considered typical of continental arc settings (Quandt, 2013; López & Zuluaga, 2016; Quandt et al., 2018). Rb/Sr (whole–rock) and K/Ar (hornblende, muscovite, and biotite) ages range from 162 to 181 Ma (Tschanz et al., 1969, 1974), while U/Pb (zircon) crystallization ages range between 176 Ma and 196 Ma (Leal–Mejía, 2011; Quandt et al., 2018). Plutons of the Sierra Nevada de Santa Marta are associated with volcanic rocks, hypabyssal intrusions, and volcaniclastic rocks with andesitic, dacitic, rhyolitic, and basaltic compositions (Tschanz et al., 1969, 1974). Several large ignimbrite bodies are recognized (Los Tábanos, La Piña, Los Clavos, La Paila, and Caja de Ahorros); these rocks were grouped informally with the Golero Rhyolite in the "Jurassic volcaniclastic and volcanic rocks"; however, this grouping did not consider a systematic difference in composition relative to the observed plutonic rocks (see Colmenares et al., 2007 and Quandt et al., 2018).

2.2. Eastern Central Zone (Santander Massif, Table 2)

The Santander Massif is largely composed of several Upper Triassic to Lower Jurassic metaluminous to strongly peraluminous granitoids intruding the Bucaramanga Gneiss and the Silgará Schist metamorphic rocks (Onzaga Granodiorite, Guaca River Diorite, San Martín Tonalite, Suratá Diorite, Tonalite and Granodiorite, Páramo Rico Tonalite and Granodiorite, La Corcova Quartz Monzonite, Pescadero Monzogranite, Santa Bárbara Quartz Monzonite, Mogotes Quartz Monzonite, Ocaña Alkaline Granite, and Rionegro Monzogranite). Compositionally, they are mainly diorite, tonalite, granodiorite, and granite; petrographic and geochemical characteristics and isotopic ages are discussed in several publications including Goldsmith et al. (1971), Ward et al. (1973), Dörr et al. (1995), Restrepo–Pace (1995), Ordóñez–Calderón (2003), Mantilla–Figueroa et al. (2009), Leal–Mejía (2011), Mantilla–Figueroa et al. (2013), van der Lelij (2013), Bissig et al. (2014), Arango et al. (2016), Correa–Martínez et al. (2016, 2018), Rodríguez et al. (2016a, 2017b, 2018c), González et al. (2015g), van der Lelij et al. (2016), Zapata et al. (2016a, 2018), Hernández et al. (2017), López et al. (2017), Rodríguez et al. (2017a), Leal–Mejía et al. (2019), and Zuluaga & López (2019). Geochemical interpretations from these publications agree that the granites have I–

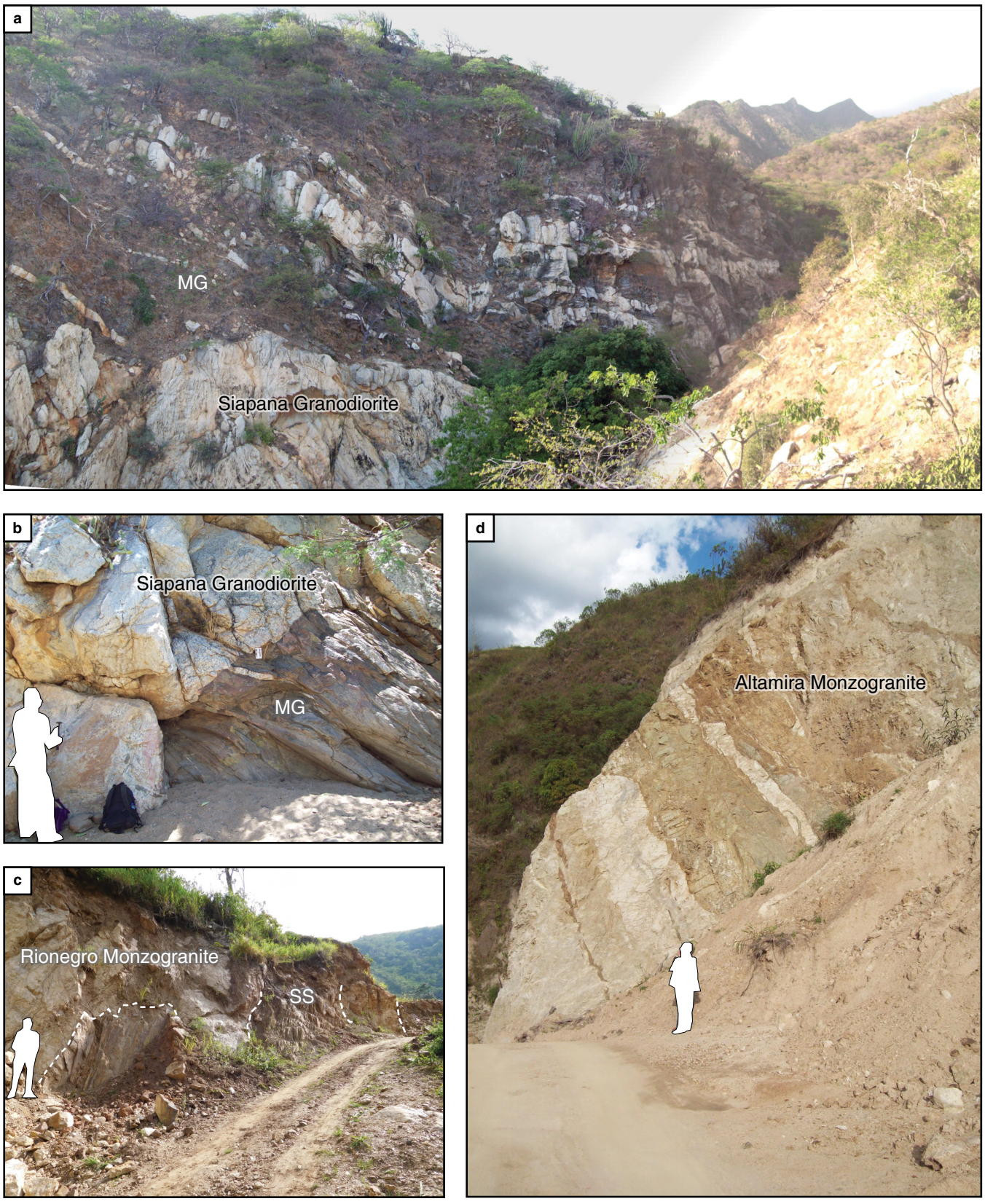

Figure 2. Typical intrusive contacts of plutonic rocks of the Late Triassic to Jurassic magmatic belt in Colombia. **(a)** Border zone of the contact between the Siapana Granodiorite and the Macuira Gneiss (MG), arroyo Guajarima, serranía de Macuira, Northern Zone. **(b)** Sharp contact between the Siapana Granodiorite and the Macuira Gneiss (MG), arroyo Guajarima, serranía de Macuira, Northern Zone. **(c)** Sharp contact between the Rionegro Monzogranite and the Silgará Formation (SS), Santander Massif, Eastern Central Zone. **(d)** Aplitic and mafic dikes intruding the Altamira Monzogranite, Garzón Massif, Eastern Cordillera, Southern Zone.

Table 1. Characteristics of the lithostratigraphic units of the Northern Zone.

Lithostratigraphic unit	Lithology	Contact type/country rock	Age (Ma)	Method	Reference
Guajira Sector					
Siapana Granodiorite	Granodiorite	Intrusive/Permian metamorphic amphibolite facies	167.0 ± 9.4	LA–ICP–MS	Cardona et al. (2006)
Cosinas Tonalite	Tonalite, quartz diorite, quartz monzodiorite.	Faulted/Cenozoic sedimentary rocks			
Ipapure Granodiorite	Tonalite, diorite, granodiorite, monzodiorite, monzogranite.	Intrusive/Jurassic volcanic rocks			
Ipapure Rhyodacite	Andesites, dacites, rhyolite, rhyodacites, tuffs.	Discordant–Intrusive/Jurassic rocks	184.0 ± 0.7 184.0 ± 0.8 181.7 ± 1.0	LA–ICP–MS	Zuluaga et al. (2015)
Sierra Nevada de Santa Marta Sector					
Triassic keratophyric porphyry	Rhyolite, latite, basalt.	Intrusive/Triassic volcanic–sedimentary successions			
Triassic spilites	Basalt, latite.	Triassic volcanic–sedimentary successions			
Pueblo Bello–Patillal Batholith	Quartz monzonite, monzogranite (locally leucocratic), granophyric granite.	Gradational intrusive/Jurassic plutonic and Neoproterozoic metamorphic granulite facies	179.8 ± 3.3 182.2 ± 1.0 179.8 ± 3.3	LA–MC–ICP–MS LA–ICP–MS	Leal–Mejía (2011) Quandt et al. (2018)
Patillal Batholith	Quartz monzonite, monzogranite (locally leucocratic), granophyric granite.	Gradational intrusive/Jurassic plutonic	186.0 ± 0.7 186.4 ± 1.6 189.4 ± 2.0 190.3 ± 1.2	LA–ICP–MS	Quandt et al. (2018)
Central Batholith	Quartz diorite, granodiorite, quartz monzonite.	Intrusive–Faulted/Neoproterozoic metamorphic granulite facies and Jurassic plutonic			
Caja de Ahorros Ignimbrite	Trachytic to andesitic tuffs and ignimbrites.	Discordant–Faulted/Jurassic volcanic–sedimentary successions			
La Paila Ignimbrite	Breccias, ignimbrites and rhyolitic to trachytic tuffs.	Discordant/Jurassic volcanic–sedimentary successions			
Ojeda Batholith	Quartz monzonite, granodiorite, granite.	Intrusive locally gradational			
Atánquez Batholith	Monzogranite, granite, granodiorite, syenite, tonalite.	Gradational intrusive–Faulted/Neoproterozoic metamorphic granulite facies and Jurassic plutonic	192.1 ± 1.7 185.7 ± 1.0	LA–ICP–MS	Quandt et al. (2018)
Aracataca Batholith	Granodiorite, quartz monzonite.	Sharp and gradational intrusive–Faulted/Neoproterozoic metamorphic granulite facies and Jurassic plutonic			
La Piña Ignimbrite	Vitreous–crystalline, trachytic quartz, latitic quartz, and rhyodacitic and lithic tuffs.	Discordant–Faulted/Jurassic volcanic–sedimentary successions			
Los Clavos Ignimbrite	Trachytic to andesitic tuffs and ignimbrites	Discordant/Jurassic plutonic	180.6 ± 1.2 187.2 ± 1.0	LA–ICP–MS	Quandt et al. (2018)
Bolívar Batholith	Tonalite, granodiorite.	Intrusive/Neoproterozoic metamorphic granulite facies and Jurassic plutonic			
Porphyritic granite	Granite	Intrusive			
Nueva Lucha Pluton	Quartz diorite	Intrusive–Faulted/Metamorphic granulite facies and volcanic–sedimentary successions			
Los Tábanos Rhyodacite	Rhyolitic and dacitic tuffs	Discordant/Jurassic volcanic–sedimentary successions	176.0 ± 0.9	LA–ICP–MS	Quandt et al. (2018)
Golero Rhyolite	Rhyolitic and rhyodacitic tuffs, rhyolitic porphyries.	Discordant–Faulted/Jurassic volcanic–sedimentary successions and plutonic rocks			
Socorro Stock	Diorite, granodiorite.	Faulted/Neoproterozoic metamorphic granulite facies			
Guatapurí Formation	Rhyodacite, rhyolite, lithic tuff.	Intrusive–Discordant	196.5 ± 4.9 183.3 ± 3.0 184.5 ± 1.4	LA–MC–ICP–MS LA–ICP–MS	Leal–Mejía (2011) Quandt et al. (2018)

Table 2. Characteristics of the lithostratigraphic units of the Eastern Central Zone.

Lithostratigraphic unit	Lithology	Contact type/country rock	Age (Ma)	Method	Reference
		Santander Sector			
Agua Blanca Batholith	Quartz monzonite, monzogranite, syenogranite, granodiorite, tonalite, gabbro, microgabbro.	Intrusive–Faulted/Ordovician metamorphic granulite – amphibolite – greenschist facies and Triassic – Jurassic volcanic rocks	202.2 ± 1.0 201.4 ± 3.6 204.9 ± 3.6 206 201.0 ± 3.6 204	LA–ICP–MS CA–ID–TIMS	van der Lelij (2013) González et al. (2015g)
Santa Bárbara Quartz Monzonite	Monzonite, monzogranite, granodiorite, syenogranite.	Intrusive–Faulted/Ordovician metamorphic granulite – amphibolite facies and Paleozoic metasedimentary rocks	190.6 ± 1.5 191.9 ± 1.1 195.1 ± 1.9 196.8 ± 2.0 200.7 ± 2.0 201.6 ± 4.0 203.0 ± 2.6 203.8 ± 2.7 213.9 ± 4.3 199.1 ± 5.7 198.0 ± 2.7 202.5 ± 7.8 209.3 ± 7.3 201.6 ± 4.0 203.8 ± 5.8 213.9 ± 4.3 200.7 ± 2.0 203.0 ± 2.6	LA–ICP–MS	Rodríguez et al. (2018b)
Mogotes Quartz Monzonite	Quartz monzonite, monzogranite, syenogranite, granodiorite, quartz monzodiorite, tonalite.	Intrusive/Ordovician metamorphic granulite – amphibolite – greenschist facies and Paleozoic metasedimentary rocks	211.8 ± 3.8 191.0 ± 3.5 198.0 ± 0.8 201.0 ± 0.9 200.4 ± 0.7 202.5 ± 1.3 198.0 ± 0.8 200.4 ± 2.2 195.7 ± 3.9 199.6 ± 1.8 199.6 ± 2.6 189.1 ± 3.6 193.7 ± 1.3 205.4 ± 3.0 202.1 ± 1.8 191.0 ± 3.5 214.0 ± 7.0 199.0 ± 6.0 203.9 ± 3.9 203.8 ± 4.2 197.6 ± 3.8 191.0 ± 6.5 199.0 ± 6.5 199.6 ± 2.6 193.0 ± 5.6 203.0 ± 4.5 201.0 ± 3.7	LA–ICP–MS CA–ID–TIMS	van der Lelij (2013) Correa–Martínez et al. (2016) Zapata et al. (2018)
La Corcova Quartz Monzonite	Monzogranite, granodiorite, syenogranite, alkali feldspar granite, quartz diorite, quartz monzonite, tonalite subordinate near the margin.	Intrusive/Ordovician metamorphic granulite – amphibolite facies	192.5 ± 2.6 198.3 ± 1.8 199.5 ± 4.6 202.7 ± 1.2 204.8 ± 6.1 210.48 ± 0.92 201.8 ± 4.0 199.5 ± 6.3 214.9 ± 7.3 200.0 ± 11.0 192.9 ± 2.7	LA–ICP–MS CA–ID–TIMS	van der Lelij (2013) Rodríguez et al. (2016a)

Table 2. Characteristics of the lithostratigraphic units of the Eastern Central Zone (*continued*).

Lithostratigraphic unit	Lithology	Contact type/country rock	Age (Ma)	Method	Reference
		Santander Sector			
Páramo Rico Tonalite–Granodiorite	Granodiorite, tonalite, monzogranite (locally) leucocratic.	Intrusive/Ordovician metamorphic granulite – amphibolite – greenschist facies and Upper Triassic plutonic rocks	208.9 211.1 205+5/–9 205–210 210.6 ± 3.5 204.3+2.7/–3.3 202.2+5.3/–3.3 199.1+2.5/–2.6 199.2+2.8/–2.7 199.0+2.5/–2.6 198.4+2.5/–2.6 198.7–2.6/–2.9 196.7+2.9/–2.8 199.8 ± 1.2 208.8 ± 4.1	LA–ICP–MS LA–MC–ICP–MS TIMS CA–ID–TIMS Total dilution	Dörr et al. (1995) Leal–Mejía (2011) Mantilla–Figueroa et al. (2009, 2013) van der Lelij (2013) Bissig et al. (2014)
Rionegro Monzogranite	Quartz monzonite, monzogranite, syenogranite, quartz diorite, quartz syenite, granodiorite, tonalite, diorite, gabbro, gabbronorite, subordinate charnockite.	Intrusive/Ordovician metamorphic granulite – amphibolite – greenschist facies	196.0 ± 1.1 184.1 ± 2.3 186.7 ± 1.9 194.5 ± 1.2 195.5 ± 3.5 196.6 ± 2.1 197.2 ± 1.5 200.8 ± 1.9 214.5 ± 2.7 189.9 ± 1.6 191.2 ± 9.7 186.4 ± 3.6 184.3 ± 6.6 213.6 ± 3.2 193.0 ± 16.0 207.3 ± 1.6 196.6 ± 2.1 195.9 ± 1.6	LA–ICP–MS CA–ID–TIMS	van der Lelij (2013) Arango et al. (2016)
Pescadero Monzogranite	Monzogranite with biotite and muscovite, syenogranite, local granodiorite.	Intrusive/Ordovician metamorphic granulite – amphibolite – greenschist facies	194.8 ± 3.2 197.3 ± 2.4 199.1 ± 1.3 198.1 ± 8.2 196.0 ± 15.0	LA–ICP–MS CA–ID–TIMS	van der Lelij (2013) Zapata et al. (2016a)
Ocaña Alkaline Granite	Quartz monzonite and monzogranite with biotite and muscovite, in complex relationships with rhyolite.	Intrusive/Ordovician metamorphic granulite – amphibolite facies	195.8 ± 1.8 195.9 ± 1.6	CA–ID–TIMS	van der Lelij (2013) Arango et al. (2016)
Onzaga Granodiorite	Granodiorite, quartz monzonite, monzonite.	Intrusive/Ordovician metamorphic granulite – amphibolite facies	200.4 ± 0.7 201.0 ± 0.9	CA–ID–TIMS	van der Lelij (2013)
Suratá Diorite, Tonalite and Granodiorite	Diorite, granodiorite, tonalite with biotite and hornblende.	Intrusive/Ordovician metamorphic granulite – amphibolite – greenschist facies	201.1 ± 1.4 200.0 ± 1.5	CA–ID–TIMS	van der Lelij (2013)
Guaca River Diorite	Diorite	Intrusive/Ordovician metamorphic granulite – amphibolite facies			
San Martín Tonalite	Monzogranite, granodiorite, tonalite, quartz diorite, quartz monzonite, quartz monzodiorite.	Intrusive/Ordovician metamorphic granulite – amphibolite facies	198.9 ± 1.8 198.0 ± 2.8 187.3 ± 7.2 196.6 ± 2.5 197.8 ± 7.0 195.0+6.0–7.7 191.0 ± 5.0	LA–ICP–MS	Rodríguez et al. (2017b)
El Uvo Rhyolites	Rhyolite	Intrusive/Upper Triassic plutonic rocks	197.5 ± 1.5	LA–ICP–MS	Zapata et al. (2018)
San Joaquín Rhyolite	Rhyolite, pheno dacite, pheno–andesite.	Intrusive–Faulted/Paleozoic metasedimentary and Upper Triassic plutonic rocks	201.0 ± 2.1	LA–ICP–MS	Rodríguez et al. (2018c)

Table 2. Characteristics of the lithostratigraphic units of the Eastern Central Zone (*continued*).

Lithostratigraphic unit	Lithology	Contact type/country rock	Age (Ma)	Method	Reference
		Santander Sector			
Alto Los Cacaos Rhyolite	Rhyolite, quartz trachyte, pheno–andesite.	Intrusive–Faulted/Ordovician metamorphic granulite – amphibolite – greenschist facies and Upper Triassic plutonic rocks	205.2 ± 2.6	LA–ICP–MS	Correa–Martínez et al. (2018)
Noreán Formation (Noreán Volcanic Complex)	Lapilli and ash crystal lithic tuffs of dacitic to rhyolitic compositions, lithic agglomerates, polymictic igneous breccias of andesitic and dacitic compositions, and rhyodacitic lavas in addition to basalts, trachytes and andesites. Hypabyssal rocks of andesitic composition.	Discordant–Intrusive/Jurassic rocks	192.4 ± 2.2 184.9 ± 2.0 175.9 ± 1.1	LA–ICP–MS	Correa–Martínez et al. (2019)

and S–type high–potassium calc–alkaline and shoshonitic series signatures and that they were likely emplaced in a continental margin arc setting. Rb/Sr (whole–rock) and U/Pb (zircon) ages range from 210 to 111 Ma. K/Ar (biotite) and Ar/Ar (biotite–hornblende) plutonic and host metamorphic rock cooling ages range between ca. 208 and 172 Ma. Cooling ages in the metamorphic host rocks suggest that the calc–alkaline magmatic event was an important regional thermal disturbance; e.g., a large volume of magma was emplaced during crustal thinning coeval with the disaggregation of the Pangaea supercontinent. The magmatic pulses also produced significant amounts of volcanic rocks, hypabyssal intrusions, and volcaniclastic rocks with andesitic, dacitic, rhyolitic, and rhyodacitic compositions (Norean Formation; Clavijo, 1995a; Rodríguez et al., 2017b, 2018c; Correa–Martínez et al., 2018; Zapata et al., 2018).

2.3. Western Central Zone (Serranía de San Lucas and Central Cordillera, Table 3)

2.3.1. Serranía de San Lucas

Plutons in the serranía de San Lucas include the San Lucas Granitoids, Norosí and Guamoco Batholiths, San Martín de Loba–Juana Sánchez Granodiorites, and Papayal Monzonite; these are Jurassic granodioritic to dioritic I–type calc–alkaline medium– to high–potassium series granites emplaced in a continental arc setting (see Mantilla–Figueroa et al., 2007; Leal–Mejía, 2011; González et al., 2015a, 2015b, 2015c, 2015d, 2015e). Rb/Sr (whole–rock), K/Ar (hornblende, muscovite, and biotite), and U/Pb (zircon) ages range from 201 to 135 Ma (Ingeominas & Universidad Industrial de Santander, 2006a, 2006b, 2006c, 2006d; Leal–Mejía, 2011; González et al., 2015a, 2015b, 2015c, 2015d, 2015e). Associated volcanic rocks include andesite to rhyodacite hypabyssal intrusions and volcaniclastic rocks. Volcanic and volcaniclastic rocks, mostly dacitic crystalline tuffs, andesitic–dacitic breccias, and basaltic flows, are grouped as the Noreán Formation or the Noreán Volcanic Complex (Clavijo et al., 1992; Clavijo, 1995a, 1995b; Ingeominas & Universidad Industrial de Santander, 2006a, 2006b, 2006c, 2006d; González et al., 2015a, 2015b, 2015c, 2015d, 2015e).

2.3.2. Central Cordillera (North of 5° N)

In the northern part of the Central Cordillera (north of 5° N), Upper Jurassic quartz diorite to tonalite calc–alkaline plutonic rocks (Segovia Diorite) and dacite to latite calc–alkaline volcanic rocks (Segovia Vulcanites and La Malena Volcanic Asssemblage) have been related to volcanic arcs in subduction settings (González & Londoño, 2002; Leal–Mejía, 2011; Universidad Pedagógica y Tecnológica de Colombia & Ingeominas, 2011; Zapata et al., 2013; González et al., 2015f). Lu/Hf and U/Pb (zircon) ages range from 158 to 183 Ma (Leal–Mejía, 2011; Zapata et al., 2013; González et al., 2015f).

2.4. Southern Zone (Upper Magdalena Valley, Table 4)

Jurassic dioritic to tonalitic stocks and batholiths, hypabyssal intrusions and dacitic crystalline tuffs, andesitic–dacitic breccias and basaltic flows in the Upper Magdalena Valley are distributed in three geographical provinces: (i) Eastern slope of the Central Cordillera, (ii) Magdalena Valley, and (iii) Eastern Cordillera. The petrological characteristics and ages of these plutons and volcanics are presented and discussed in Álvarez (1983), Jaillard et al. (1990), Bayona et al. (1994), Núñez et al. (1996), Gómez (2002), González & Núñez (2002), Núñez (2002), Leal–Mejía (2011), Villagómez et al. (2011), Álvarez (2013), Cochrane et al. (2014b), Arango et al. (2015a, 2015b, 2015c), Rodríguez et al. (2015a, 2015b, 2015c, 2015d, 2016a,

Table 3. Characteristics of the lithostratigraphic units of the Western Central Zone.

Lithostratigraphic unit	Lithology	Contact type/country rock	Age (Ma)	Method	Reference
Serranía de San Lucas Sector					
Noreán Formation (Noreán Volcanic Complex)	Lapilli and ash crystal lithic tuffs of dacitic to rhyolitic compositions, lithic agglomerates, polymictic igneous breccias of andesitic and dacitic compositions, and rhyodacitic lavas in addition to basalts, trachytes and andesites. Hypabyssal rocks of andesitic composition.	Discordant–Intrusive/Jurassic plutonic rocks	196.1 ± 4.4 190.1 ± 3.2 189.0 ± 3.3 190.0 ± 2.2 194.0 ± 2.3 201.6 ± 3.6 189.0 ± 3.0 187.0 ± 0.96 178.1 ± 5.6 201.6 ± 3.6 174.3 ± 2.7 192.0 ± 3.2 189.6 ± 1.7 187.44 ± 0.96 189.0 ± 3.0 187.0 ± 0.96	LA–ICP–MS LA–MC–ICP–MS	Leal–Mejía (2011) González et al. (2015a, 2015b, 2015e)
Norosí Granite (Norosí Batholith)	Monzogranite, syenogranite, tonalite, granodiorite, monzodiorite, microdiorite, subordinate gabbronorite, with pyroxene (clino– and orthopyroxene).	Intrusive/Jurassic volcanic–sedimentary successions	184.6 ± 3.6 193.4 ± 5.8 189.0 ± 2.8 187.2 ± 2.8 180 178.2 ± 4.3 181.8 ± 3.2 173 184 193.0 ± 3.3 189.0 ± 2.8	LA–MC–ICP–MS	Ordóñez–Carmona et al. (2009) Leal–Mejía (2011) Cuadros (2012) Cuadros et al. (2013) González et al. (2015b)
Guamoco Granodiorite (Guamoco Batholith)	Granodiorite, tonalite, monzogranite, quartz monzodiorite, quartz diorite, syenogranite, granites.	Intrusive–Faulted/Mesoproteroizoic metamorphic granulite – amphibolite facies, Paleozoic metasedimentary rocks and Triassic – Jurassic volcanic–sedimentary successions	186.8 ± 2.9 190.3 ± 3.1 190.3 ± 1.6 186.0 ± 2.5 183.3 ± 4.4 183.0 ± 2.5 184.0 ± 3.5 183.2 ± 2.8 185.4 ± 3.4 189.6 ± 2.8 189.4 ± 1.3 187.2 ± 2.9 186.6 ± 1.6 188.8 ± 2.6 185.3 ± 2.6 182.1 ± 3.0 181.9 ± 2.7 185.7 ± 2.6 188.8 ± 1.3 185.4 ± 2.1 185.3 ± 1.4 185.7 ± 2.6 192.0 ± 3.2	LA–MC–ICP–MS	Leal–Mejía (2011) González et al. (2015e)
San Martín de Loba–Juana Sánchez Granodiorites	Granodiorite, with pyroxene (clino– and orthopyroxene).	Intrusive/Jurassic volcanic–sedimentary successions	182.0 ± 3.0 186.3 ± 5.2 189.0 ± 4.0 184.6 ± 4.8	SHRIMP LA–MC–ICP–MS	Leal–Mejía (2011)
Papayal Monzonite	Monzonite	Intrusive/Jurassic volcanic–sedimentary successions	193.6 ± 5.4	LA–MC–ICP–MS	Leal–Mejía (2011)

Table 3. Characteristics of the lithostratigraphic units of the Western Central Zone (*continued*).

Lithostratigraphic unit	Lithology	Contact type/country rock	Age (Ma)	Method	Reference
Central Cordillera (north of 5° N) Sector					
Segovia Vulcanites	Dacites, andesites, latites, subordinate tuffs.	Intrusive–Faulted/Paleozoic? metamorphic amphibolite facies and Jurassic plutonic rocks	165.5 ± 2.1	LA–MC–ICP–MS	González et al. (2015f)
La Malena Volcanic Assemblage	Dacitic, latitic, trachytic, basaltic, rhyolitic and rhyodacitic volcanic flows, volcanic breccias, lamprophyres, crystalline, crystal–vitreous and lithic ash tuffs, and andesitic and trachytic porphyries.	Discordant–Faulted–Intrusive/ Metasedimentary and plutonic rocks	183.2 ± 3.0 163.1 ± 2.18 163.51 ± 0.95	LA–ICP–MS	González et al. (2015e)
Segovia Diorite	Granodiorite, tonalite, diorite, quartz diorite, gabbro, quartz monzonite, monzogranite, syenogranite, subordinate alkali feldspar granite.	Intrusive–Faulted/Paleozoic? metamorphic amphibolite facies and Jurassic volcanic–sedimentary rocks	166.5+2.3/2.5 164.6 ± 2.4 158.7 ± 2.0 160.7+2.4/–2.3 159.0 ± 2.4 162.7 ± 2.6 163.1 ± 2.8 160.0 ± 2.4 158.0 ± 2.4 158.0 ± 0.87 155.37 ± 0.81 162.0 ± 2.5 157.0 ± 7.2 158.0 ± 0.87 154.0 ± 1.6 151.1 ± 7.2 161.0 ± 2.7	LA–MC–ICP–MS	Frantz et al. (2007) Leal–Mejía (2011) González et al. (2015b, 2015f)

2016b, 2018a), Spikings et al. (2015), Bustamante et al. (2016), van der Lelij et al. (2016), Zapata et al. (2016b), García–Chinchilla (2018), and Rodríguez (2018). The main named bodies include Las Minas Monzonite, Garzón Granite, Altamira, Algeciras, and Mocoa Monzogranites, San Cayetano, Anchique, Dolores, Sombrerillos, and Los Naranjos Quartz Monzonites, El Astillero Quartz Monzodiorite, Teruel Quartz Latite, Del Páez Quartz Monzodiorite, Ibagué Batholith, and the Saldaña Formation. These rocks have been classified as I–type granites (Cordilleran or Andean) of the calc–alkaline and high–K calc–alkaline series related to magmatic arc settings on continental margins. U/Pb (zircon) ages allow the identification of two groups likely related to magmatic pulses: (i) a pulse that produced most plutonic rocks with ages ranging from 203 to 162 Ma (including an age group at the southern end of the Ibagué Batholith of 192 to 152 Ma) and (ii) a pulse that produced acidic volcanic rocks (Saldaña Formation) with ages ranging from 200 to 146 Ma and probably the northern sector of the Ibagué Batholith with ages ranging from 164 to 138 Ma. The remnants of the calc–alkaline magmatic belt in the Upper Magdalena Valley intrude the metamorphic basement of the Garzón Massif and the eastern flank of the Central Cordillera (Bayona et al., 1994; Altenberger & Concha, 2005; Bustamante et al., 2010, 2016; Leal–Mejía, 2011; Villagómez et al., 2011; Cochrane et al., 2014b; García–Chinchilla, 2018).

3. Age Data Compilation

Three hundred ten U/Pb crystallization ages for intrusive and effusive igneous rocks were compiled from Dörr et al. (1995), Bustamante et al. (2010, 2016), Leal–Mejía (2011), Mantilla–Figueroa et al. (2013), Cochrane (2013), Salazar–Torres et al. (2013), van der Lelij (2013), Bissig et al. (2014), Cochrane et al. (2014a, 2014b), Arango et al. (2015a, 2015b, 2015c, 2015d, 2015e, 2016), Gómez et al. (2015), González et al. (2015a, 2015b, 2015c, 2015d, 2015e, 2015f, 2015g), Rodríguez et al. (2015a, 2015b, 2015c, 2015d, 2016a, 2016b, 2017a, 2017b, 2018a, 2018b, 2018c), Bustamante (2016), Correa–Martínez et al. (2016, 2018), Quiceno–Colorado et al. (2016), van der Lelij et al. (2016), Zapata et al. (2016a, 2016b, 2018), García–Chinchilla (2018), Quandt et al. (2018), and Leal–Mejía et al. (2019). Age compilation combines data obtained by laser ablation inductively coupled plasma mass spectrometer (LA–ICP–MS), laser ablation multi–collector inductively coupled plasma mass spectrometer (LA–MC–ICP–MS), sensitive high–resolution ion microprobe (SHRIMP), and chemical decomposition (dilution) of zircons.

Table 4. Characteristics of the lithostratigraphic units of the Southern Zone.

Lithostratigraphic unit	Lithology	Contact type/country rock	Age (Ma)	Method	Reference
		Central Cordillera Sector			
Ibagué Batholith	North: Tonalite, granodiorite, diorite, granite (ca. 154 Ma). South: Quartz monzodiorite, diorite, quartz diorite, granodiorite, quartz monzonite, monzonite, monzodiorite (ca. 182 Ma).	Intrusive–Faulted/Neoproterozoic? metamorphic amphibolite – granulite facies, Paleozoic metamorphic greenschist – amphibolite facies and Triassic calcareous rocks.	138.7 ± 1.0 145.56 ± 0.92 149.3 ± 2.8 152.9 ± 3.1 153.9 ± 1.1 155.4 ± 2.2 156.5 ± 1.1 164.4 ± 1.1 186.8 ± 2.8 182.7 ± 2.7 188.4+2.8/–2.7 186.0 ± 3.1 188.5 ± 3.3 192.3 ± 3.1 166.0 ± 10.0 159.6 ± 2.4 175.0 ± 2.0 173.6 ± 1.5 164.4 ± 1.1 168.8 ± 0.7 156.5 ± 1.1 155.7 ± 2.2 188.9 ± 2.0 169.6 ± 2.4 180.4 ± 1.6 180.5 ± 2.7 185.9 ± 1.4 186.0 ± 2.6 141.9+1.1–0.8 158.2+1.2–0.4 152.61+1.82–0.74	LA–MC–ICP–MS LA–ICP–MS	Bustamante et al. (2010) Leal–Mejía (2011) Villagómez et al. (2011) Cochrane et al. (2014b) Bustamante et al. (2016) Zapata et al. (2016b) Rodríguez et al. (2018a)
Payandé Stock	Granodiorite	Intrusive/Triassic calcareous rocks and Permian? plutonic rocks	164.07 +2.11/–0.96 164.59 +1.05/–2.76	LA–ICP–MS	Bustamante (2016)
Del Páez Quartz Monzodiorite	Quartz monzodiorite, monzodiorite, gabbro, diorite, monzogranite, tonalite, granodiorite, with pyroxene (clino– and orthopyroxene).	Intrusive–Faulted/Neoproterozoic? metamorphic amphibolite – granulite facies; Jurassic volcanic–sedimentary successions and Cretaceous sedimentary rocks.	181.7 ± 3.8 193.13 ± 1.4	LA–MC–ICP–MS LA–ICP–MS	Rodríguez et al. (2018a)
Anchique Quartz Monzonite	Quartz monzonite, monzonite, granite, with pyroxene (clinopyroxene).	Intrusive/Jurassic volcanic–sedimentary successions	183.5 ± 3.0 186.4 ± 1.4	LA–MC–ICP–MS LA–ICP–MS	Arango et al. (2015c) Rodríguez et al. (2018a)
El Astillero Quartz Monzodiorite	Quartz monzodiorite, monzodiorite, quartz diorite, quartz monzonite, with pyroxene (clino– and orthopyroxene).	Intrusive/Jurassic volcanic–sedimentary successions	187.0 ± 3.3	LA–MC–ICP–MS LA–ICP–MS	Rodríguez et al. (2015c) Rodríguez et al. (2018a)
Sombrerillos Quartz Monzonite (Quartz Monzodiorite)	Granodiorite, syenogranite, tonalite, quartz monzonite, and quartz monzodiorite, with pyroxene (clino– and orthopyroxene).	Intrusive–Faulted/Paleozoic sedimentary rocks and Jurassic volcanic–sedimentary successions	189.0 ± 7.0 187.0 ± 1.0 187.0 ± 2.0 203.9 ± 2.3 180.3 ± 2.9 174.0 ± 1.5	LA–MC–ICP–MS LA–ICP–MS	García–Chinchilla (2018) Rodríguez et al. (2018a)

Table 4. Characteristics of the lithostratigraphic units of the Southern Zone (*continued*).

Lithostratigraphic unit	Lithology	Contact type/country rock	Age (Ma)	Method	Reference
Magdalena Valley Sector					
San Cayetano Quartz Monzonite	Quartz monzonitie and quartz monzodioritie, with pyroxene (clino– and orthopyroxene).	Intrusive/Jurassic volcanic–sedimentary successions	195.8 ± 1.5 173.3 ± 1.3	LA–MC–ICP–MS LA–ICP–MS	Rodríguez et al. (2018a)
Los Naranjos Quartz Monzonite	Quartz monzonite, monzonite and granite, with pyroxene (clinopyroxene).	Intrusive/Jurassic volcanic–sedimentary successions	187.9 ± 1.3	LA–MC–ICP–MS LA–ICP–MS	Rodríguez et al. (2015b) Rodríguez et al. (2018a)
Teruel Quartz Latite (Teruel Latite, Teruel Batholith)	Quartz latite, rhyolite, dacite, with pyroxene (clinopyroxene).	Intrusive–Faulted/Jurassic volcanic–sedimentary successions and Cretaceous sedimentary rocks	174.1 ± 2.0 170.5 ± 1.1	LA–MC–ICP–MS LA–ICP–MS	Arango et al. (2015b) Rodríguez et al. (2018a)
Eastern Cordillera Sector					
Dolores Quartz Monzonite (Dolores Stock)	Quartz monzonite, quartz syenite.	Faulted/Cretaceous sedimentary rocks			
Algeciras Monzogranite	Monzogranite, granodiorite, with pyroxene (clinopyroxene).	Intrusive–Faulted/Paleozoic sedimentary rocks, Jurassic volcanic–sedimentary successions and Paleogene – Neogene sedimentary rocks	176.0 ± 2.0 179.0 ± 1.9 169.6 ± 1.2	LA–MC–ICP–MS LA–ICP–MS	Rodríguez et al. (2015d) García–Chinchilla (2018) Rodríguez et al. (2018a)
Garzón Granite	Granodiorite, monzodiorite, quartz monzodiorite, with pyroxene (clinopyroxene).	Faulted/Cenozoic sedimentary rocks	177.8 ± 4.2 165.3 ± 4.0 170.8 ± 2.4	LA–MC–ICP–MS LA–ICP–MS	Bustamante et al. (2010) Rodríguez et al. (2015a) Rodríguez et al. (2018a)
Altamira Monzogranite	Monzogranite, quartz monzonite, syenogranite.	Intrusive–Faulted/Jurassic volcanic–sedimentary successions and Cenozoic sedimentary rocks	181.6 ± 1.3 181.7 ± 6.3 162.0 ± 3.0 178.97 ± 0.4 169.4 ± 3.2	LA–MC–ICP–MS LA–ICP–MS	Bustamante et al. (2010) Arango et al. (2015d) García–Chinchilla (2018) Rodríguez et al. (2018a)
Mocoa Monzogranite	Monzogranite, granodiorite, syenogranite, tonalite, quartz diorite, quartz monzonite, quartz monzodiorite.	Intrusive/Jurassic volcanic–sedimentary successions	170.2 ± 2.7 180.4 ± 1.6 181.8 ± 1.3 170.7 ± 2.1	LA–MC–ICP–MS LA–ICP–MS	Leal–Mejía (2011) Arango et al. (2015e) Zapata et al. (2016b) Rodríguez et al. (2018a)
Serranía de Las Minas (transition between the Upper Magdalena Valley and the Central Cordillera) Sector					
Las Minas Monzonite	Quartz monzodiorite, diorite–monzodiorite, dioritic, with pyroxene (clino– and orthopyroxene).	Intrusive/Jurassic volcanic–sedimentary successions, Neoproterozoic? metamorphic amphibolite – granulite facies and Paleozoic sedimentary rocks.	193.4 ± 1.0 197.6 ± 1.9 187.4 ± 2.3 181.6 ± 3.4	LA–MC–ICP–MS LA–ICP–MS	Arango et al. (2015a) Bustamante et al. (2010) Rodríguez et al. (2018a)
Andesitic–dacitic porphyry	Andesite, dacite.	Intrusive/Jurassic volcanic–sedimentary successions			
Hypabyssal porphyries	Rhyolite, dacite.	Intrusive/Jurassic plutonic rocks	172.0 ± 1.0 175.0 ± 3.0 167.0 ± 2.0	LA–MC–ICP–MS LA–ICP–MS	García–Chinchilla (2018)
Saldaña Formation	Glassy, lithic and crystal tuffs, lavas of andesitic, dacitic, trachyandesitic, quartz latitic, and rhyolitic compositions, and hypabyssal andesitic and dacitic rocks.	Discordant–Intrusive	185.9 ± 1.4 186.0 ± 2.6 179.0 ± 2.0 181.5 ± 1.6 158.5 ± 1.0 146.8 ± 1.5	LA–ICP–MS	Cochrane et al. (2014b) Rodríguez et al. (2016b) Zapata et al. (2016b)

The following list gives the geochronological data distribution: (i) 19 U/Pb ages for the Northern Zone, (ii) 86 U/Pb ages for the Southern Zone, (iii) 132 U/Pb ages for the Eastern Central Zone, and (iv) 73 U/Pb ages for the Western Central Zone.

U/Pb (zircon) geochronological data were plotted in histograms with a 2 my bin width overlain by the kernel density estimates (KDEs; Vermeesch, 2012). The histograms were constructed using a constant bin size for visually evaluating the numbers of samples forming age peaks between the geochronological U/Pb (zircon) data, allowing comparisons between the age populations in the four zones. We adopted the KDE calculation, which visually has an appearance similar to that of probability density plots (PDPs), in which the bandwidth is varied according to the local density (Vermeesch, 2012). KDE calculation was accomplished using an open–source Java application developed by Vermeesch (2012) that enables the visualization of U/Pb age data (Density Plotter – a Java application for kernel density estimation, downloaded from https://www.ucl.ac.uk/~ucfbpve/densityplotter/). For the spatiotemporal distribution and the representation of magmatic activity in terms of the episodic pattern behavior (magmatic tempo) of arc magmatism, we use the terms flare–up (periods with high magma addition rates or waxing magmatism) and lulls (periods with low magma addition rates or reduced magmatism) in the sense of De Silva et al. (2015), Ducea et al. (2015), Paterson & Ducea (2015), and Kirsch et al. (2016).

4. Geochemical Data Compilation

This review is based on a compilation of published and unpublished whole–rock geochemical data for Colombia and contains major (1059) and trace (1006) element analyses at different locations along the Late Triassic to Jurassic magmatic belt. The published geochemical data set was compiled using information from Dörr et al. (1995), Bustamante et al. (2010; 2016), Mantilla–Figueroa et al. (2013), Cochrane (2013), Salazar–Torres et al. (2013), van der Lelij (2013), Bissig et al. (2014), Cochrane et al. (2014b), Arango et al. (2015a, 2015b, 2015c, 2015d, 2016), González et al. (2015a, 2015b, 2015c, 2015d, 2015e, 2015f, 2015g), Rodríguez et al. (2015a, 2015b, 2015c, 2015d, 2016a, 2016b, 2017a, 2017b, 2018a, 2018b, 2018c), Correa–Martínez et al. (2016, 2018), Quiceno–Colorado et al. (2016), van der Lelij et al. (2016), Zapata et al. (2016a, 2016b, 2018), García–Chinchilla (2018), Quandt et al. (2018), Leal–Mejía et al. (2019), and Zuluaga & López (2019). New whole–rock geochemical data for the San Cayetano Stock and the Saldaña Formation complement the compilation presented here (see Table 1 of the Supplementary Information). The compilation includes 713 samples of plutonic rocks, 51 samples of hypabyssal rocks, and 224 samples of volcanic rocks, all distributed along the four zones: (i) 193 analyses for the Northern Zone, (ii) 235 analyses for the Southern Zone, (iii) 275 analyses for the Eastern Central Zone, and (iv) 285 analyses for the Western Central Zone. The dataset was filtered in order to exclude geochemical analyses with loss on ignition (LOI) greater than 2.5% (71 analyses). During processing, the results obtained with major elements were contrasted with results obtained from trace elements to ensure consistency. All graphics were obtained using the open–source (freeware) R language package called Geochemical Data Toolkit (GCDkit), which provides a flexible and comprehensive environment for efficient data processing and visualization (Janoušek et al., 2004).

5. Spatiotemporal Distribution of Upper Triassic to Jurassic Igneous Rocks in Colombia

In the current tectonic configuration of northwestern South America, the Upper Triassic to Jurassic plutonic suites are spatially located in the mountain ridges and piedmonts (Central and Eastern Cordilleras, Sierra Nevada de Santa Marta, and serranía de Perijá), whereas Jurassic volcaniclastic successions are mainly distributed towards the margins of intramontane valleys (Magdalena and Cesar Rivers); these magmatic suites are distributed across a total area of approximately 50 500 km^2. U/Pb (zircon) ages from the Late Triassic to Jurassic magmatic belt show several peaks interpreted as results of periods of increase and decrease in magmatic activity (Figure 3). A peak of approximately 200 Ma characterizes the Eastern Central Zone, and this peak represents the oldest pulse in the belt (Figure 3a). Magmatic activity is null in this zone from ca. 184 Ma; this magmatic quiescence contrasts with the presence of peaks of high magmatic activity in the Southern, Western Central, and Northern zones at ca. 186 Ma (Figure 3b–d) and suggests a migration of the magmatic front towards the west. In the Southern Zone, an important peak is observed at ca. 170 Ma (Figure 3b), whereas in the Western Central and Northern zones, there is a lull during this time (Figure 3c, 3d). The final magmatic episode is registered in the Southern and Western Central zones with a peak at ca. 158 Ma (Figure 3b, 3c). Overall, the magmatic activity in the northwestern margin of South America spanned a time of approximately 60 my. This activity had lull periods during the Late Triassic and Early Jurassic – Early Cretaceous (Figure 3e). The described pattern for the Late Triassic to Jurassic magmatic belt is a probable record of a magmatic flare–up with magmatic tempos between 10 and 20 my (cf., Paterson & Ducea, 2015; Kirsch et al., 2016).

6. Geochemical Characteristics of the Late Triassic to Jurassic Magmatic Belt in Colombia

Harker diagrams show that most major element concentrations ($Fe_2O_{3(T)}$, TiO_2, MgO, CaO, Al_2O_3, and P_2O_5) decrease with in-

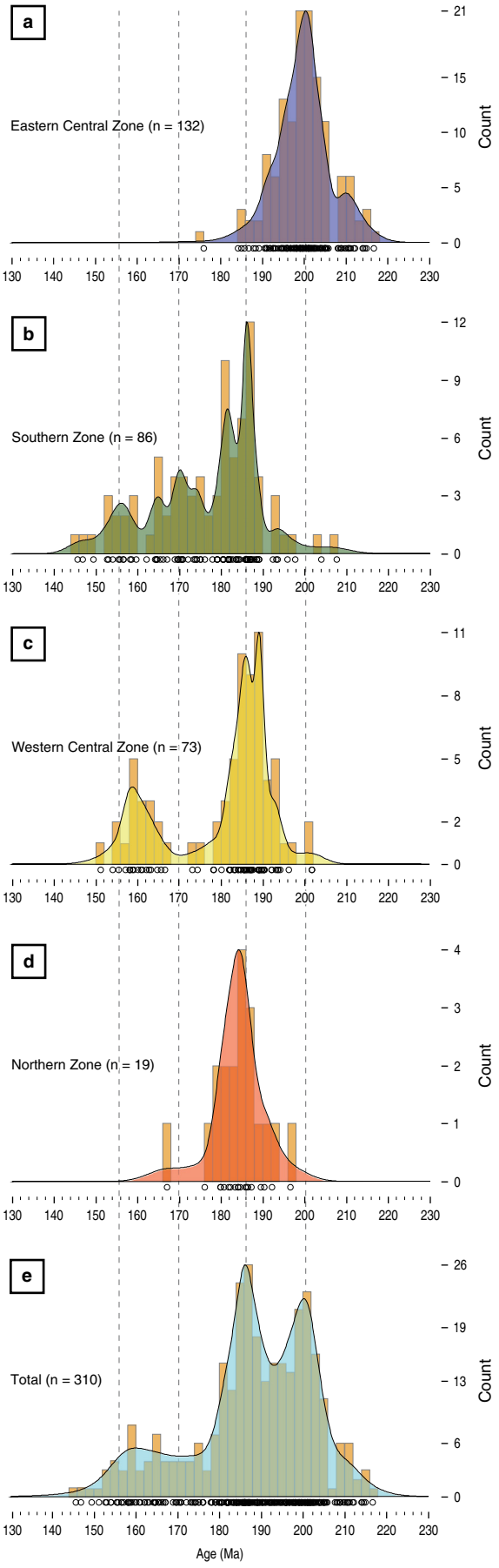

Figure 3. Igneous U/Pb zircon age spectra providing a temporal record of arc magmatism between 230 and 130 Ma. **(a)** Eastern Central Zone. **(b)** Southern Zone. **(c)** Western Central Zone. **(d)** Northern Zone. **(e)** Total U/Pb ages. Individual diagrams include LA–ICP–MS, LA–MC–ICP–MS, and SHRIMP age data presented as histograms with a 2 my bin width and adaptive Kernel density estimation (KDE) functions (see text). The number of analyses (n) given in each plot represents the number of crystallization ages.

creasing SiO_2. In contrast, K_2O shows random variations within very narrow ranges of SiO_2 concentrations (but with an overall increasing trend), and there are slight increases in Na_2O with increasing SiO_2. Trace elements show marked negative trends for Sr and slight negative trends for Y in all regions. Zr tends to have negative trends in the Central Eastern and Northern zones and random trends in the Central Western and Southern zones as well as low average values in the Central Western Zone. Ba has random trends, albeit with slight negative trends in the Central Eastern and Central Western zones.

6.1. Volcanic Rocks

The major element contents generally range from 45.62 to 82.6% SiO_2, 0.01 to 9.93% K_2O, 0.04 to 8.1% Na_2O, and 0.02 to 15.15% CaO. Trace element concentrations range from 4.0 to 351 ppm Rb, 12 to 8220 ppm Sr, 19 to 3523.74 ppm Ba, 1.3 to 736.81 ppm Cr, 0.025 to 533.1 ppm Ni, 0.5 to 173.61 ppm La, 0.23 to 62.66 ppm Eu, 1.8 to 351.26 ppm Y, and 1.2 to 503.41 ppm Zr. In the SiO_2 vs. Zr/TiO_2 diagram (Winchester & Floyd, 1977), they plot within the andesitic basalt, andesite, dacite, rhyodacite, and rhyolite fields following a subalkaline trend and within the transitional and calc–alkaline fields based on the Th/Yb vs. Zr/Y diagram (cf., Ross & Bédard, 2009). On the ternary La/10–Y/15–Nb/8 diagram, rocks plot mainly in the calc–alkaline orogenic to postorogenic fields (Figure 4a), suggesting an association of marginal arcs and crustal intracontinental domains (Figure 4b).

6.2. Plutonic Rocks–Granitoids

In plutonic rocks, major element concentrations range from 50.3 to 82.47% SiO_2, 0.04 to 8.83% K_2O, 0.03 to 8.42% Na_2O, and 0.02 to 16% CaO. Their $(La/Yb)_N$ ratios range from 0.64 to 263.33, and the Eu/Eu* ratios range from 0.06 to 3.27. Trace element concentrations range from 1.5 to 385 ppm Rb, 5 to 7430 ppm Sr, 8.5 to 3451.3 ppm Ba, 0.25 to 217 ppm Cr, 0.05 to 525.2 ppm Ni, 1.3 to 130.3 ppm La, 0.01 to 4.8 ppm Eu, 0.32 to 130.5 ppm Y, and 0.53 to 1895.47 ppm Zr. Plutons are mostly normal (SiO_2 < 70%) and silica–rich (SiO_2 > 70%) granitoids with ASI > 1.5 (peraluminous leucogranites), calcic to calc–alkalic magnesian and ferrous, and calc–alkalic and alkali–calcic granite signatures (Frost et al., 2016).

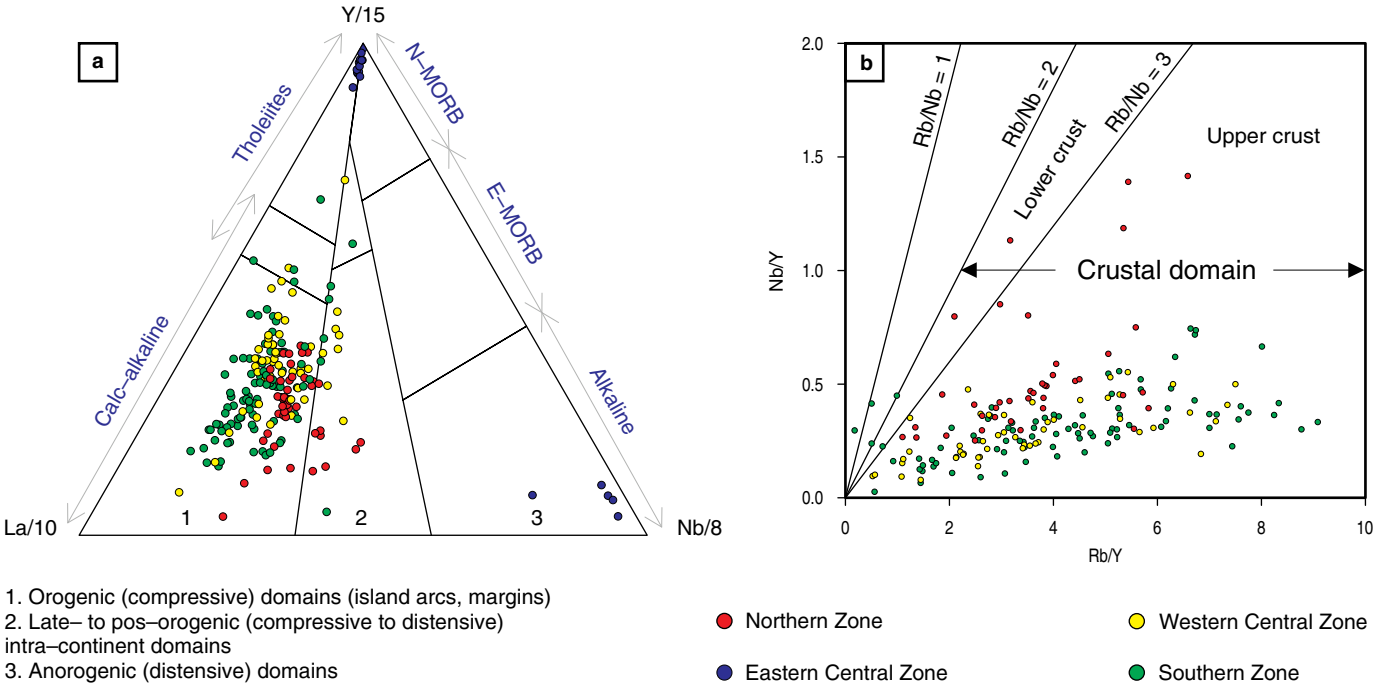

Figure 4. Discrimination diagrams for volcanic rocks. (**a**) Ternary La/10–Y/15–Nb/8 diagram (Cabanis & Lecolle, 1989) for the discrimination of tectonic regimes. Note that the rocks are grouped in the calc–alkaline orogenic domain. **(b)** Nb/Y vs. Rb/Y diagram (Chazot & Bertrand, 1995) showing the distribution of the samples associated with a crustal domain.

In Figure 5, several discrimination diagrams support a calc–alkaline, transitional, and tholeiitic magma series affinity interpretation (Figure 5a); some diagrams also indicate a high–potassium calc–alkaline and shoshonitic character (Figure 5b, 5c). The A/CNK Shand indexes range from 0.53 to 11.8 and indicate peraluminous to metaluminous characters consistent with the results from the multicationic B–A diagram (Figure 5d) of Debon & Le Fort (1983). Rocks also have agpaitic indexes ranging from 0.044 to 0.965, which confirms the absence of peralkaline associations.

Chemical analyses plotted in the S–I–A–M classification diagrams (Figure 6) show that most plutons are primarily classified as I–type. A few samples have A–type signatures (mostly A2 – postcollisional field in Figure 6a, 6b), and some others, primarily those in the Eastern Central Zone, have diffuse S–type trends (Figure 6c). Although the differentiation of granitoids into the S–I–A–M types is considered highly ambiguous (cf., Chappell, 1984; Chappell & White, 1974, 1992, 2001; Whalen et al., 1987; Eby, 1990, 1992; Castro, 2004; Castro et al., 1991a, 1991b; Chappell et al., 2012), results from these diagrams are consistent with other geochemical parameters from the dataset.

Differentiation trends as seen in the Ba–Rb–Sr diagram show that (Figure 7a) (i) the Eastern Central Zone primarily contains anomalous, normal, and strongly differentiated granites with diorites, quartz diorites, and subordinate granodiorites; (ii) the Northern Zone contains anomalous granites to normal granites, quartz diorites, and subordinate granodiorites; (iii) the Southern Zone shows an increasing trend from the quartz diorite and granodiorite fields to that of the anomalous granites with strongly differentiated normal granites and subordinate diorites; and (iv) the Western Central Zone shows an increasing trend from the diorite field to those of quartz diorites and granodiorites with anomalous and strongly differentiated subordinate granites. Note that rocks from the Eastern Central Zone tend to be the most differentiated, whereas those of the Western Central Zone tend to be the least differentiated. The low Ba–Sr granites from the Eastern Central Zone with an increasing Rb trend (and decreasing Ba) could be associated with a source likely related to volcanic or syncollisional arc settings, whereas the high Ba–Sr granites of the Northern, Southern, and Western Central zones may be connected to mixing with mantle components (Figure 7b). The presence of both strongly fractionated and unfractionated granitic rocks is also evident in Figure 7c, where rocks range from unevolved to strongly evolved and fractionated.

Petrographic (modal) and total rock geochemical (Q–P) classification diagrams show the wide lithological range of the assemblages: granites (syenogranites and monzogranites), quartz monzodiorites, granodiorites, tonalites, gabbros, monzogabbros, quartz diorites, quartz monzonites, monzonites, and subordinate syenites. All of these rocks likely originated

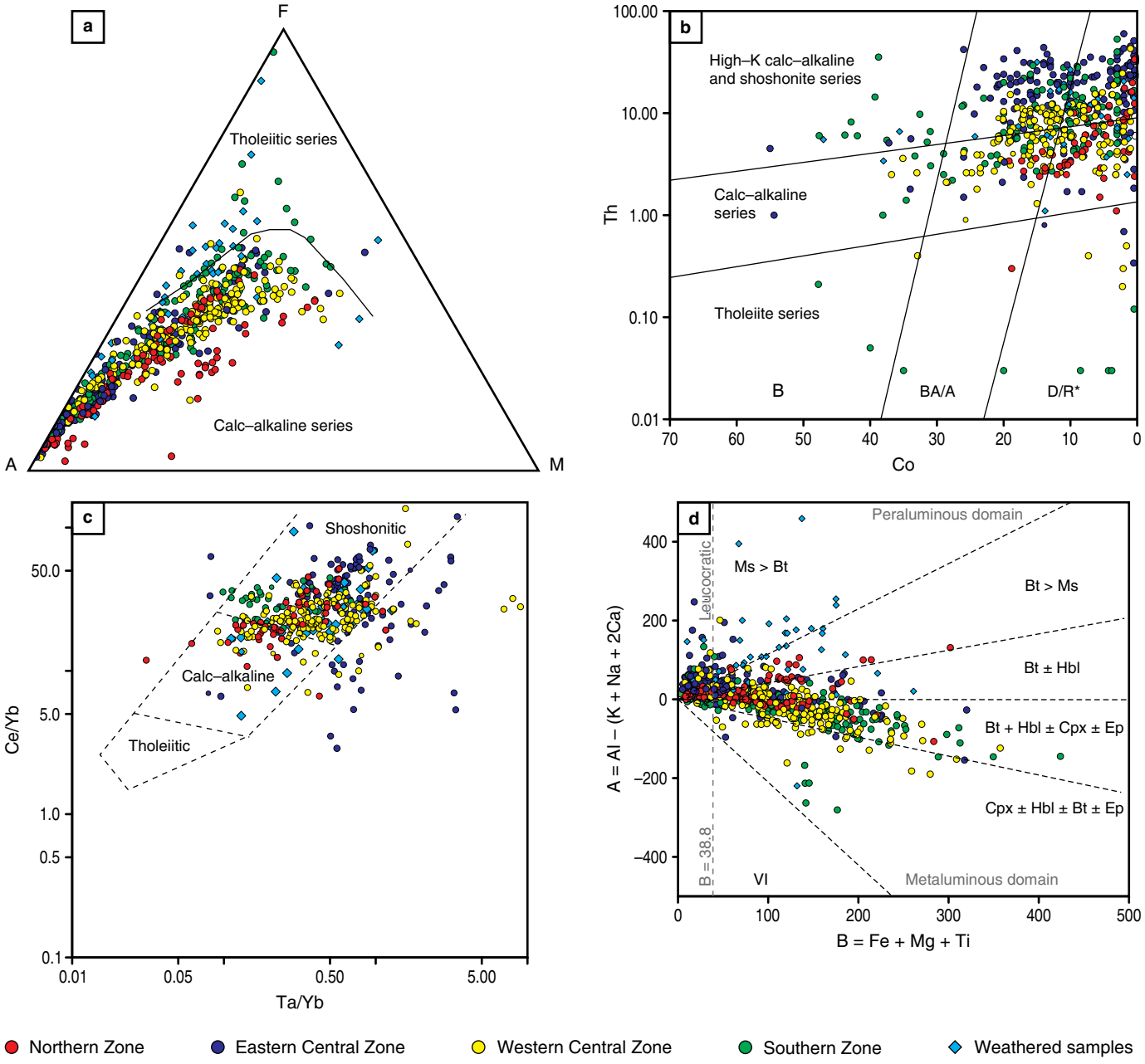

Figure 5. Discrimination of magmatic series. **(a)** Alkali–FeO–MgO (AFM) diagram (Irvine & Baragar, 1971) showing a calc–alkaline trend in the Late Triassic to Jurassic magmatic belt. **(b)** Th (ppm) vs. Co (ppm) diagram (Hastie et al., 2007) grouping rocks of the Late Triassic to Jurassic magmatic belt into the fields for the calc–alkaline, high–potassium/calc–alkaline and shoshonitic series. **(c)** Ce/Yb vs. Ta/Yb diagram (Müller et al., 1992) grouping the units primarily into the shoshonitic and calc–alkaline fields. **(d)** B–A multicationic diagram (Debon & Le Fort, 1983) showing that the plutonic rocks vary between the peraluminous and metaluminous domains.

in a typical arc, as indicated by the diagram in Figure 8a and by the already mentioned geochemical characteristics. The ample chemical variations allow the suite to have associations from leucocratic (Central Eastern Zone) to sodic and mesocratic (Northern, Central Western, and Southern zones; Figure 8b). The suite also has a wide distribution between ferrous and magnesian varieties (Figure 8c), but it is mostly constrained to alkali–calcic and calc–alkaline characters (Figure 8d).

7. Discussion

7.1. Tectonic Environment and Petrogenesis

Late Triassic – Jurassic magmatism in Colombia is of subalkaline affinity (primarily of the calc–alkaline and shoshonitic series), suggesting the presence of subduction fluids in the magma source (cf., Bustamante et al., 2010; Leal–Mejía,

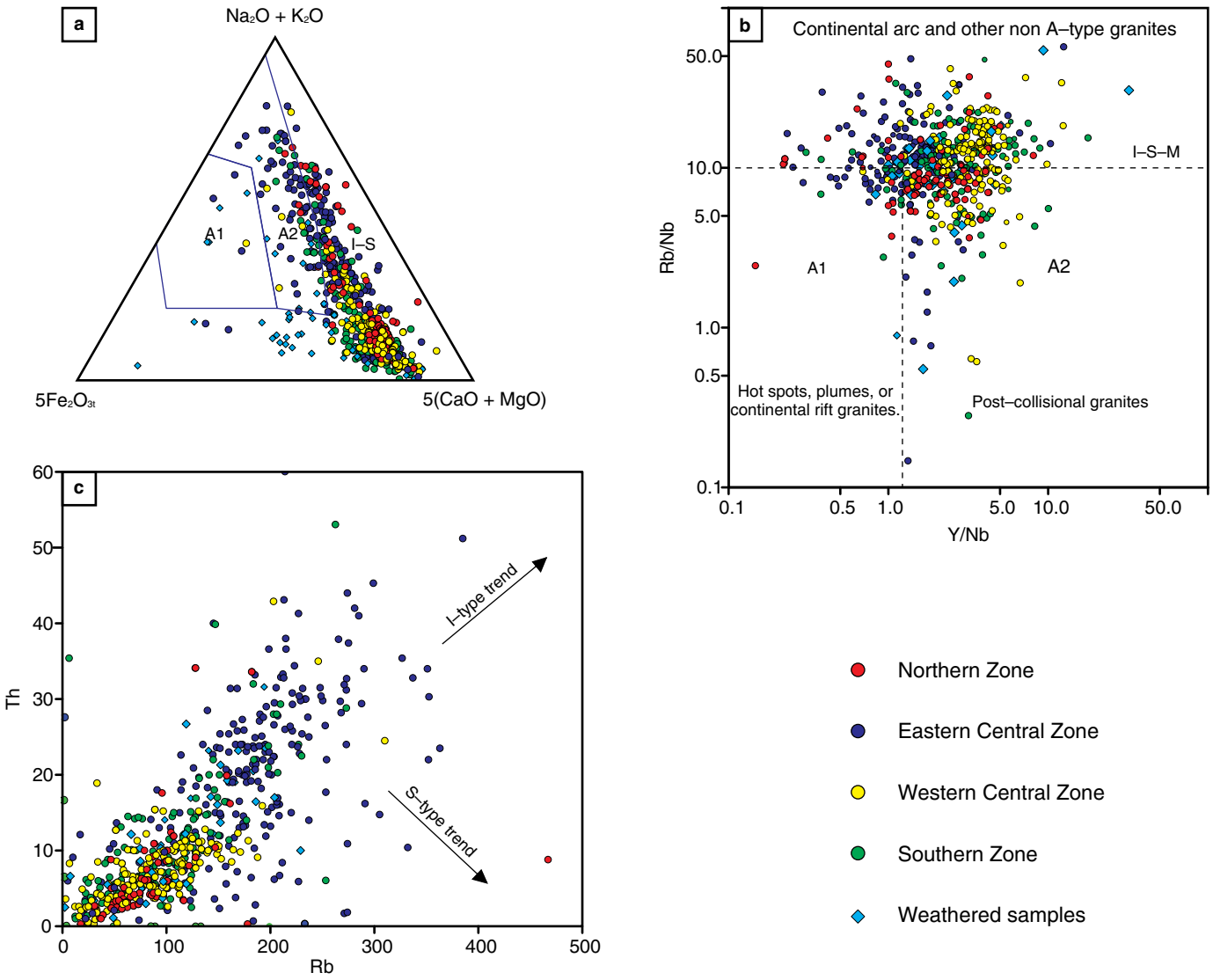

Figure 6. Discrimination among I–, S–, and A–type granites. **(a)** $5Fe_2O_{3t} - Na_2O + K_2O - 5(CaO + MgO)$ diagram (Grebennikov, 2014) discriminating A–type granites from I– and S–type granites. **(b)** Y/Nb vs. Rb/Nb discrimination diagram (Bahajroy & Taki, 2014) classifying the granites as postcollisional (A2), continental arc and other non A–type granites (I–S–M) subordinately associated with hotspots, mantle plumes, or continental rifts (A1). **(c)** Rb (ppm) vs. Th (ppm) diagram (Chappell, 1999). Note the distribution of samples following an I–type trend.

2011; Cochrane, 2013; Cochrane et al., 2014a, 2014b; Spikings et al., 2015; Zuluaga et al., 2015; van der Lelij et al., 2016; García–Chinchilla, 2018; Quandt et al., 2018; Rodríguez et al., 2018a). The magmatism ranges from metaluminous to strongly peraluminous and contains no rocks with peralkaline affinity, which precludes the presence of anorogenic magmatism typical of an intracontinental rift (see, e.g., Bowden et al., 1984; Brown et al., 1984; Pearce et al., 1984; Whalen et al., 1987; Maniar & Piccoli, 1989; Barbarin, 1990, 1999; Bonin, 1990, 1998, 2007; Bonin et al., 1998; Eby, 1990; Frost et al., 2001; Nédélec & Bouchez, 2015).

Volcanic rocks vary compositionally between andesitic basalts and rhyolites, which are typical arc rocks (cf., Figure 4), whereas the granitic rocks include (i) peraluminous granitoids with muscovite; (ii) high–potassium calc–alkaline to shoshonitic granitoids; (iii) calc–alkaline metaluminous granitoids with amphibole, biotite, and pyroxene; and (iv) granitoids discriminated as I–, S–, and A–type. Note that the compositional groups suggest the contribution of crustal melts and mixing with slab– (and mantle–?) derived components in an active continental margin setting (cf., Barbarin, 1999; Castro, 2014; Zhao et al., 2019).

In addition to the plots presented in the previous sections, the convergent geodynamic setting is supported by other discrimination diagrams that suggest an active continental margin regime in an orogenic domain with a syncollisional to post-

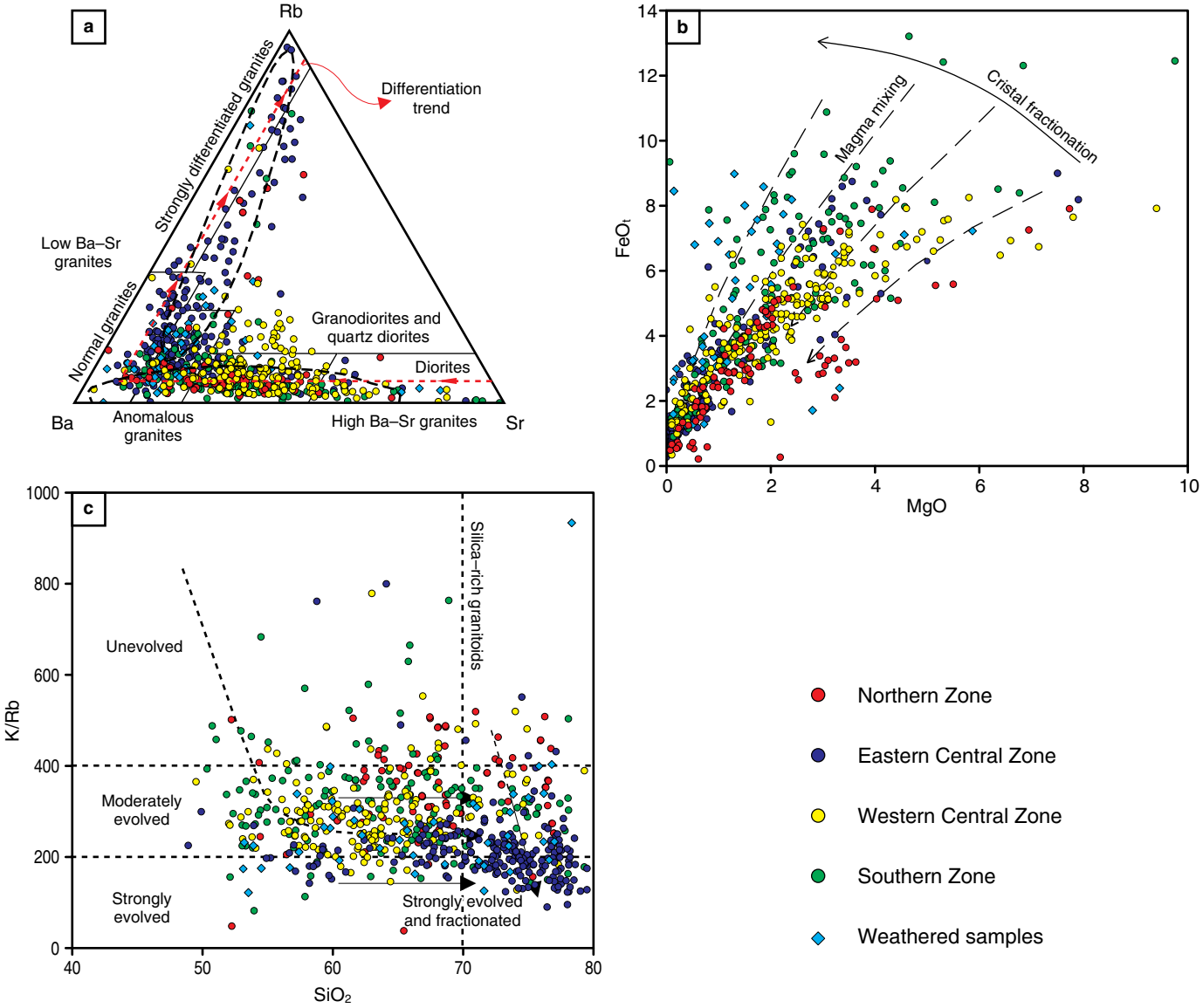

Figure 7. Fractionation grades of granitic rocks. **(a)** Ba–Rb–Sr diagram (El Bouseily & El Sokkary, 1975) showing that rocks in the Eastern Central Zone are the most differentiated, whereas rocks in the Western Central Zone are the least differentiated. High– and low–Ba–Sr granite fields complemented by Tarney & Jones (1994). **(b)** MgO vs. FeO_t diagram (Zorpi et al., 1989; Goswami & Bhattacharyya, 2014) showing that magma mixing processes were important mechanisms in the formation of the Late Triassic to Jurassic magmatic belt. **(c)** SiO_2 vs. K/Rb discrimination diagram (Blevin, 2004) classifying the rocks as a function of the evolution and fractionation of melts.

collisional (syn–subduction) regime and with a predominant calc–alkaline volcanic arc signature (Figure 9a–d).

The mineralogy of plutonic and volcanic rocks indicates associations of metaluminous and peraluminous magmas, which suggests one or more of the following processes: assimilation of country rock, incorporation of mantle–derived melts, contamination of magmas with melts from slab sediments, and magma mingling and mixing. Geochemical characteristics extracted from the dataset help to discriminate among the variety of sources and mechanisms pointing to (i) peraluminous leucogranites resulting from partial melting of pelitic rocks; (ii) calc–alkaline ferrous rocks from the partial melting of tonalites and granodiorites; (iii) alkali–calcic ferrous rocks from melting and/or differentiation of tholeiites, and (iv) magnesian rocks from the differentiation of high–aluminum basalts or andesites (see, e.g., Frost et al., 2016). However, magma mixing processes likely played a key role in the formation of the Late Triassic – Jurassic magmatic belt, as suggested by MgO–FeOt trends and a lack of correlation between Zr and Y (Goswami & Bhattacharyya, 2014). This point is significant because FeOt–MgO trends can be affected by other mechanisms, such as the variable onset of crystallization of iron oxides in magmas with distinct oxygen fugacities and/or water contents (cf., Figure 7b).

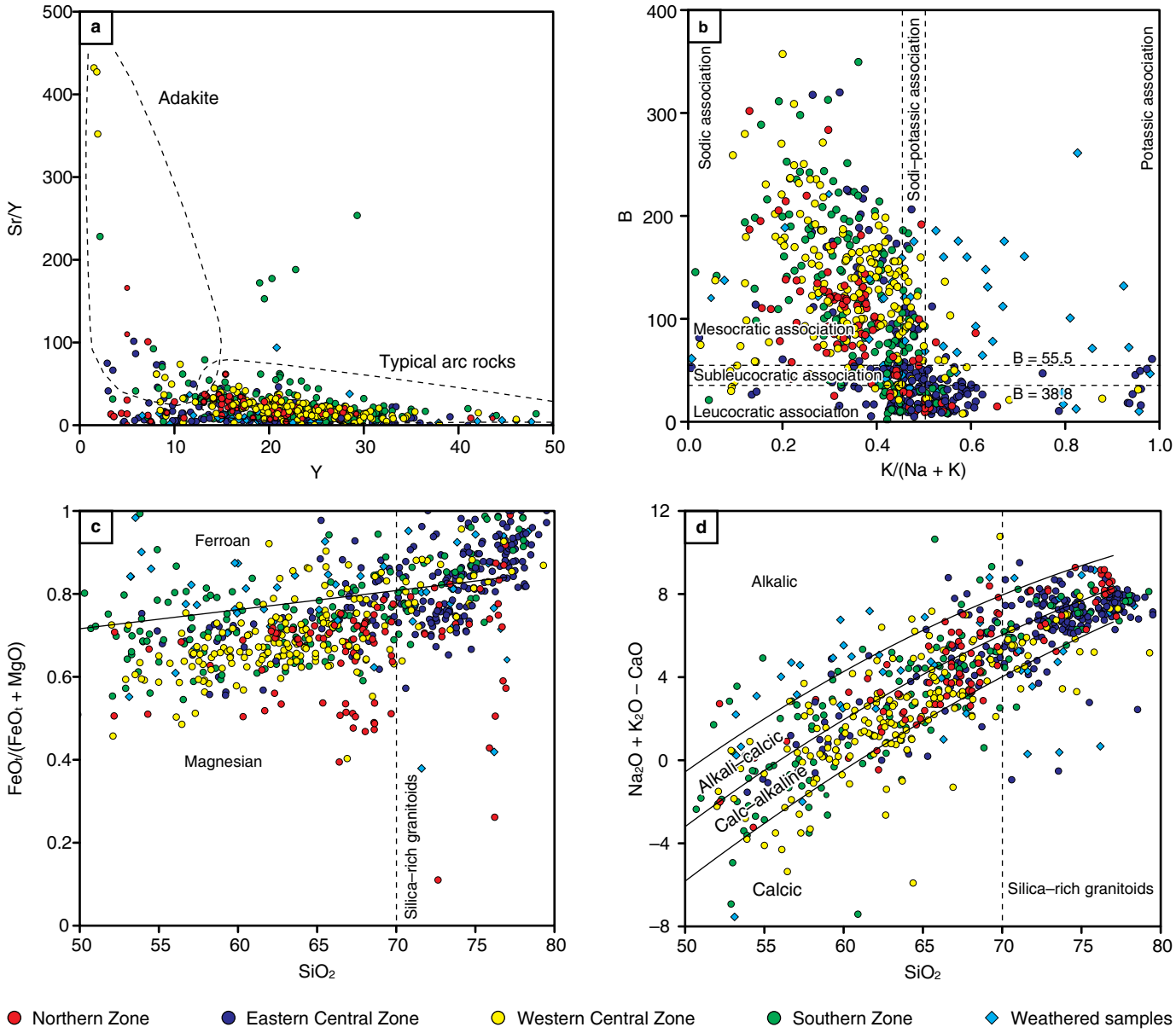

Figure 8. Discrimination diagrams for plutonic rocks. **(a)** Y (ppm) vs. Sr/Y diagram (Drummond & Defant, 1990) grouping the rocks within the fields of typical arc rocks and adakitic rocks. **(b)** K/(Na + K) vs. B diagram (Debon & Le Fort, 1983, 1988) relating the color index (B) to the alkali ratio (K/(Na + K)). **(c)** Modified SiO_2 vs. modified alkali–lime index (MALI) diagram (Frost & Frost, 2008; Frost et al., 2001, 2016). **(d)** SiO_2 vs. $Na_2O + K_2O$ – CaO diagram (Frost & Frost, 2008; Frost et al., 2001, 2016).

The suite has mostly rocks with moderate potassium concentrations suggesting potassium–depleted sources, but there are also high–potassium rocks that could have been generated by partial melting of potassium–enriched mantle sources (Bao et al., 2018), which further supports the interpretation of different sources for magmatism. Potassic rocks are assemblages that include the specimens richest in potassium on the calc–alkaline spectrum and are geochemically different from other geochemical varieties (Müller et al., 1992). To obtain better control on the interpretation of this group and following Müller et al. (1992), rocks were hierarchically discriminated first based on the La–TiO_2/100–10Hf diagram (Figure 10a) and then on the 50Nb–3Zr–Ce/P_2O_5 diagram (Figure 10b). Most of the rocks plot in the continental arc potassic (CAP) field, which suggests the recycling of oceanic crust in a subduction environment. In the diagram of Figure 10a, some rocks associated with oceanic potassic arcs (especially from the Western Central Zone) plot in the IOP–LOP field, suggesting ambiguity regarding the element concentrations considered, which is probably related to mixing and metasomatic enrichment by fluids derived from the underlying mantle wedge (Müller et al., 1992).

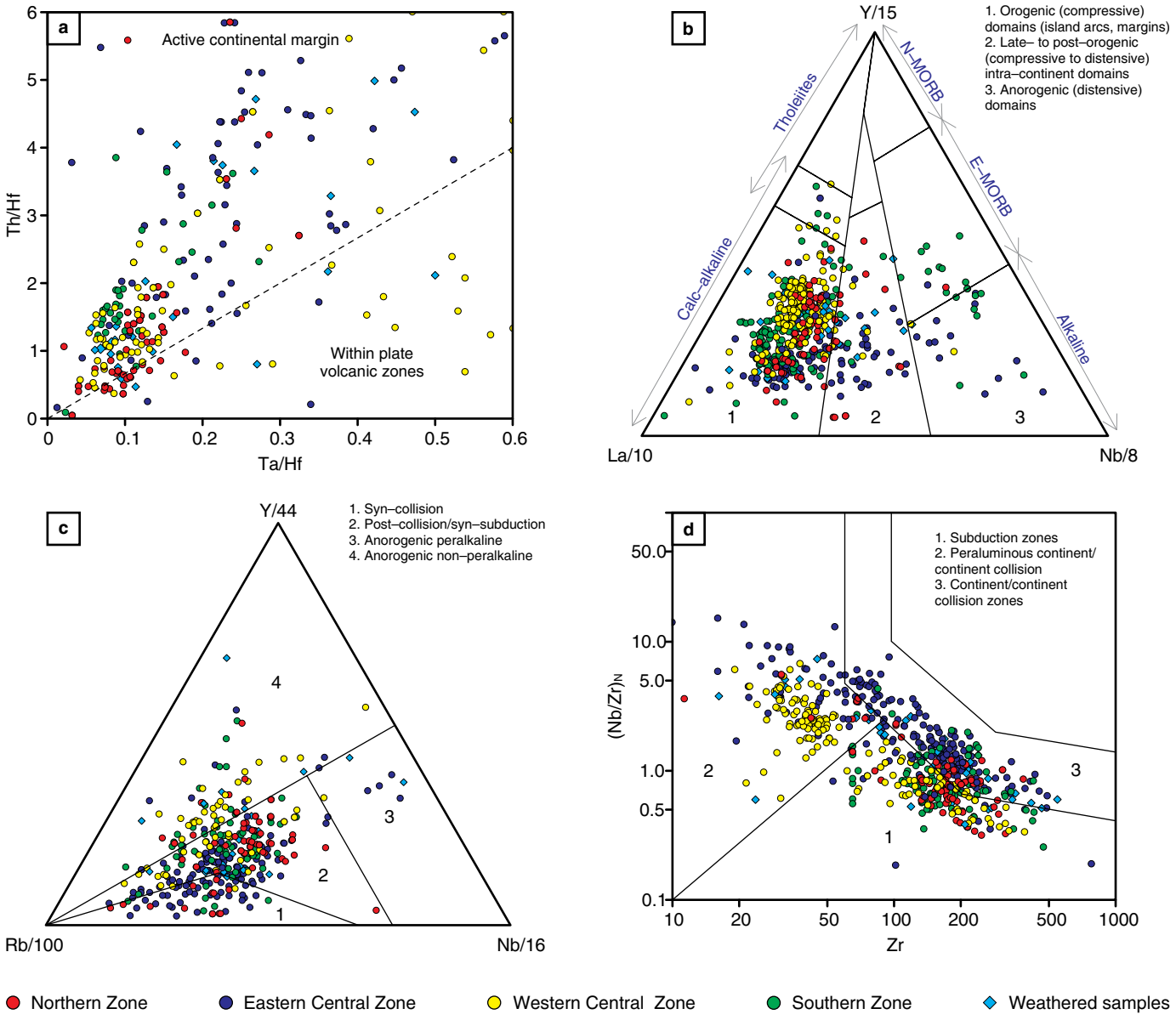

Figure 9. Tectonic discrimination diagrams. **(a)** Ta/Hf vs. Th/Hf discrimination diagram (Schandl & Gorton, 2002) suggests an active continental margin regime. **(b)** La/10–Y/15–Nb/8 plot (Cabanis & Lecolle, 1989) shows an orogenic domain for the granitic rocks. **(c)** Rb/100–Y/44–Nb/16 discrimination diagram (Thiéblemont & Cabanis, 1990) shows a syncollisional to postcollisional (syn–subduction) tectonic regime. **(d)** Zr (ppm) vs. $(Nb/Zr)_N$ diagram (Thiéblemont & Tégyey, 1994) showing a transition between the fields of continent–continent collision (fields 2 and 3) and subduction zones (field 1).

The Zr saturation temperatures tend to be higher than 600 °C and reach approximately 1000 °C (Figure 10c), which suggests the presence of high– and low–temperature granites (Watson & Harrison, 1983; Miller et al., 2003). High–temperature granites have Zr saturation temperatures higher than 750 °C and generally contain no zircon xenocrysts inherited from the regions of the magma source, which is consistent with the fractionation of mantle–derived magmas (Miller et al., 2003). Note that there is a negative correlation between Zr saturation temperatures and SiO_2 in samples from the Eastern Central Zone, suggesting that zircon saturation in these samples occurred early in the fractionation process (Janoušek et al., 2004; Figure 10d). Therefore, Zr saturation temperatures indicate the liquidus temperature of the granitic melt (Watson & Harrison, 1983). In some cases, the Zr concentrations confirm the tholeiitic affinities shown by some lithological assemblages (for example, the Central Western Zone), which suggests very little contamination of the parental magma by continental crust and is cor-

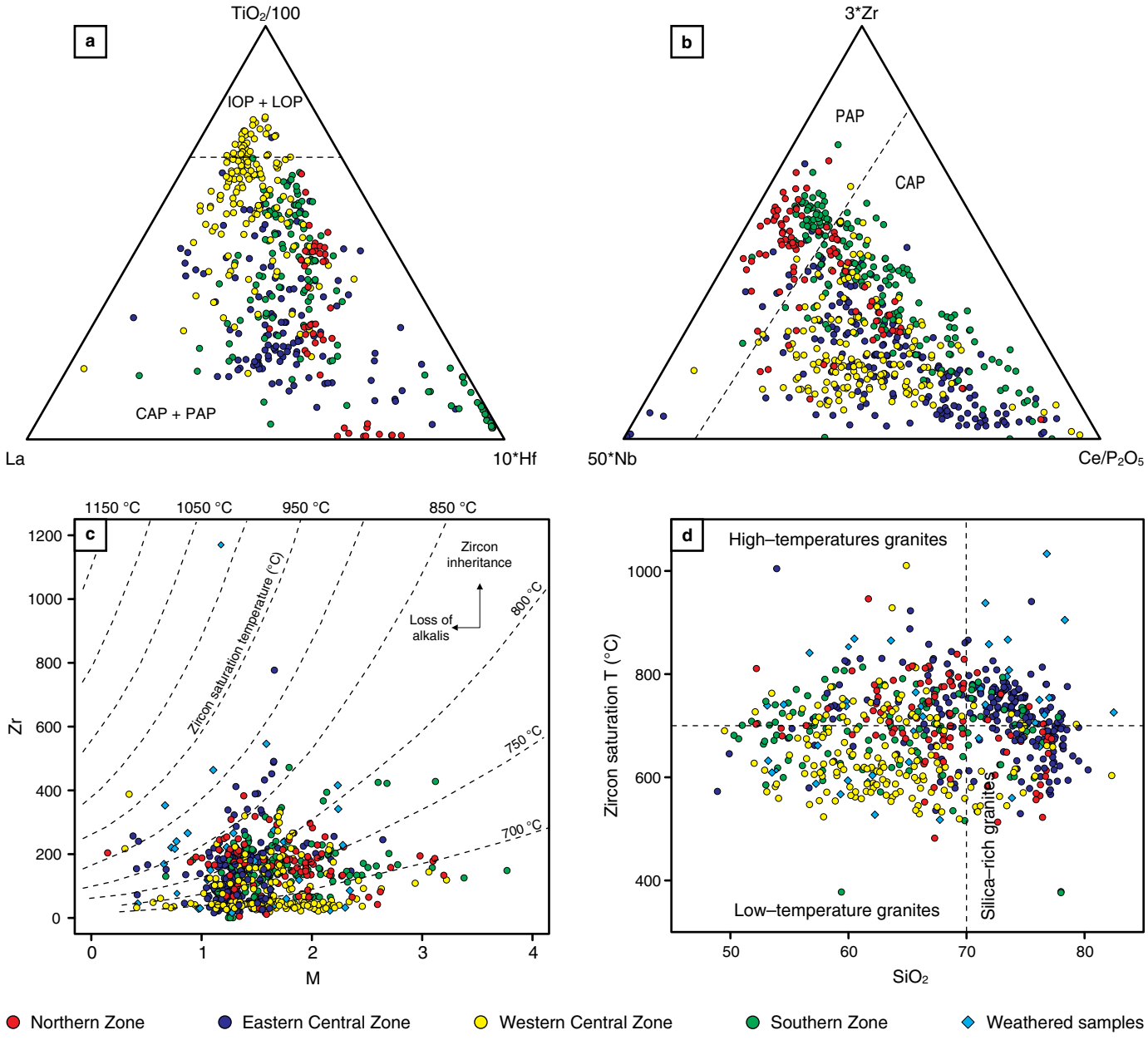

Figure 10. Discrimination diagrams for potassic rocks and zirconium saturation temperature. **(a)** La (ppm) –TiO_2/100–10*Hf discrimination diagrams differentiating continental and postcollisional (CAP + PAP) arc potassic rocks from initial and late oceanic (IOP + LOP) arc potassic rocks. **(b)** 50*Nb–3*Zr–Ce/P_2O_5 discrimination diagrams plotting the rocks in the fields of continental arc potassic (CAP) rocks. **(c)** M vs. Zr (ppm) diagram (Janoušek et al., 2004). Note that the Zr saturation temperatures tend to be higher than 600 °C and reach approximately 1000 °C. **(d)** SiO_2 vs. Zr saturation diagram. Note the distribution of lithological units into high– and low–temperature granite fields.

roborated by the concentrations of Y. Additionally, the Nb/Yb and Th/Yb ratios suggest contributions from subduction–related fluids and magma evolution by either fractional crystallization with assimilation or a process related to the melting–assimilation–storage–homogenization (MASH) zone in a volcanic arc setting with interaction between the enriched mantle and the crust (Pearce, 2008).

Chondrite–normalized spider diagrams show the presence of negative Nb, Ta, and Ti anomalies (Figure 11a), consistent with retention of oxide phases during partial melting in subduction zones (see Pearce, 1982; Pearce et al., 1984, 1990; Müller et al., 1992; Pe–Piper et al., 2009; Goswami & Bhattacharyya, 2014; Moreno et al., 2014). Negative Eu anomalies (Figure 11b) are observed in the chondrite C1–normalized diagrams of the Eastern Central and Western zones, suggesting fractional crystallization of plagioclase and alkali feldspar, whereas the Eu anomalies of the Northern and Southern zones tend to be flat to positive, which suggests the likely

accumulation of plagioclase in the source (Hess, 1989; Keshavarzi et al., 2014). Overall, REE patterns show steep slopes for LREE, suggesting melting of a substantial proportion of clinopyroxene or melting of enriched amphibolite metabasalt (Pe–Piper et al., 2009), and flat curves for HREE, suggesting the addition of a small proportion of partial melts of garnet (Pe–Piper et al., 2009). Several processes from trace element ratio diagrams (Figure 11c–d) can be highlighted: variable differentiation grades, residual garnet (Eastern Central Zone), mixing of components from different sources including a subduction component, crustal contamination, and crystallization of accessory phases (Kay et al., 2013).

Note that there is an apparent contradiction between the $(Y/Nb)_N$ and $(Ce/Pb)_N$ ratios since observed $(Y/Nb)_N$ ratios <1 suggest that mantle sources were not involved in the genesis of the magmas or that this ratio decreased during the evolution of the continental margin magma, while $(Ce/Pb)_N$ ratios > 1 suggest that the crust is not a key factor in the genesis of the magmas (Figure 11e, 11f). Here, it is important to remember that we discard intracontinental rift magmatism based on the absence of peralkaline rocks and the postorogenic tectonic affinity. The apparent contradiction is resolved by considering the mixing of melts from different sources (crustal and mantle melts). Magma mixing is also indicated by high $(Th/Nb)_N$ and $(Th/Ta)_N$ ratios (higher than those observed in island arc magmas and higher than the crustal trend).

To evaluate the geochemical links between granitic melts and their sources, we use the methodology of Moyen et al. (2017). In the diagrams of Figure 12 (projected from biotite + quartz + H_2O), all liquids from the same source should plot along a tight array, pointing to the Na + K + Al apex (the granite minimum) and have a slope that depends solely on the nature of the source (Moyen et al., 2017). In this diagram, two lines are important: (i) the line connecting the feldspars and representing peraluminous rocks (horizontal in the figure, corresponding to A/CNK = 1) and (ii) the line connecting the 3Al + 2(Na + K) and the (Ca + Al) apices. This line separates mafic from felsic sources. Some samples from the Northern and Western Central zones can be interpreted as crystallized melts that originated with some influence from felsic sources. Samples from the Northern, Western Central, and Southern zones plot in a nearly horizontal trend along the line A/CNK = 1, suggesting melting of the supra–subduction mantle wedge. Samples from the Eastern Central Zone plot above the A/CNK = 1 line towards the 3Al + 2(Na + K) apex, which suggests a felsic crustal aluminous source (metasediments or metaigneous) and peraluminous affinity.

7.2. Evolution of the Magmatic Belt in Colombia

The age distribution within the belt allows the identification of several patterns: (i) the oldest magmas occur in the Eastern Central Zone with ages ranging from 216 to 186 Ma and a magmatic peak at ca. 200 Ma (see Figure 3); (ii) in the Northern, Western Central, and Southern zones, uninterrupted magmatic activity began at approximately 196 Ma, with a peak of magmatic activity at ca. 186 Ma; magmatic activity was interrupted in the Northern Zone at ca. 174 Ma; (iii) the youngest peaks of magmatic activity are observed in the Western Central and Southern zones (ca. 156 and 158 Ma); and (iv) magmatic activity between 165 and 175 Ma seems to have been concentrated in the Southern Zone. Note that the youngest magmatism has the most basic compositions (quartz diorites, tonalites, diorites, and granodiorites), whereas the oldest magmatism has more felsic compositions (monzogranites and subordinate syenogranites). Figure 13 illustrates how the magmatism varied spatially and temporally during the evolution of the belt. Plutons from the Eastern Central Zone are mostly peraluminous, while there is a slight tendency towards a metaluminous character in the plutons from the Southern, Western Central, and Northern zones.

In the diagrams of Figure 14, it is evident that plutonic rocks from the Eastern Central Zone, which record the oldest magmatism, cluster around the syncollisional field (Figure 14a). Plutonic rocks from the Southern, Western Central, and Northern zones have a wider distribution with compositions that vary progressively from subduction to late–orogenic regimes (Figure 14b–d), which reflects general and consistent increases in K and Na (Batchelor & Bowden, 1985). The previous discriminations suggest that a subduction regime prevailed with the development of active continental margin magmatism (see also Figure 9); this interpretation is also consistent with what is observed in $(Th/Ta)_N$ vs. $(Y/Nb)_N$ and $(Ce/Pb)_N$ vs. $(Y/Nb)_N$ diagrams (Figure 11e, 11f).

Note that published Pb, Nd, and Sr isotope compositions reveal an increased juvenile magmatic component in progressively younger rocks, which is consistent with Hf isotope data, and demonstrate an increased proportion of juvenile mass within the crystallizing magma (Leal–Mejía, 2011; Bissig et al., 2014; Cochrane et al., 2014b; Bustamante et al., 2016). This interpretation is also supported by trends in εNd_i and εHf_i from negative values in Early Jurassic time to positive values in Early Cretaceous time (Ordóñez–Calderón, 2003; Ordóñez–Carmona et al., 2006; Cochrane et al., 2014b; Spikings et al., 2015; Bustamante et al., 2016). Negative εNd_i and εHf_i values in the oldest samples of the suite suggest an important crustal component in the parental magma (Figure 14e), which is coherent with the observed high $^{87}Sr/^{86}Sr$ ratios (>0.705). Spatially, a greater contribution of lithospheric mantle and crustal assimilation in the arc magmas towards the east has also been suggested (Ordóñez–Calderón, 2003; Quandt et al., 2018). Pb isotope data further indicate a mostly "orogenic" or arc–type juvenile crust source (Figure 14f), with a more radiogenic lead contribution from the upper continental crust (Leal–Mejía, 2011; Quandt et al., 2018). Hf isotope data point

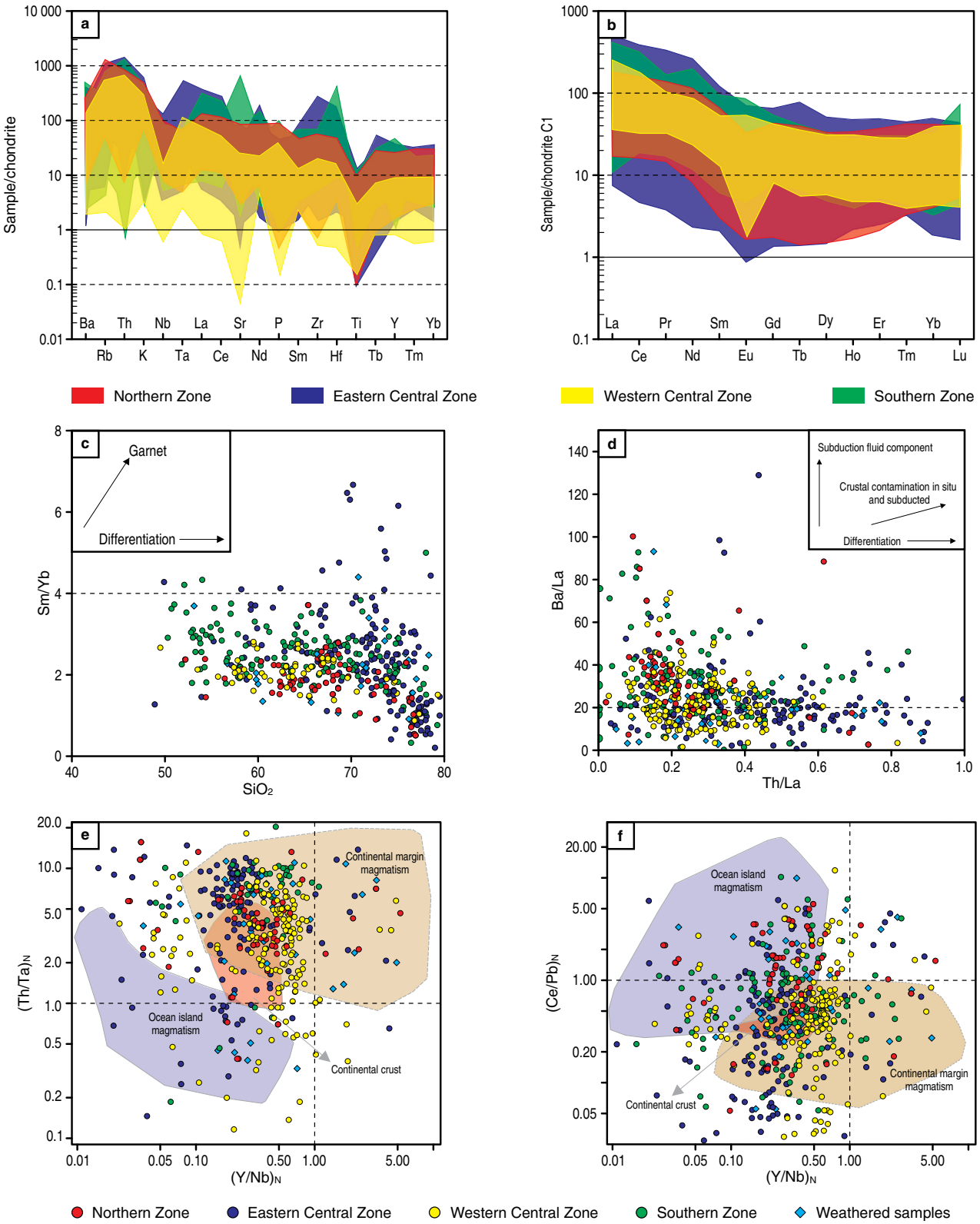

Figure 11. Geochemical REE patterns for the different regions of the Late Triassic to Jurassic magmatic belt in Colombia. **(a)** Chondrite–normalized (Thompson, 1982) spider diagrams show the presence of negative Nb, Ta, and Ti anomalies. **(b)** Chondrite C1–normalized (McDonough & Sun, 1995) diagrams show sloping patterns for LREE and flat patterns for HREE. **(c)** SiO_2 vs. Sm/Yb ratio (Kay et al., 2013); the Sm/Yb ratio greater than ca. 4 suggests Yb retention in residual garnet formed at high pressure. **(d)** Th/La vs. Ba/La ratios (Kay et al., 2013). Note the relevance of the subduction fluid component in relation to the crustal contamination. **(e, f)** $(Th/Ta)_N$ vs. $(Y/Nb)_N$ and $(Ce/Pb)_N$ vs. $(Y/Nb)_N$ discrimination diagrams (Moreno et al., 2014) showing that the evolution of magmatism is mainly consistent with an active continental margin environment. Note the high values of the $(Ce/Pb)_N$ ratios, which suggest a contribution from mantle melts.

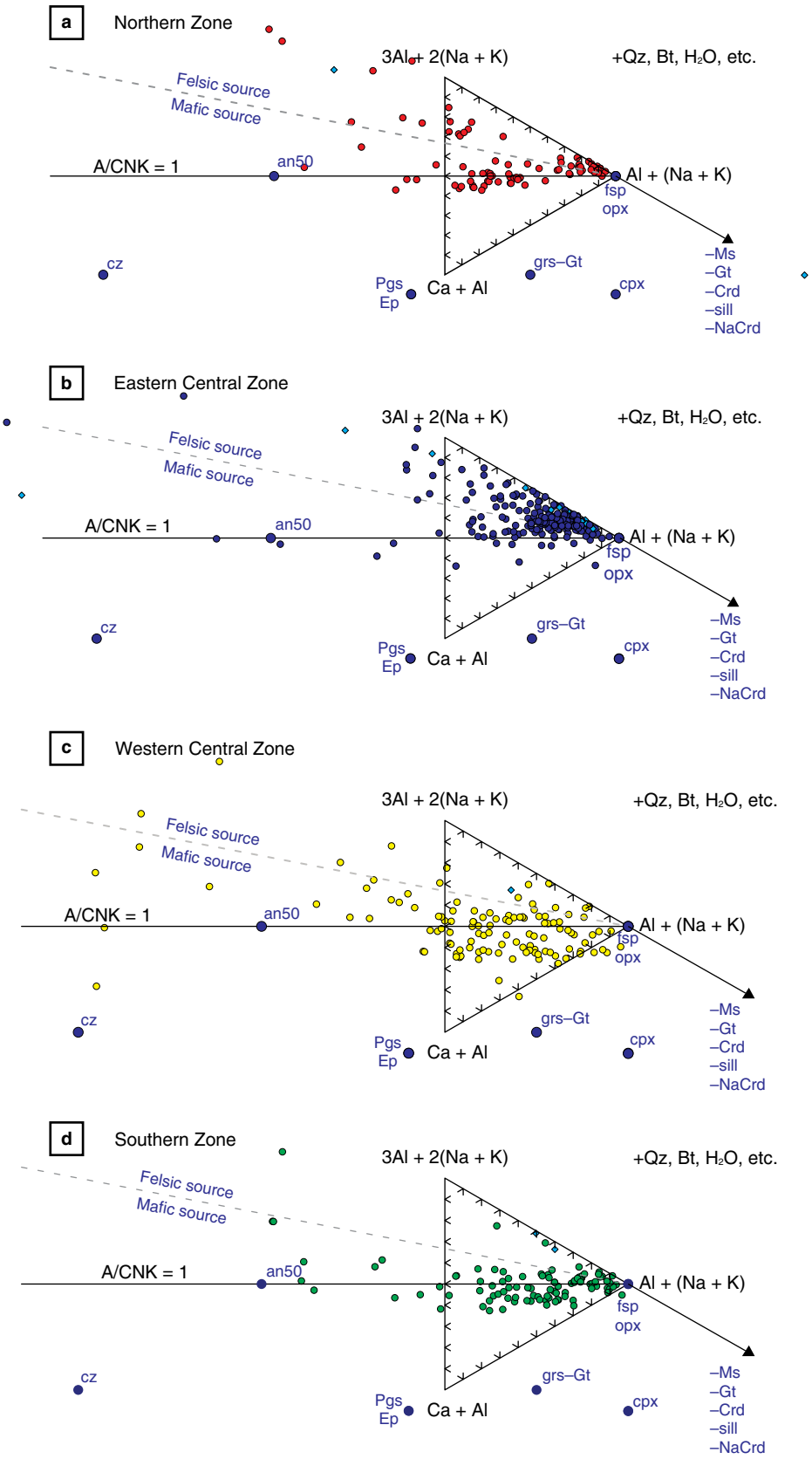

Figure 12. Ca + Al – Al + (Na + K) – 3Al + 2(Na + K) diagram (Moyen et al., 2017) for the sources of granitic rocks. **(a)** Northern Zone. **(b)** Eastern Central Zone. **(c)** Western Central Zone. **(d)** Southern Zone.

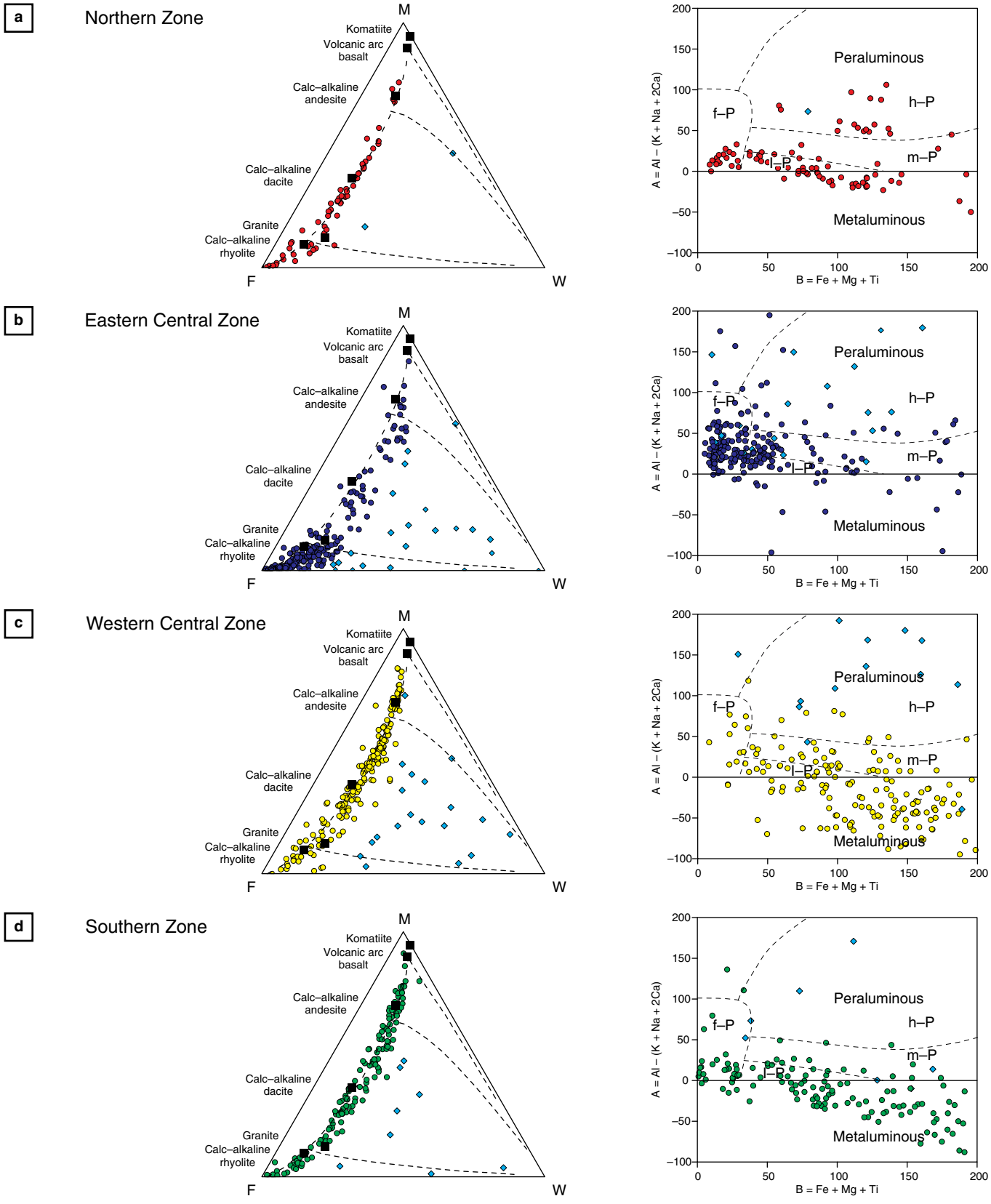

Figure 13. M–F–W diagrams (Ohta & Arai, 2007) showing the effects of differentiation and alteration on igneous rocks by combining several indicators, in which M corresponds to mafic rocks, F to felsic rocks, and W to weathered compositions (left) and a B–A multicationic diagram (Villaseca et al., 1998) showing that the plutonic rocks vary between the peraluminous and metaluminous domains (right). **(a)** Northern Zone. **(b)** Eastern Central Zone. **(c)** Western Central Zone. **(d)** Southern Zone. The blue diamonds represent weathered samples.

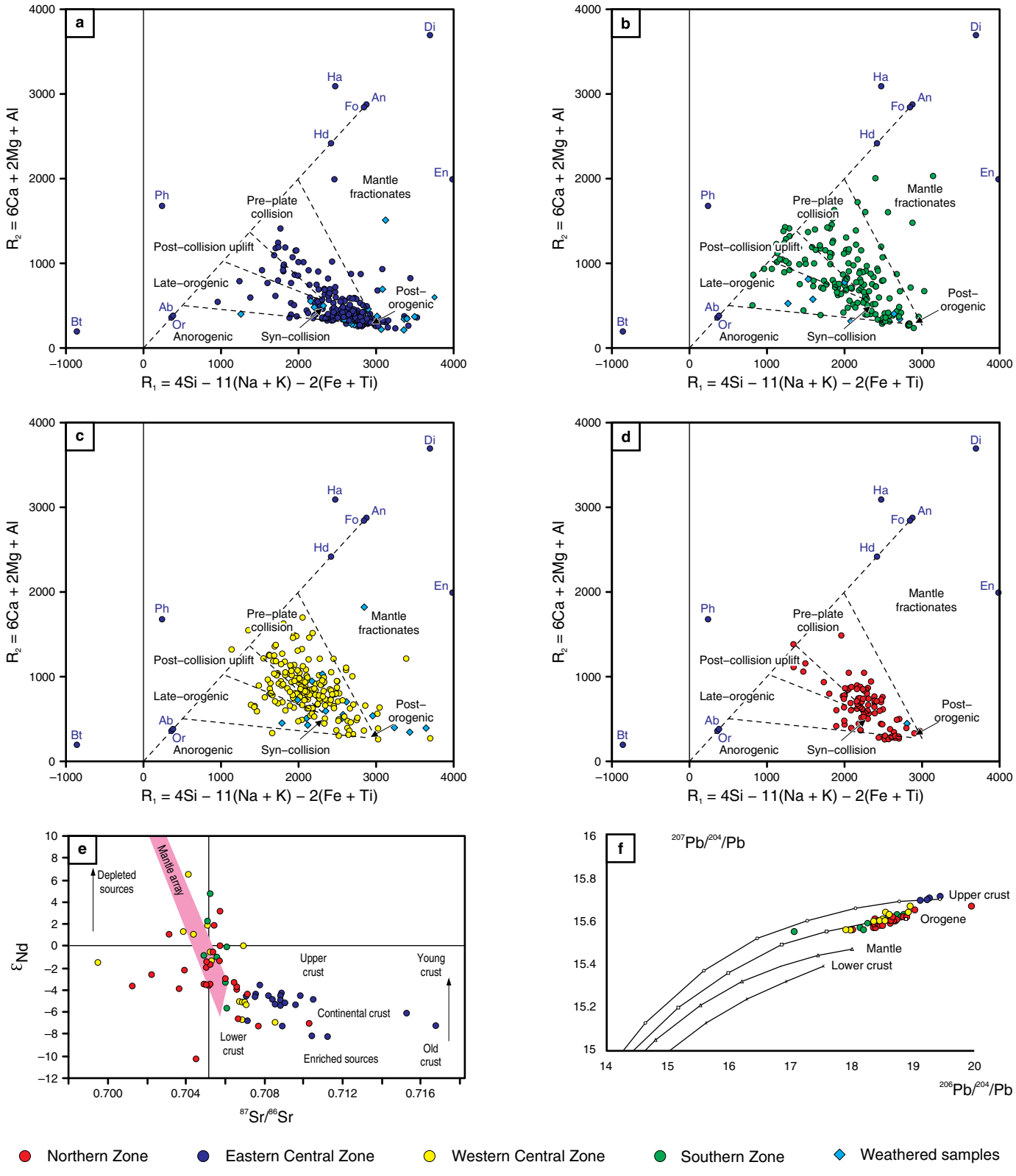

Figure 14. Discrimination diagrams of the tectonic settings of granitic rocks from the R1–R2 cationic values (Batchelor & Bowden, 1985). (**a)** Northern Zone. **(b)** Eastern Central Zone. **(c)** Western Central Zone. **(d)** Southern Zone. **(e)** $^{86}Sr/^{87}Sr$ vs. ε_{Nd} plot for the Late Triassic to Jurassic magmatic belt. **(f)** Lead isotope compositions of the Late Triassic to Jurassic magmatic belt. Lead isotope evolution curves after the Plumbotectonics model of Zartman & Doe (1981) are shown for comparison.

to an increasing proportion of juvenile input in the magmas from Early Jurassic to Early Cretaceous times (20% to 80%); this feature is also observed spatially along an oceanward trend (Cochrane et al., 2014b).

8. Conclusions

The elongated shapes of the Late Triassic to Jurassic magmatic belt and individual plutons (cf., Figure 1) suggest that the generation of spaces to accommodate the magmatic pulses was related to transtensional environments, which in turn were related to crustal evolution in a tectonic framework dominated by oblique subduction. This interpretation is consistent with an extensional environment in the northern corner of South America during the Late Triassic to Jurassic, which has been reported by several authors (Mojica et al., 1996; Cediel et al., 2003; Pindell & Kennan, 2009; van der Lelij, 2013; van der Lelij et al., 2016), but the triggering mechanism has not been provided. In turn, extensional environments promote crustal thinning and favor a high–temperature thermal regime in the continental crust, which can trigger partial melting at the base of the crust or the decompression of intermediate to mafic rocks as an alternative mechanism for the occurrence of high–potassium granites. The interpretation of a thermal anomaly at the base of the crust due to the action of the enriched mantle (mantle wedge), in a tectonic setting of oblique subduction, is supported by the high–potassium calc–alkaline to shoshonitic affinities, magma mixing, and negative Nb, Ta, and Ti anomalies typical of subduction. High Ce and Pb concentrations and positive Pb, Rb, K, and Ba anomalies are attributed to metasomatism of the mantle wedge by fluids derived by melting during slab subduction and/or contamination by the continental crust (see, for example, Keshavarzi et al., 2014). This interpretation is also supported by the presence of S–, I–, and A–type granitic rocks recording high and low temperatures; these rocks range from strongly peraluminous to metaluminous and have geochemical signatures suggesting crustal contamination, as interpreted here and previously by other authors (e.g., van der Lelij et al., 2016), and different sources of melts.

Plutonic, hypabyssal, and volcanic successions are distributed in four zones: Northern, Eastern Central, Western Central, and Southern, covering a total area of approximately 50 500 km^2. The effusive volcanism and subvolcanic plutons indicate the presence of magmatic arcs along belts from south to north in Colombia (cf., Figure 1), through the Northern Andean Block, and from the Ecuadorian Andes to the Venezuelan Andes. The presence of abundant associations of S–type granites followed by associations of slightly peraluminous to metaluminous I–type granites and subordinate associations of A–type granites combined with a clear evolutionary trend towards I–type granites suggests the occurrence of processes that greatly modified the magma composition.

Magmatism on the continental margin varied spatially and temporally from a postcollisional extensional setting (associated with orogenic collapse?) to a volcanic arc setting in an active continental margin dominated by subduction over a time span of approximately 60 my. The S–, I–, and A–type granites of high–potassium calc–alkaline to shoshonitic affinity with strong peraluminous to metaluminous characters in the belt are key features to develop interpretations about the origin and evolution of these magmas and to understand the tectonics of the northwestern margin of Gondwana between the Late Triassic and the Jurassic. The age distribution and geochemistry indicate a trend where the youngest and most metaluminous mafic compositions of the tholeiitic to calc–alkaline series are located in the west, while the oldest and most alkaline compositions of the high–potassium calc–alkaline and peraluminous series are located in the eastern part of the belt. The youngest magmatism is typical of environments related to subduction associated with active continental margins, whereas the oldest magmatism is characteristic of syncollisional to postcollisional (postorogenic) settings. The magmatic age distribution is also characterized by several peaks and lulls interpreted as records of magmatic flare–ups with magmatic tempos between 10 and 20 Ma (Figure 3); however, it is likely that at least some of the age distribution was controlled by exhumation and erosional processes, as well as the preservation bias inherent in the geological record. The most noticeable gap in the age distribution that may indicate an important interruption (a lull) in magmatic activity is observed between 165 and 175 Ma in all but the Southern Zone.

Figure 15 shows the spatiotemporal distribution of plutons in the magmatic belt; this figure also portrays the interpreted spatial location of the transition from the postcollisional stage to the arc stage and the location of the subduction zone. The oldest magmas from the postcollisional stage are interpreted as a result of melting of the lower crust due to a thermal anomaly (possibly associated with the mantle wedge, slab breakoff, or slab tearing of the subducting plate along a transform fault) during oblique subduction. Magmas from the arc stage are mostly "orogenic" or arc–type juvenile crust, with contributions from the lithospheric mantle and crustal assimilation in a supra–subduction regime; these magmas show an increasing proportion of juvenile mass within the crystallizing magma in progressively younger rocks. Note that this framework interpretation is consistent with those observed in many cordilleran–type magmatic belts containing multiple intrusions with variable composition and arranged as nested complexes in linear arrays (Cobbing & Pitcher, 1972; Pitcher, 1997; Winter, 2014). The most basic compositions of tholeiitic to potassium–depleted calc–alkaline affinity are located near

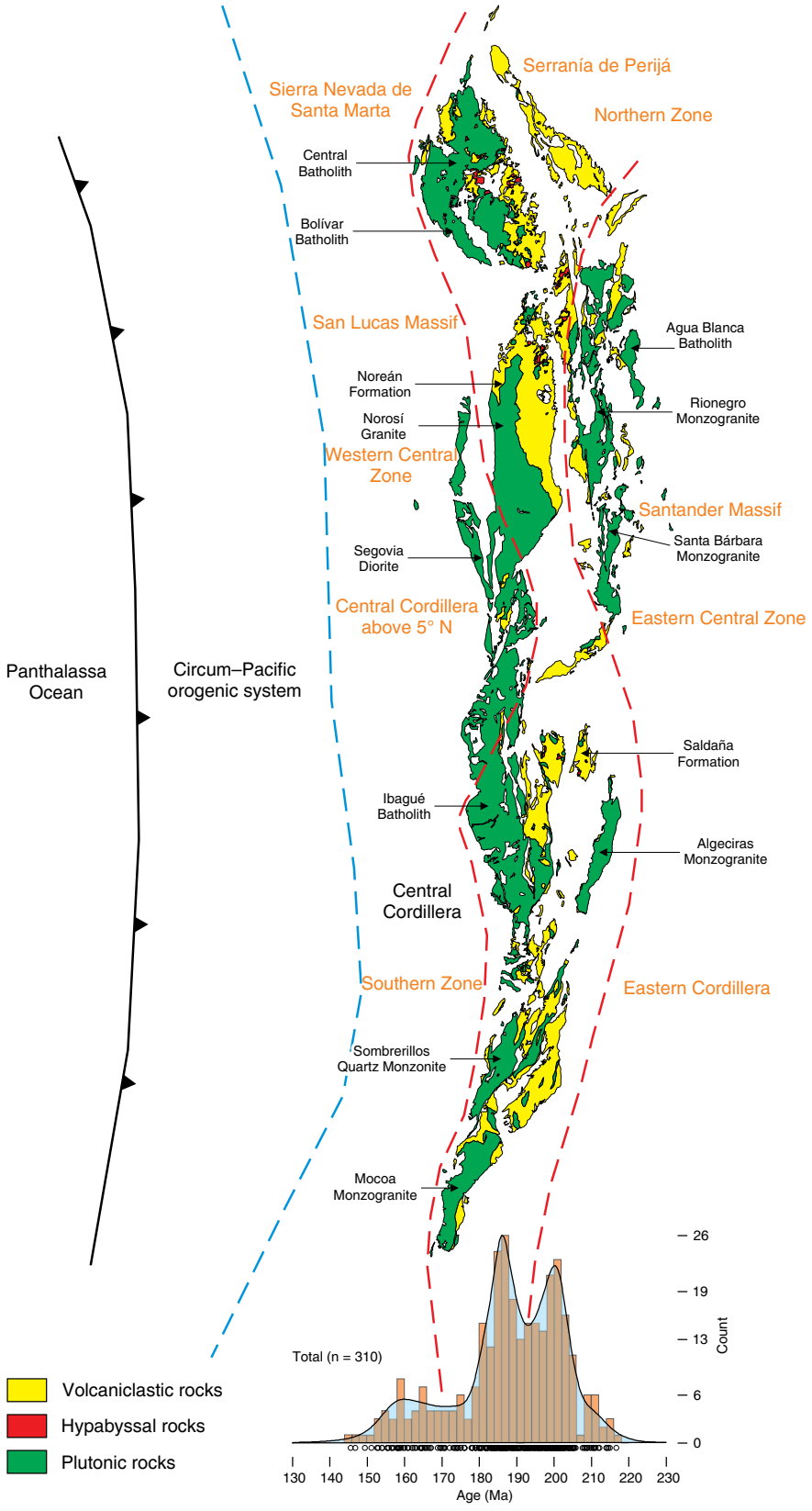

Figure 15. Schematic diagram showing the spatial and temporal variations in the Late Triassic to Jurassic magmatic belt along the continental margin in a supra–subduction tectonic regime. The oldest magmatism has more felsic compositions (monzogranites and subordinate syenogranites) and is typical of syncollisional to postcollisional (postorogenic) settings. The youngest magmatism has the most basic compositions (quartz diorites, tonalites, diorites, and granodiorites), which are typical of subduction–related environments associated with active continental margins.

the trench, whereas the most evolved, potassium–rich calc–alkaline affinities are found towards the back–arc region and ultimately change to the shoshonitic or trans–alkaline series (Brown, 1981; Lameyre, 1988; Winter, 2014).

Acknowledgments

The authors are grateful to the Universidad Nacional de Colombia and the Servicio Geológico Colombiano and the support of these two institutions through several projects from the outcomes of this research. Special thanks to Jorge GÓMEZ TAPIAS for fostering the publication of this study. We appreciate helpful and constructive reviews from David BUCHS and Yamirka ROJAS AGRAMONTE. We also recognize that this work would not have been possible without all the contributions made by different authors concerning the characterization of the Triassic to Jurassic magmatic belt in Colombia; to all of them, thank you for your valuable work.

References

Aggarwal, Y.P. 1983. Seismic slip rates and earthquakes ruptures zones in the southern Caribbean: Implications for plate motions and earthquake hazard in this region. 10th Caribbean Geological Conference. Memoirs, p. 157. Cartagena.

Altenberger, U. & Concha, A. 2005. Late Lower to early Middle Jurassic arc magmatism in the northern Ibagué–Batholith, Colombia. Geología Colombiana, 30: 87–97.

Álvarez, A.J. 1983. Geología de la cordillera Central y el occidente colombiano y petroquímica de los intrusivos granitoides meso–cenozoicos. Boletín Geológico, 26(2): 1–175.

Álvarez, M.J. 2013. Petrologia, geoquímica isotópica e metalogenia dos depósitos de ouro El Silencio e La Gran Colômbia, Distrito Mineiro Segovia–Remedios, Colômbia. Master thesis, Universidade de Brasilia, 178 p. Brasilia.

Arango, M.I., Rodríguez, G., Bermúdez, J.G. & Zapata, G. 2015a. Catálogo de unidades litoestratigráficas de Colombia: Cuarzomonzodiorita de Las Minas, cordillera Central. Servicio Geológico Colombiano, 26 p. Bogotá.

Arango, M.I., Rodríguez, G., Zapata, G. & Bermúdez, J.G. 2015b. Catálogo de unidades litoestratigráficas de Colombia: Cuarzolatita de Teruel, cordillera Central. Servicio Geológico Colombiano, 25 p. Bogotá.

Arango, M.I., Rodríguez, G., Bermúdez, J.G. & Zapata, G. 2015c. Catálogo de unidades litoestratigráficas de Colombia: Cuarzomonzonita de Anchique, cordillera Central. Servicio Geológico Colombiano, 26 p. Bogotá.

Arango, M.I., Rodríguez, G., Zapata, G. & Bermúdez, J.G. 2015d. Catálogo de unidades litoestratigráficas de Colombia: Monzogranito de Altamira, cordilleras Oriental y Central. Servicio Geológico Colombiano, 31 p. Bogotá.

Arango, M.I., Rodríguez, G., Zapata, G. & Bermúdez, J.G. 2015e. Catálogo de unidades litoestratigráficas de Colombia: Monzogranito de Mocoa, cordillera Oriental. Servicio Geológico Colombiano, 41 p. Bogotá.

Arango, M.I., Rodríguez, G., Zapata, G. & Correa–Martínez, A.M. 2016. Catálogo de unidades litoestratigráficas de Colombia: Monzogranito de Rionegro, cordillera Oriental. Servicio Geológico Colombiano, 128 p. Bogotá.

Aspden, J.A., McCourt, W.J. & Brook, M. 1987. Geometrical control of subduction–related magmatism: The Mesozoic and Cenozoic plutonic history of western Colombia. Journal of the Geological Society, 144(6): 893–905. https://doi.org/10.1144/gsjgs.144.6.0893

Aspden, J.A., Harrison, S.H. & Rundle, C.C. 1992. New geochronological control for the tectono–magmatic evolution of the metamorphic basement, Cordillera Real and El Oro Province of Ecuador. Journal of South American Earth Sciences, 6(1–2): 77–96. https://doi.org/10.1016/0895-9811(92)90019-U

Bahajroy, M. & Taki, S. 2014. Study of the mineralization potential of the intrusives around Valis (Tarom–Iran). Earth Sciences Research Journal, 18(2): 123–129. https://doi.org/10.15446/esrj.v18n2.44799

Bao, Z., Cai, K., Sun, M., Xiao, W., Wan, B., Wang, Y., Wang, X. & Xia, X. 2018. Continental crust melting induced by subduction initiation of the south Tianshan Ocean: Insight from the latest Devonian granitic magmatism in the southern Yili Block, NW China. Journal of Asian Earth Sciences, 153: 100–117. https://doi.org/10.1016/j.jseaes.2017.04.026

Barbarin, B. 1990. Plagioclase xenocrysts and mafic magmatic enclaves in some granites of the Sierra Nevada Batholith, California. Journal of Geophysical Research: Solid Earth, 95(B11): 17747–17756. https://doi.org/10.1029/JB095iB11p17747

Barbarin, B. 1999. A review of the relationships between granitoid types, their origins and their geodynamic environments. Lithos, 46(3): 605–626. https://doi.org/10.1016/S0024-4937(98)00085-1

Batchelor, R.A. & Bowden, P. 1985. Petrogenetic interpretation of granitoid rock series using multicationic parameters. Chemical Geology, 48(1–4): 43–55. https://doi.org/10.1016/0009-2541(85)90034-8

Bayona, G., García, D.F. & Mora, G. 1994. La Formación Saldaña: Producto de la actividad de estratovolcanes continentales en un dominio de retroarco. En: Etayo–Serna, F. (editor), Estudios Geológicos del Valle Superior del Magdalena, Universidad Nacional de Colombia. Capítulo 1, 21 p. Bogotá.

Bayona, G., Cardona, A., Vásquez, M. & Montes, C. 2012. Subduction to rift–related evolution of Triassic and Jurassic rocks in the northern Andes. 108th Annual Meeting, Geological Society of America, Cordilleran Section, Abstracts with Programs, 44(3), p. 23. Queretaro. https://gsa.confex.com/gsa/2012CD/webprogram/Paper201809.html

Belica, M.E., Tohver, E., Pisarevsky, S.A., Jourdan, F., Denyszyn, S. & George, A.D. 2017. Middle Permian paleomagnetism of the Sydney Basin, eastern Gondwana: Testing Pangaea models and the timing of the end of the Kiaman Reverse Superchron. Tectonophysics, 699: 178–198. https://doi.org/10.1016/j.tecto.2016.12.029

Bissig, T., Mantilla–Figueroa, L.C. & Hart, C.J.R. 2014. Petrochemistry of igneous rocks of the California–Vetas mining district, Santander, Colombia: Implications for northern Andean tectonics and porphyry Cu (–Mo, Au) metallogeny. Lithos, 200–201: 355–367. https://doi.org/10.1016/j.lithos.2014.05.003

Blevin, P. 2004. Metallogeny of granitic rocks. The Ishihara Symposium: Granites and associated metallogenesis. Geoscience Australia, 37 p. Canberra.

Bonin, B. 1990. From orogenic to anorogenic settings: Evolution of granitoid suites after a major orogenesis. Geological Journal, 25(3–4): 261–270. https://doi.org/10.1002/gj.3350250309

Bonin, B. 1998. Alkaline rocks and geodynamics. Turkish Journal of Earth Sciences, 7: 105–118.

Bonin, B. 2007. A–type granites and related rocks: Evolution of a concept, problems and prospects. Lithos, 97(1–2): 1–29. https://doi.org/10.1016/j.lithos.2006.12.007

Bonin, B., Azzouni–Sekkal, A., Bussy, F. & Ferrag, S. 1998. Alkali–calcic and alkaline post–orogenic (PO) granite magmatism: Petrologic constraints and geodynamic settings. Lithos, 45(1–4): 45–70. https://doi.org/10.1016/S0024-4937(98)00025-5

Bowden, P., Batchelor, R.A., Chappell, B.W., Didier, J. & Lameyre, J. 1984. Petrological, geochemical and source criteria for the classification of granitic rocks: A discussion. Physics of the Earth and Planetary Interiors, 35(1–3): 1–11. https://doi.org/10.1016/0031-9201(84)90029-3

Brown, G.C. 1981. Space and time in granite plutonism. Philosophical Transactions of the Royal Society A, 301(1461): 321–336. https://doi.org/10.1098/rsta.1981.0114

Brown, G.C., Thorpe, R.S. & Webb, P.C. 1984. The geochemical characteristics of granitoids in contrasting arcs and comments on magma sources. Journal of the Geological Society, 141(3): 413–426. https://doi.org/10.1144/gsjgs.141.3.0413

Bustamante, C. 2016. Geoquímica e geocronologia do plutonismo de arco Meso–Cenozoico na Cordilheira Central da Colômbia e os processos de acresção crustal nos Andes do Norte. Doctoral thesis, Universidade de São Paulo, 130 p. São Paulo.

Bustamante, C., Cardona, A., Bayona, G., Mora, A., Valencia, V., Gehrels, G. & Vervoort, J. 2010. U–Pb LA–ICP–MS geochronology and tectonic correlation of Middle Jurassic intrusive rocks from the Garzón Massif, Upper Magdalena Valley and the Central Cordillera, southern Colombia. Boletín de Geología, 32(2): 93–109.

Bustamante, C., Archanjo, C., Cardona, A. & Vervoort, J. 2016. Late Jurassic to Early Cretaceous plutonism in the Colombian Andes: A record of long–term arc maturity. Geological Society of America Bulletin, 128(11–12): 1762–1779. https://doi.org/10.1130/B31307.1

Cabanis, B. & Lecolle, M. 1989. Le diagramme La/10–Y/15–Nb/8: Un outil pour la discrimination des series volcaniques et la mise en evidence des processus de mélange et/ou de contamination crustale. Comptes Rendus l'Académie des Sciences, Série 2, Mécanique, Physique, Chimie, Sciences de l'univers, Sciences de la Terre, 309: 2023–2029. Paris.

Cardona, A., Cordani, U. & MacDonald, W.D. 2006. Tectonic correlations of pre–Mesozoic crust from the northern termination of the Colombian Andes, Caribbean region. Journal of South American Earth Sciences, 21(4): 337–354. https://doi.org/10.1016/j.jsames.2006.07.009

Cardona, A., Valencia, V., Garzón, A., Montes, C., Ojeda, G., Ruiz, J. & Weber, M. 2010. Permian to Triassic I to S–type magmatic switch in the northeast Sierra Nevada de Santa Marta and adjacent regions, Colombian Caribbean: Tectonic setting and implications within Pangea paleogeography. Journal of South American Earth Sciences, 29(4): 772–783. https://doi.org/10.1016/j.jsames.2009.12.005

Castro, A. 2004. The source of granites: Inferences from the Lewisian Complex. Scottish Journal of Geology, 40(1): 49–65. https://doi.org/10.1144/sjg40010049

Castro, A. 2014. The off–crust origin of granite batholiths. Geoscience Frontiers, 5(1): 63–75. https://doi.org/10.1016/j.gsf.2013.06.006

Castro, A., Moreno–Ventas, I. & De La Rosa, J.D. 1991a. H–type (hybrid) granitoids: A proposed revision of the granite–type classification and nomenclature. Earth–Science Reviews, 31(3–4): 237–253. https://doi.org/10.1016/0012-8252(91)90020-G

Castro, A., Moreno–Ventas, I. & De La Rosa, J.D. 1991b. Multistage crystallization of tonalitic enclaves in granitoid rocks (Hercynian belt, Spain): Implications for magma mixing. Geologische Rundschau, 80(1): 109–120. https://doi.org/10.1007/BF01828770

Cediel, F., Shaw, R.P. & Cáceres, C. 2003. Tectonic assembly of the northern Andean Block. In: Bartolini, C., Buffler, R.T. & Blickwede, J. (editors), The circum–Gulf of Mexico and the Caribbean: Hydrocarbon habitats, basin formation, and plate tectonics. American Association of Petroleum Geologists, Memoir 79, p. 815–848. Tulsa, USA.

Chappell, B.W. 1984. Source rocks of I– and S–type granites in the Lachlan fold belt, southeastern Australia. Philosophical Transactions of the Royal Society A, 310(1514): 693–706. https://doi.org/10.1098/rsta.1984.0015

Chappell, B.W. 1999. Aluminium saturation in I– and S–type granites and the characterization of fractionated haplogranites. Lithos, 46(3): 535–551. https://doi.org/10.1016/S0024-4937(98)00086-3

Chappell, B.W. & White, A.J.R. 1974. Two contrasting granite types. Pacific Geology, 8: 173–174.

Chappell, B.W. & White, A.J.R. 1992. I– and S–type granites in the Lachlan fold belt. In: Brown, P.E. & Chappell, B.W. (editors), The Second Hutton Symposium on the Origin of Granites and Related Rocks. Geological Society of America, Special Paper 272, p. 1–26. https://doi.org/10.1130/SPE272-p1

Chappell, B.W. & White, A.J.R. 2001. Two contrasting granite types: 25 years later. Australian Journal of Earth Sciences, 48(4): 489–499. https://doi.org/10.1046/j.1440-0952.2001.00882.x

Chappell, B.W., Bryant, C.J. & Wyborn, D. 2012. Peraluminous I–type granites. Lithos, 153: 142–153. https://doi.org/10.1016/j.lithos.2012.07.008

Chazot, G. & Bertrand. H. 1995. Genesis of silicic magmas during Tertiary continental rifting in Yemen. Lithos, 36(2): 69–83. https://doi.org/10.1016/0024-4937(95)00012-5

Chen, L. & Zhao, Z.F. 2017. Origin of continental arc andesites: The composition of source rocks is the key. Journal of Asian Earth Sciences, 145(part A): 217–232. https://doi.org/10.1016/j.jseaes.2017.04.012

Clarke, D.B. 1981. The mineralogy of peraluminous granites: A review. Canadian Mineralogist, 19(1): 3–17.

Clarke, D.B. 1992. Granitoid rocks. Springer Science & Business Media, 284 p. London.

Clavijo, J. 1995a. La Formación Noreán: Nueva evidencia de volcanismo explosivo en la paleocuenca del Magdalena (Colombia) y su relación con otras unidades del Jurásico norandino. IX Congreso Latinoamericano de Geología. Memoirs, 10 p. Caracas, Venezuela.

Clavijo, J. 1995b. Memoria explicativa: Mapa geológico de la plancha 75 Aguachica. Scale 1:100 000. Ingeominas, 48 p. Bucaramanga.

Clavijo, J., Barbosa, G., Camacho, J.A., Bernal, L.E., Royero, J.M. & Castro, G.E. 1992. Geología de la plancha 75 Aguachica. Scale 1:100 000. Ingeominas. Bogotá.

Cobbing, E.J. & Pitcher, W.S. 1972. The Coastal Batholith of central Peru. Journal of the Geological Society, 128(5): 421–451. https://doi.org/10.1144/gsjgs.128.5.0421

Cochrane, R.S. 2013. U–Pb thermochronology, geochronology and geochemistry of NW South America: Rift to drift transition, active margin dynamics and implications for the volume balance of continents. Doctoral thesis, University of Geneva, 118 p. Geneva, Switzerland. https://doi.org/10.13097/archive-ouverte/unige:30029

Cochrane, R., Spikings, R., Gerdes, A., Ulianov, A., Mora, A., Villagómez, D., Putlitz, B. & Chiaradia, M. 2014a. Permo–Triassic anatexis, continental rifting and the disassembly of western Pangaea. Lithos, 190–191: 383–402. https://doi.org/10.1016/j.lithos.2013.12.020

Cochrane, R., Spikings, R., Gerdes, A., Winkler, W., Ulianov, A., Mora, A. & Chiaradia, M. 2014b. Distinguishing between in–situ and accretionary growth of continents along active margins. Lithos, 202–203: 382–394. https://doi.org/10.1016/j.lithos.2014.05.031

Colmenares, F.H., Mesa, A.M., Roncancio, J.H., Arciniegas, E.G., Pedraza, P.E., Cardona, A., Romero, A.J., Silva, C.A., Alvarado, S.I., Romero, O.A. & Vargas, A.F. 2007. Geología de las planchas 11, 12, 13, 14, 18, 19, 20, 21, 25, 26, 27, 33, 34 y 40. Proyecto: Evolución geohistórica de la Sierra Nevada de Santa Marta. Invemar–Ingeominas–ICP–Ecopetrol–Geosearch Ltda., 401 p. Bogotá.

Correa–Martínez, A.M., Rodríguez, G., Arango, M.I., Zapata, G. & Bermúdez, J.G. 2016. Catálogo de unidades litoestratigráficas de Colombia: Batolito de Mogotes, cordillera Oriental. Servicio Geológico Colombiano, 112 p. Medellín.

Correa–Martínez, A.M., Rodríguez, G., Bermúdez, J.G., Arango, M.I. & Zapata, G. 2018. Catálogo de unidades litoestratigráficas de Colombia: Riolitas del Alto Los Cacaos, cordillera Oriental. Servicio Geológico Colombiano, 47 p. Medellín.

Correa–Martínez, A.M., Rodríguez, G., Arango, M.I. & Zapata–García, G. 2019. Petrografía, geoquímica y geocronología U–Pb de las rocas volcánicas y piroclásticas de la Formación Noreán al NW del Macizo de Santander, Colombia. Boletín de Geología, 41(1): 29–54. http://dx.doi.org/10.18273/revbol.v41n1-2019002

Craddock, J.P., Malone, D.H., Porter, R., Compton, J., Luczaj, J., Konstantinou, A., Day, J.E. & Johnston, S.T. 2017. Paleozoic reactivation structures in the Appalachian–Ouachita–Marathon foreland: Far–field deformation across Pangea. Earth–Science Reviews, 169: 1–34. https://doi.org/10.1016/j.earscirev.2017.04.002

Cuadros, F.A. 2012. Caracterização geoquímica e geocronológica do embasamento mesoproterozóico da parte norte da serranía de San Lucas (Colômbia). Master thesis, Universidade de Brasilia, 113 p. Brasilia.

Cuadros, F.A., Botelho, N.F., Ordoñez–Carmona, O. & Matteini, M. 2013. Edades U–Pb en zircón por LA–MC–ICP–MS del Gneis de San Lucas y el Batolito de Norosí en la parte septentrional de la serranía de San Lucas. XIV Congreso Colombiano de Geología y Primer Simposio de Exploradores. Memoirs, p. 193–194. Bogotá.

Debon, F. & Le Fort, P. 1983. A chemical–mineralogical classification of common plutonic rocks and associations. Earth and Environmental Science Transactions of the Royal Society of Edinburgh, 73(3): 135–149. https://doi.org/10.1017/S0263593300010117

Debon, F. & Le Fort, P. 1988. A cationic classification of common plutonic rocks and their magmatic associations: Principles, method, applications. Bulletin de Minéralogie, 111: 493–510. https://doi.org/10.3406/bulmi.1988.8096

Dera, G., Prunier, J., Smith, P.L., Haggart, J.W., Popov, E., Guzhov, A., Rogov, M., Delsate, D., Thies, D., Cuny, G., Pucéat, E., Charbonnier, G. & Bayon, G. 2015. Nd isotope constraints on ocean circulation, paleoclimate, and continental drainage during the Jurassic breakup of Pangea. Gondwana Research, 27(4): 1599–1615. https://doi.org/10.1016/j.gr.2014.02.006

De Silva, S.L., Riggs, N.R. & Barth, A.P. 2015. Quickening the pulse: Fractal tempos in continental arc magmatism. Elements, 11(2): 113–118. https://doi.org/10.2113/gselements.11.2.113

Dörr, W., Grösser, J.R., Rodríguez, G.I. & Kramm, U. 1995. Zircon U–Pb age of the Paramo Rico tonalite–granodiorite, Santander Massif (cordillera Oriental, Colombia) and its geotectonic significance. Journal of South American Earth Sciences, 8(2): 187–194. https://doi.org/10.1016/0895-9811(95)00004-Y

Drummond, M.S. & Defant, M.J. 1990. A model for trondhjemite–tonalite–dacite genesis and crustal growth via slab melting: Archean to modern comparisons. Journal of Geophysical Research: Solid Earth, 95(B13): 21503–21521. https://doi.org/10.1029/JB095iB13p21503

Ducea, M.N., Paterson, S.R. & DeCelles, P.G. 2015. High–volume magmatic events in subduction systems. Elements, 11(2): 99–104. https://doi.org/10.2113/gselements.11.2.99

Eby, G.N. 1990. The A–type granitoids: A review of their occurrence and chemical characteristics and speculations on their petrogenesis. Lithos, 26(1–2): 115–134. https://doi.org/10.1016/0024-4937(90)90043-Z

Eby, G.N. 1992. Chemical subdivision of the A–type granitoids: Petrogenetic and tectonic implications. Geology, 20(7): 641–644. https://doi.org/10.1130/0091-7613(1992)020<0641:CSOTAT>2.3.CO;2

El Bouseily, A.M. & El Sokkary, A.A. 1975. The relation between Rb, Ba and Sr in granitic rocks. Chemical Geology, 16(3): 207–219. https://doi.org/10.1016/0009-2541(75)90029-7

Elliott, T. 2003. Tracers of the slab. In: Eiler, J. (editor), Inside the subduction factory. Geophysical Monograph Series 138, p. 23–45.

Frantz, J.C., Ordoñez, O. & Chemale, F. 2007. Caracterización de ambientes geológicos con mineralizaciones de oro en los Andes colombianos. VIII Congreso Colombiano de Minería. Memoirs, CD. Medellín.

Frost, B.R. & Frost, C.D. 2008. A geochemical classification for feldspathic igneous rocks. Journal of Petrology, 49(11): 1955–1969. https://doi.org/10.1093/petrology/egn054

Frost, B.R., Barnes, C.G., Collins, W.J., Arculus, R.J., Ellis, D.J. & Frost, C.D. 2001. A geochemical classification of granitic rocks. Journal of Petrology, 42(11): 2033–2048. https://doi.org/10.1093/petrology/42.11.2033

Frost, C.D., Frost, B.R. & Beard, J.S. 2016. On silica–rich granitoids and their eruptive equivalents. American Mineralogist, 101(6): 1268–1284. https://doi.org/10.2138/am-2016-5307

Ganne, J. & Feng, X. 2018. Magmatism: A crustal and geodynamic perspective. Journal of Structural Geology, 114: 329–335. https://doi.org/10.1016/j.jsg.2018.02.002

Ganne, J., Schellart, W.P., Rosenbaum, G., Feng, X. & De Andrade, V. 2017. Probing crustal thickness evolution and geodynamic processes in the past from magma records: An integrated approach. In: Bianchini, G., Bodinier, J.L., Braga, R. & Wilson, M. (editors), The crust–mantle and lithosphere–asthenosphere boundaries: Insights from xenoliths, orogenic deep sections, and geophysical studies. Geological Society of America, Special Paper 526, 25 p. https://doi.org/10.1130/2017.2526(01)

Gansser, A. 1973. Facts and theories on the Andes. Journal of the Geological Society of London, 129(2): 93–13l. https://doi.org/10.1144/gsjgs.129.2.0093

García–Chinchilla, D.A. 2018. Petrogênese e evolução tectônica de rochas graníticas da região de Garzón, Cordilheira Oriental da Colômbia. Doctoral thesis, Universidade de São Paulo, 214 p. São Paulo. https://doi.org/10.11606/T.44.2018.tde-10072018-150324

Goldsmith, R., Marvin, R.F. & Mehnert, H.H. 1971. Radiometric ages in the Santander Massif, Eastern Cordillera, Colombian Andes. United States Geological Survey, Professional Paper 750, p. D41–D49.

Gómez, J. 2002. Catálogo de unidades litoestratigráficas de Colombia: Cuarzomonzonita de Dolores, cordillera Oriental. Ingeominas, 15 p. Bogotá.

Gómez, J., Montes, N.E., Alcárcel, F.A. & Ceballos, J.A. 2015. Catálogo de dataciones radiométricas de Colombia en ArcGIS y Google Earth. In: Gómez, J. & Almanza, M.F. (editors), Compilando la geología de Colombia: Una visión a 2015. Servicio Geológico Colombiano, Publicaciones Geológicas Especiales 33, p. 63–419. Bogotá.

González, H. & Londoño, A.C. 2002. Catálogo de las unidades litoestratigráficas de Colombia: Diorita de Segovia, cordillera Central. Ingeominas, 17 p. Bogotá.

González, H. & Núñez, A. 2002. Catálogo de las unidades litoestratigráficas de Colombia: Monzogranito de Mocoa. Ingeominas, unpublished report, 30 p. Bogotá.

González, H., Maya, M., Camacho, J., Cardona, O.D. & Vélez, W. 2015a. Memoria explicativa: Plancha 74 Guaranda. Scale 1:100 000. Servicio Geológico Colombiano, 184 p. Medellín.

González, H., Maya, M., García, J.F., Gómez, J.P., Palacio, A.F. & Vélez, W. 2015b. Memoria explicativa: Plancha 84 Los Canelos. Scale 1:100 000. Servicio Geológico Colombiano, 147 p. Medellín.

González, H., Maya, M., García, J.F., Gómez, J.P., Palacio, A.F. & Vélez, W. 2015c. Memoria explicativa: Plancha 95 Buenavista. Scale 1:100 000. Servicio Geológico Colombiano. 128 p. Medellín.

González, H., Maya, M., Tabares, L.F., Palacio, A.F., Gómez, J.P., Montoya, A. & Vélez, W. 2015d. Memoria explicativa: Plancha 107 Cerro Azul. Scale 1:100 000. Servicio Geológico Colombiano, 167 p. Medellín.

González, H., Maya, M., Tabares, L.F., Montoya, A., Palacio, A.F., Sánchez, C., Barajas, A. & Vélez, W. 2015e. Memoria explicativa: Plancha 118 San Francisco. Scale 1:100 000. Servicio Geológico Colombiano, 220 p. Medellín.

González, H., Maya, M., García, J.F., Camacho, J.A., Gómez, J.P., Cardona, O.D., Palacio, A.F. & Vélez, W. 2015f. Memoria explicativa: Plancha 94 El Bagre. Scale 1:100 000. Servicio Geológico Colombiano, 196 p. Medellín.

González, H., Salinas, R., Cárdenas, J.I., Muñoz, C.M. Dávila, G.C. & Vélez, W. 2015g. Memoria explicativa: Plancha 77 Campo Dos. Scale 1:100 000. Servicio Geológico Colombiano, 234 p. Medellín.

Gorton, M.P. & Schandl, E.S. 2000. From continents to island arcs: A geochemical index of tectonic setting for arc–related and within–plate felsic to intermediate volcanic rocks. The Canadian Mineralogist, 38(5): 1065–1073. https://doi.org/10.2113/gscanmin.38.5.1065

Goswami, B. & Bhattacharyya, C. 2014. Petrogenesis of shoshonitic granitoids, eastern India: Implications for the late Grenvillian post–collisional magmatism. Geoscience Frontiers, 5(6): 821–843. https://doi.org/10.1016/j.gsf.2013.09.003

Grebennikov, A.V. 2014. A–type granites and related rocks: Petrogenesis and classification. Russian Geology and Geophysics, 55(11): 1354–1366. https://doi.org/10.1016/j.rgg.2014.10.011

Harris, N.B.W., Pearce, J.A. & Tindle, A.G. 1986. Geochemical characteristics of collision–zone magmatism. In: Coward, M.P. & Ries, A.C. (editors), Collision tectonics. Geological Society of London, Special Publication 19, p. 67–81. https://doi.org/10.1144/GSL.SP.1986.019.01.04

Hastie, A.R., Kerr, A.C., Pearce, J.A. & Mitchell, S.F. 2007. Classification of altered volcanic island arc rocks using immobile trace elements: Development of the Th–Co discrimination diagram. Journal of Petrology, 48(12): 2341–2357. https://doi.org/10.1093/petrology/egm062

Hernández, S.A., López, J.A. & Zuluaga, C.A. 2017. Petrografía y geoquímica del Batolito de Rionegro al sur del municipio de Cáchira, Macizo de Santander, Colombia. XVI Congreso Colombiano de Geología. Memoirs, p. 1294–1301. Santa Marta.

Hess, P.C. 1989. Origins of igneous rocks. Harvard University Press, 336 p. Cambridge, USA.

Ingeominas & Universidad Industrial de Santander. 2006a. Memoria explicativa: Cartografía geológica de la plancha 55 El Banco. Scale 1:100 000. Ingeominas, 192 p. Bogotá.

Ingeominas & Universidad Industrial de Santander. 2006b. Memoria explicativa: Cartografía geológica de la plancha 64 Barranco de Loba. Scale 1:100 000. Ingeominas, 201 p. Bogotá.

Ingeominas & Universidad Industrial de Santander. 2006c. Memoria explicativa: Cartografía geológica de la plancha 85 Simití. Scale 1:100 000. Ingeominas, 140 p. Bogotá.

Ingeominas & Universidad Industrial de Santander. 2006d. Memoria explicativa: Cartografía geológica de la plancha 96 Bocas del Rosario. Scale 1:100 000. Ingeominas, 126 p. Bogotá.

Irvine, T.N. & Baragar, W.R.A. 1971. A guide to the chemical classification of the common volcanic rocks. Canadian Journal of Earth Sciences, 8(5): 523–548. https://doi.org/10.1139/e71-055

Jaillard, E., Soler, P., Carlier, G. & Mourier, T. 1990. Geodynamic evolution of the northern and central Andes during early to middle Mesozoic times: A Tethyan model. Journal of the Geological Society, 147(6): 1009–1022. https://doi.org/10.1144/gsjgs.147.6.1009

Janoušek, V., Finger, F., Roberts, M., Frýda, J., Pin, C. & Dolejš, D. 2004. Deciphering the petrogenesis of deeply buried granites: Whole–rock geochemical constraints on the origin of largely undepleted felsic granulites from the Moldanubian Zone of the Bohemian Massif. Earth and Environmental Science Transactions of the Royal Society of Edinburgh, 95(1–2): 141–159. https://doi.org/10.1017/S0263593300000985

Kay, S.M., Mpodozis, C. & Gardeweg, M. 2013. Magma sources and tectonic setting of Central Andean andesites (25.5–28° S) related to crustal thickening, forearc subduction erosion and delamination. In: Gómez–Tuena, A., Straub, S. M. & Zellmer, G. F. (editors). Orogenic andesites and crustal growth. Geological Society, London, Special Publication 385: 303–334.

Keshavarzi, R., Esmaili, D., Kahkhaei, M.R., Mokhtari, M.A.A. & Jabari, R. 2014. Petrology, geochemistry and tectonomagmatic setting of Neshveh Intrusion (NW Saveh). Open Journal of Geology, 4(5): 177–189. https://doi.org/10.4236/ojg.2014.45013

Kirsch, M., Paterson, S.R., Wobbe, F., Martínez–Ardila., A.M., Clausen, B.L. & Alasino, P.H. 2016. Temporal histories of cordilleran continental arcs: Testing models for magmatic episodicity. American Mineralogist, 101(10): 2133–2154. https://doi.org/10.2138/am-2016-5718

Lameyre, J. 1988. Granite settings and tectonics. Rendiconti della Società Italiana di Mineralogia e Petrologia, 43(2): 215–236.

Leal–Mejía, H. 2011. Phanerozoic gold metallogeny in the Colombian Andes: A tectono–magmatic approach. Doctoral thesis, Universitat de Barcelona, 989 p. Barcelona.

Leal–Mejía, H., Melgarejo, C. & Shaw, R. 2011. Phanerozoic gold metallogeny in the Colombian Andes. In: Proceedings Let´s talk ore deposits. Society for Geology Applied to Mineral Deposits, SGA Biennial Meeting. Extended abstracts, p. 209–211. Antofagasta, Chile.

Leal–Mejía, H., Shaw, R.P. & Melgarejo i Draper, J.C. 2019. Spatial–temporal migration of granitoid magmatism and the Phanerozoic tectono–magmatic evolution of the Colombian Andes. In: Cediel, F. & Shaw, R.P. (editors), Geology and tectonics of northwestern South America: The Pacific–Caribbean–Andean junction. Frontiers in Earth Sciences. Springer, p. 253–410. Cham, Germany. https://doi.org/10.1007/978-3-319-76132-9_5

Litherland, M., Aspden, J.A. & Jemielita, R.A. 1994. The metamorphic belts of Ecuador. Overseas Memoir of the British Geological Survey 11, 147 p. Nottingham, England.

López, J.A. & Zuluaga, C.A. 2016. Geoquímica de roca total y ambiente geodinámico del magmatismo calcoalcalino de edad Triásico–Jurásico de la Sierra Nevada de Santa Marta y Alta Guajira. The Colombian and Venezuelan Caribbean–Geology Workshop. Abstracts, 2 p. Bogotá.

López, J.A., Cuellar, M.A., Aguirre, R., Valencia, M. & Sánchez, C.A. 2007. Evidencias petrográficas y de campo de una intrusión sintectónica en la cordillera Central de Colombia: El caso de la Milonita Granítica del Guacaica. XI Congreso Colombiano de Geología. Memoirs, p. 17. Bucaramanga.

López, J.A., Zuluaga, C.A. & Tassinari, C.C.G. 2017. Geoquímica de roca total de la Cuarzomonzonita de Santa Bárbara, Macizo de Santander. XVI Congreso Colombiano de Geología. Memoirs, p. 1326–1332. Santa Marta.

MacDonald, W.D. 1964. Geology of the serranía de Macuira area, Guajira Peninsula, Colombia. Doctoral thesis, Princeton University, 237 p. Princeton, USA.

Maloney, K.T., Clarke, G.L., Klepeis, K.A. & Quevedo, L. 2013. The Late Jurassic to present evolution of the Andean margin: Drivers and the geological record. Tectonics, 32(5): 1049–1065. https://doi.org/10.1002/tect.20067

Maniar, P.D. & Piccoli, P.M. 1989. Tectonic discrimination of granitoids. Geological Society of America Bulletin, 101(5): 635–643. https://doi.org/10.1130/0016-7606(1989)101<0635:TDOG>2.3.CO;2

Mantilla–Figueroa, L.C., Bernal, L.E., Clavijo, J., Pinto, J.E., Osorio, J., Ibáñez, D., Castro, E., López, E., Duarte, R., Celada, C.M., Gómez, E., Quintero, I., Pérez, A., Páez, L.A., García, C., Colegial, J.D., Correa, K., Serrano, J., Gaviria, J., Casas, R., Lasso, S., Niz, L., García, M., Nava, G., Martínez, A.M., Silva, A., Prada, D., Calderón, H., Jiménez, G., Cuellar, M., Franco, R. & Caballero, V. 2007. Generalidades sobre la geología de la serranía de San Lucas: Planchas 55, 64, 85 y 96. XI Congreso Colombiano de Geología. Memoirs, p. 14–17. Bucaramanga.

Mantilla–Figueroa, L.C., Valencia, V.A., Barra, F., Pinto, J. & Colegial, J. 2009. Geocronología U–Pb del distrito aurífero de Vetas–California (departamento de Santander, Colombia). Boletín de Geología, 31(1): 31–43.

Mantilla–Figueroa, L.C., Bissig, T., Valencia, V. & Hart, C.J.R. 2013. The magmatic history of the Vetas–California mining district, Santander Massif, Eastern Cordillera, Colombia. Journal of South American Earth Sciences, 45: 235–249. https://doi.org/10.1016/j.jsames.2013.03.006

Martini, M. & Ortega–Gutiérrez, F. 2018. Tectono–stratigraphic evolution of eastern Mexico during the break–up of Pangea: A review. Earth–Science Reviews, 183: 38–55. https://doi.org/10.1016/j.earscirev.2016.06.013

Matthews, K.J., Maloney, K.T., Zahirovic, S., Williams, S.E., Seton, M. & Müller, R.D. 2016. Global plate boundary evolution and kinematics since the late Paleozoic. Global and Planetary Change, 146: 226–250. https://doi.org/10.1016/j.gloplacha.2016.10.002

McDonough, W.F. & Sun, S.S. 1995. The composition of the Earth. Chemical Geology, 120(3–4): 223–253. https://doi.org/10.1016/0009-2541(94)00140-4

Miller, C.F. 1985. Are strongly peraluminous magmas derived from pelitic sedimentary sources? The Journal of Geology, 93(6): 673–689. https://doi.org/10.1086/628995

Miller, C.F., McDowell, S.M. & Mapes, R.W. 2003. Hot and cold granites? Implications of zircon saturation temperatures and preservation of inheritance. Geology, 31(6): 529–532. https://doi.org/10.1130/0091-7613(2003)031<0529:HACGIO>2.0.CO;2

Mišković, A., Spikings, R.A., Chew, D.M., Košler, J., Ulianov, A. & Schaltegger, U. 2009. Tectonomagmatic evolution of western Amazonia: Geochemical characterization and zircon U–Pb geochronologic constraints from the Peruvian Eastern Cordilleran granitoids. Geological Society of America Bulletin, 121(9–10): 1298–1324. https://doi.org/10.1130/B26488.1

Mojica, J. & Kammer, A. 1996. Resumen del Jurásico en Colombia. Contribution International Geological Correlation Programme (IGCP) 322: Jurassic events in South America. Geología Colombiana, 20: 160–162.

Mojica, J., Kammer, A. & Ujueta, G. 1996. El Jurásico del sector noroccidental de Suramérica y guía de la excursión al Valle Superior del Magdalena (Nov. 1–4/95), regiones de Payandé y Prado, departamento del Tolima, Colombia. Geología Colombiana, 21: 3–40.

Moreno, J.A., Molina, J.F., Montero, P., Abu–Anbar, M., Scarrow, J.H., Cambeses, A. & Bea, F. 2014. Unraveling sources of A–type magmas in juvenile continental crust: Constraints from compositionally diverse Ediacaran post–collisional granitoids in the Katerina Ring Complex, southern Sinai, Egypt. Lithos, 192–195: 56–85. https://doi.org/10.1016/j.lithos.2014.01.010

Moyen, J.F., Laurent, O., Chelle–Michou, C., Couzinié, S., Vanderhaeghe, O., Zeh, A., Villaros, A. & Gardien, V. 2017. Collision vs. subduction–related magmatism: Two contrasting ways of granite formation and implications for crustal growth. Lithos, 277: 154–177. https://doi.org/10.1016/j.lithos.2016.09.018

Müller, D., Rock, N.M.S. & Groves, D.I. 1992. Geochemical discrimination between shoshonitic and potassic volcanic rocks in different tectonic settings: A pilot study. Mineralogy and Petrology, 46: 259–289. https://doi.org/10.1007/BF01173568

Muttoni, G., Gaetani, M., Kent, D.V., Sciunnach, D., Angiolini, L., Berra, F., Garzanti, E., Mattei, M. & Zanchi, A. 2009. Opening of the Neo–Tethys Ocean and the Pangea B to Pangea A transformation during the Permian. GeoArabia, 14(4): 17–48.

Nance, R.D., Murphy, J.B. & Santosh, M. 2014. The supercontinent cycle: A retrospective essay. Gondwana Research, 25: 4–29. https://doi.org/10.1016/j.gr.2012.12.026

Nédélec, A. & Bouchez, J.L. 2015. Granites: Petrology, structure, geological setting, and metallogeny. Oxford University Press, 335 p. Oxford. https://doi.org/10.1093/acprof:oso/9780198705611.001.0001

Noguera, M.I., Wright, J.E., Urbani, F. & Pindell, J. 2011. U–Pb geochronology of detrital zircons from the Venezuelan passive margin: Implications for an Early Cretaceous proto–Orinoco river system and proto–Caribbean ocean basin paleogeography. Geologica Acta, 9(3–4): 265–272. https://doi.org/10.1344/105.000001698

Núñez, A. 2002. Catálogo de unidades litoestratigráficas de Colombia: Batolito de Ibagué, cordillera Central. Ingeominas, 26 p. Bogotá.

Núñez, A., Bocanegra, A. & Gómez, J. 1996. Los plutones jurásicos del Valle Superior del Magdalena (Colombia). VII Con-

greso Colombiano de Geología. Memoirs, II, p. 226–239. Bogotá.

Ohta, T. & Arai, H. 2007. Statistical empirical index of chemical weathering in igneous rocks: A new tool for evaluating the degree of weathering. Chemical Geology, 240(3–4): 280–297. https://doi.org/10.1016/j.chemgeo.2007.02.017

Ordóñez–Calderón, J.C. 2003. Petrology of the granitoid rocks in the Santander Massif, northeast Colombia. Master thesis. Shimane University, 122 p. Shimane, Japan.

Ordóñez–Carmona, O., Restrepo, J.J. & Pimentel, M.M. 2006. Geochronological and isotopical review of pre–Devonian crustal basement of the Colombian Andes. Journal of South American Earth Sciences, 21(4): 372–382. https://doi.org/10.1016/j.jsames.2006.07.005

Ordóñez–Carmona, O., Frantz, J.C., Chemale, F. & Londoño, C. 2009. Serranía de San Lucas: Mineralizaciones auríferas, intrusiones de 1500 Ma, metamorfismo Grenville y magmatismo jurásico. XII Congreso Colombiano de Geología. Memoirs in CD ROM, T003–R117, 1 p. Paipa, Boyacá.

Paterson, S.R. & Ducea, M.N. 2015. Arc magmatic tempos: Gathering the evidence. Elements, 11(2): 91–98. https://doi.org/10.2113/gselements.11.2.91

Paul, A.N., Spikings, R.A., Ulianov, A. & Ovtcharova, M. 2018. High temperature (>350 ºC) thermal histories of the long lived (>500 Ma) active margin of Ecuador and Colombia: Apatite, titanite and rutile U–Pb thermochronology. Geochimica et Cosmochimica Acta, 228: 275–300. https://doi.org/10.1016/j.gca.2018.02.033

Pearce, J.A. 1982. Trace element characteristics of lavas from destructive plate boundaries. In: Thorpe, R.S. (editor), Andesites. John Wiley & Sons, p. 525–548. New York.

Pearce, J.A. 1983. Role of sub–continental lithosphere in magma genesis at active continental margins. In: Hawkesworth, C.J. & Nurry, M.J. (editors), Continental basalts and mantle xenoliths. Shiva Publications, p. 230–249. Nantwich, UK.

Pearce, J.A. 2008. Geochemical fingerprinting of oceanic basalts with applications to ophiolite classification and the search for Archean oceanic crust. Lithos, 100(1–4): 14–48. https://doi.org/10.1016/j.lithos.2007.06.016

Pearce, J.A., Harris, N.B.W. & Tindle, A.G. 1984. Trace elements discrimination diagrams for the tectonic interpretation of granitic rocks. Journal of Petrology, 25(4): 956–983. https://doi.org/10.1093/petrology/25.4.956

Pearce, J.A., Bender, J.F., De Long, S.E., Kidd, W.S.F., Low, P.J., Guner, Y., Saroglu, F., Yilmaz, Y., Moorbath, S. & Mitchell, J.G. 1990. Genesis of collision volcanism in eastern Anatolia, Turkey. Journal of Volcanology and Geothermal Research, 44(1–2): 189–229. https://doi.org/10.1016/0377-0273(90)90018-B

Pennington, W.D. 1981. Subduction of eastern Panama Basin and seismotectonics of northwestern South America. Journal of Geophysical Research: Solid Earth, 86(B11): 10753–10770. https://doi.org/10.1029/JB086iB11p10753

Pe–Piper, G., Piper, D.J.W., Koukouvelas, I., Dolansky, L.M. & Kokkalas, S. 2009. Postorogenic shoshonitic rocks and their origin by melting underplated basalts: The Miocene of Limnos, Greece. Geological Society of America Bulletin, 121(1–2): 39–54. https://doi.org/10.1130/B26317.1

Pindell, J.L. 1985. Alleghenian reconstruction and subsequent evolution of the Gulf of Mexico, Bahamas, and proto–Caribbean. Tectonics, 4(1): 1–39. https://doi.org/10.1029/TC004i001p00001

Pindell, J.L. & Dewey, J.F. 1982. Permo–Triassic reconstruction of western Pangea and the evolution of the Gulf of Mexico/Caribbean region. Tectonics, 1(2): 179–211. https://doi.org/10.1029/TC001i002p00179

Pindell, J.L. & Kennan, L. 2009. Tectonic evolution of the Gulf of Mexico, Caribbean and northern South America in the mantle reference frame: An update. In: James, K.H., Lorente, M.A. & Pindell, J.L. (editors), The origin and evolution of the Caribbean Plate. Geological Society of London, Special Publication 328, p. 1–55. https://doi.org/10.1144/SP328.1

Pinilla–Ocampo, A. 2013. Modelo del ambiente tectónico a partir de estudios petrográficos y geoquímicos de la Riodacita de Ipapure–Cerro La Teta. Master thesis, Universidad Nacional de Colombia, 157 p. Bogotá.

Pitcher, W.S. 1988. Andean batholiths and marginal basins. Rendiconti della Società Italiana di Mineralogia e Petrologia, 43(2): 275–280.

Pitcher, W.S. 1997. The nature and origin of granite. Chapman & Hall, 387 p. https://doi.org/10.1007/978-94-011-5832-9

Quandt, D. 2013. The magmatic evolution of the Sierra Nevada de Santa Marta during the Jurassic. Master thesis, University of Postdam, 190 p. Berlin, Germany.

Quandt, D., Trumbull., R.B., Altenberger, U., Cardona, A., Romer, R.L., Bayona, G., Ducea, M., Valencia, V., Vásquez, M., Cortés, E. & Guzman, G. 2018. The geochemistry and geochronology of Early Jurassic igneous rocks from the Sierra Nevada de Santa Marta, NW Colombia, and tectono–magmatic implications. Journal of South American Earth Sciences, 86: 216–230. https://doi.org/10.1016/j.jsames.2018.06.019

Quiceno–Colorado, J., Osorio–Ocampo, S., Vallejo–Hincapié, F., Salazar–Ríos, A., Ossa–Meza, C.A., Giraldo–Alzate, L. & Romero–Arboleda, L. 2016. Petrografía y geoquímica del Stock de Payandé y su posible relación con el magmatismo Jurásico al sur de Colombia. Boletín de Geología, 38(2): 39–53.

Ramos, V.A. 1999. Plate tectonic setting of the Andean Cordillera. Episodes, 22(3): 183–190.

Ramos, V.A. 2009. Anatomy and global context of the Andes: Main geologic features and the Andean orogenic cycle. In: Kay, S.M., Ramos, V.A. & Dickinson, W.R. (editors), Backbone of the Americas: Shallow subduction, plateau uplift, and ridge and terrane collision. Geological Society of America, Memoirs 204, p. 31–65. https://doi.org/10.1130/2009.1204(02)

Restrepo–Pace, P. 1995. Late Precambrian to early Mesozoic tectonic evolution of the Colombian Andes based on new geochronological, geochemical and isotopic date. Doctoral thesis, University of Arizona, 189 p. Tucson.

Riel, N., Jaillard, E., Martelat, J.E., Guillot, S. & Braun, J. 2018. Permian – Triassic Tethyan realm reorganization: Implications for the outward Pangea margin. Journal of South American Earth Sciences, 81: 78–86. https://doi.org/10.1016/j.jsames.2017.11.007

Ríos–Blandón, P.A. 2016. Petrografía y geoquímica de la Granodiorita de Ipapure y su relación con las rocas encajantes en la Alta Guajira–Colombia. Master thesis, Universidad Nacional de Colombia, 103 p. Bogotá.

Rodríguez, G. 2018. Caracterización petrográfica, química y edad Ar–Ar de cuerpos porfídicos intrusivos en la Formación Saldaña. Boletín Geológico, 44: 5–23. https://doi.org/10.32685/0120-1425/boletingeo.44.2018.5

Rodríguez, G., Arango, M.I., Bermúdez, J.G. & Zapata, G. 2015a. Catálogo de unidades litoestratigráficas de Colombia: Granito de Garzón, cordillera Oriental. Servicio Geológico Colombiano, 23 p. Medellín.

Rodríguez, G., Arango, M.I., Bermúdez, J.G. & Zapata, G. 2015b. Catálogo de unidades litoestratigráficas de Colombia: Cuarzomonzonita de Los Naranjos, cordillera Central. Servicio Geológico Colombiano, 28 p. Medellín.

Rodríguez, G., Arango, M.I., Zapata, G. & Bermúdez, J.G. 2015c. Catálogo de unidades litoestratigráficas de Colombia: Cuarzomonzodiorita de El Astillero, serranía de Las Minas. Servicio Geológico Colombiano, 27 p. Medellín.

Rodríguez, G., Zapata, G., Arango, M.I. & Bermúdez, J.G. 2015d. Catálogo de unidades litoestratigráficas de Colombia: Monzogranito de Algeciras, cordillera Oriental. Servicio Geológico Colombiano, 36 p. Medellín.

Rodríguez, G., Correa, A.M., Zapata, G. & Arango, M.I. 2016a. Catálogo de unidades litoestratigráficas de Colombia: Monzogranito de La Corcova, cordillera Oriental. Servicio Geológico Colombiano, 106 p. Medellín.

Rodríguez, G., Arango, M.I., Zapata, G. & Bermúdez, J.G. 2016b. Catálogo de unidades litoestratigráficas de Colombia: Formación Saldaña, cordilleras Central y Oriental. Servicio Geológico Colombiano, 92 p. Medellín.

Rodríguez, G., Zapata, G., Correa–Martínez, A.M. & Arango, M.I. 2017a. Caracterización petrográfica, química y geocronológica del magmatismo triásico–jurásico del Macizo de Santander, Colombia. XVI Congreso Colombiano de Geología y III Simposio de Exploradores. Memoirs, p. 1430–1433. Santa Marta.

Rodríguez, G., Arango, M.I., Zapata, G. & Correa–Martínez, A.M. 2017b. Catálogo de unidades litoestratigráficas de Colombia: Tonalita de San Martín, cordillera Oriental. Servicio Geológico Colombiano, 56 p. Medellín.

Rodríguez, G., Arango, M.I., Zapata, G. & Bermúdez, J.G. 2018a. Petrotectonic characteristics, geochemistry, and U–Pb geochronology of Jurassic plutons in the Upper Magdalena Valley, Colombia: Implications on the evolution of magmatic arcs in the NW Andes. Journal of South American Earth Sciences, 81: 10–30. https://doi.org/10.1016/j.jsames.2017.10.012

Rodríguez, G., Zapata, G., Arango, M.I. & Correa, A.M. 2018b. Catálogo de unidades litoestratigráficas de Colombia: Monzogranito de Santa Bárbara, cordillera Oriental. Servicio Geológico Colombiano, 96 p. Medellín.

Rodríguez, G., Arango, M.I., Correa, A.M. & Zapata, G. 2018c. Catálogo de unidades litoestratigráficas de Colombia: Riolita de San Joaquín, cordillera Oriental. Servicio Geológico Colombiano, 46 p. Medellín.

Rolon, L.F. 2004. Structural geometry of the jura–Cretaceous rift of the Middle Magdalena Valley Basin–Colombia. Master thesis, West Virginia University, 63 p. Morgantown, USA.

Ross, P.S. & Bédard, J.H. 2009. Magmatic affinity of modern and ancient subalkaline volcanic rocks determined from trace–element discriminant diagrams. Canadian Journal of Earth Sciences, 46(11): 823–839. https://doi.org/10.1139/E09-054

Salazar–Torres, J.C., Agudelo, W.J., Toro–Toro, L.M., Moreno–Sánchez, M. & Gómez–Cruz, A.J. 2013. Petrografía y geoquímica de las rocas volcánicas del cerro La Teta y el arroyo Jurarein, Alta Guajira colombiana. Boletín de Geología, 35(2): 53–63.

Sarmiento–Rojas, L.F. 2001. Mesozoic rifting and Cenozoic Basin inversion history of the Eastern Cordillera, Colombian Andes: Inferences from tectonic models. Doctoral thesis, Vrije Universiteit, 295 p. Amsterdam, the Netherlands.

Sarmiento–Rojas, L.F., van Wess, J.D. & Cloetingh, S. 2006. Mesozoic transtensional basin history of the Eastern Cordillera, Colombian Andes: Inferences from tectonic models. Journal of South American Earth Sciences, 21(4): 383–411. https://doi.org/10.1016/j.jsames.2006.07.003

Schandl, E.S. & Gorton, M.P. 2002. Application of high field strength elements to discriminate tectonic settings in VMS environments. Economic Geology, 97(3): 629–642. https://doi.org/10.2113/gsecongeo.97.3.629

Scotese, C.R. 2014a. Atlas of permo–Triassic paleogeographic maps (Mollweide Projection). Maps 43–52, volumes 3 & 4 of the PALEOMAP Atlas for ArcGIS. PALEOMAP Project. Evanston, USA. https://doi.org/10.13140/2.1.2609.9209

Scotese, C.R. 2014b. Atlas of Jurassic paleogeographic maps (Mollweide Projection). Maps 32–42, volume 3 of the PALEOMAP Atlas for ArcGIS. PALEOMAP Project. Evanston, USA. https://doi.org/10.13140/2.1.4850.4321

Song, S.G., Wang, M.J., Wang, C. & Niu, Y.L. 2015. Magmatism during continental collision, subduction, exhumation and mountain collapse in collisional orogenic belts and continental net growth: A perspective. Science China, Earth Sciences, 58(8):1284–1304. https://doi.org/10.1007/s11430-015-5102-x

Spikings, R., Cochrane, R., Villagómez, D., van der Lelij, R., Vallejo, C., Winkler, W. & Beate, B. 2015. The geological history of northwestern South America: From Pangaea to the early col-

lision of the Caribbean Large Igneous Province (290–75 Ma). Gondwana Research, 27(1): 95–139. https://doi.org/10.1016/j.gr.2014.06.004

Stampfli, G.M., Hochard, C., Vérard, C., Wilhem, C. & von Raurmer, J. 2013. The formation of Pangea. Tectonophysics, 593: 1–19. https://doi.org/10.1016/j.tecto.2013.02.037

Tarney, J. & Jones, C.E. 1994. Trace element geochemistry of orogenic igneous rocks and crustal growth models. Journal of the Geological Society, 151(5): 855–868. https://doi.org/10.1144/gsjgs.151.5.0855

Thiéblemont, D. & Cabanis, B. 1990. Utilisation d'un diagramme (Rb/100)–Tb–Ta pour la discrimination géochimique et l'etude pétrogénétique des roches magmatiques acides. Bulletin de la Société Géologique de France, 8–6(1): 23–35. https://doi.org/10.2113/gssgfbull.VI.1.23

Thiéblemont, D. & Tégyey, M. 1994. Une discrimination géochimique des roches différenciés témoin de la diversité d'origine et de situation tectonique des magmas calco–alcalins. Comptes Rendus Académie des Sciences, 319 (série II): 87–94. Paris.

Thompson, R.N. 1982. Magmatism of the British Tertiary Volcanic Province. Scottish Journal of Geology, 18(1): 49–107. https://doi.org/10.1144/sjg18010049

Tschanz, C.M., Jimeno, A. & Cruz, J. 1969. Geology of the Sierra Nevada de Santa Marta area (Colombia): Preliminary report. Ingeominas, 288 p. Bogotá.

Tschanz, C.M., Marvin, R.F., Cruz, J., Mehnert, H.H. & Cebula, G.T. 1974. Geologic evolution of the Sierra Nevada de Santa Marta, northeastern Colombia. Geological Society of America Bulletin, 85(2): 273–284. https://doi.org/10.1130/0016-7606(1974)85<273:GEOTSN>2.0.CO;2

Universidad Pedagógica y Tecnológica de Colombia & Ingeominas. 2011. Memoria explicativa: Cartografía geológica de la plancha 133 Puerto Berrío. Scale 1:100 000. Ingeominas, 145 p. Sogamoso.

van der Lelij, R. 2013. Reconstructing north–western Gondwana with implications for the evolution of the Iapetus and Rheic Oceans: A geochronological, thermochronological and geochemical study. Doctoral thesis, University of Geneva, 248 p. Geneva. https://doi.org/10.13097/archive-ouverte/unige:31653

van der Lelij, R., Spikings, R., Ulianov, A., Chiaradia, M. & Mora, A. 2016. Palaeozoic to Early Jurassic history of the northwestern corner of Gondwana, and implications for the evolution of the Iapetus, Rheic and Pacific Oceans. Gondwana Research, 31: 271–294. https://doi.org/10.1016/j.gr.2015.01.011

van der Meer, D.G., Torsvik, T.H., Spakman, W., van Hinsbergen, D.J.J. & Amaru, M.L. 2012. Intra–Panthalassa Ocean subduction zones revealed by fossil arcs and mantle structure. Nature Geoscience, 5: 215–219. https://doi.org/10.1038/ngeo1401

Vermeesch, P. 2012. On the visualisation of detrital age distributions. Chemical Geology, 312–313: 190–194. https://doi.org/10.1016/j.chemgeo.2012.04.021

Villagómez, D., Spikings, R., Magna, T., Kammer, A., Winkler, W. & Beltrán, A. 2011. Geochronology, geochemistry and tectonic evolution of the Western and Central Cordilleras of Colombia. Lithos, 125(3–4): 875–896. https://doi.org/10.1016/j.lithos.2011.05.003

Villaseca, C., Barbero, L. & Herreros, V. 1998. A re–examination of the typology of peraluminous granite types in intracontinental orogenic belts. Earth and Environmental Science Transactions of the Royal Society of Edinburgh, 89(2): 113–119. https://doi.org/10.1017/S0263593300007045

Vinasco, C.J., Cordani, U.G., González, H., Weber, M. & Peláez, C. 2006. Geochronological, isotopic, and geochemical data from Permo–Triassic granitic gneises and granitoids of the Colombian Central Andes. Journal of South American Earth Sciences, 21(4): 355–371. https://doi.org/10.1016/j.jsames.2006.07.007

Ward, D.E., Goldsmith, R., Cruz, J. & Restrepo, H. 1973. Geología de los cuadrángulos H–12 Bucaramanga y H–13 Pamplona, departamento de Santander. Boletín Geológico, 21(1–3): 132 p.

Watson, E.B. & Harrison, T.M. 1983. Zircon saturation revisited: Temperature and composition effects in a variety of crustal magma types. Earth and Planetary Science Letters, 64(2): 295–304. https://doi.org/10.1016/0012-821X(83)90211-X

Whalen, J.B., Currie, K.L. & Chappell, B.W. 1987. A–type granites: Geochemical characteristics, discrimination and petrogenesis. Contributions to Mineralogy and Petrology, 95(4): 407–419. https://doi.org/10.1007/BF00402202

Winchester, J.A. & Floyd, P.A. 1977. Geochemical discrimination of different magma series and their differentiation products using immobile elements. Chemical Geology, 20: 325–343. https://doi.org/10.1016/0009-2541(77)90057-2

Winter, J. 2014. An introduction to igneous and metamorphic petrology. Prentice Hall Inc., 697 p. Upper Saddle River, USA.

Zapata, S., Cardona, A., Bayona, G., Bustamante, C., Mora, A., Silva–Tamayo, J.C. & Valencia, V. 2012. Tracing major changes in middle Mesozoic plate convergence in the northern Andes: Insights from the Jurassic magmatic record of southern Colombia. 108th Annual Meeting, Geological Society of America, Cordilleran Section, Abstracts with programs, 44(3), p. 24. Queretaro. https://gsa.confex.com/gsa/2012CD/webprogram/Paper201832.html

Zapata, G., Bermúdez, J.G., Rodríguez, G. & Arango, M.I. 2013. Memoria explicativa: Cartografía geológica de la plancha 83 Nechí. Scale 1:100 000. Servicio Geológico Colombiano, 93 p. Medellín.

Zapata, G., Correa, A.M., Rodríguez, G. & Arango, M.I. 2016a. Catálogo de unidades litoestratigráficas de Colombia: Granito de Pescadero, cordillera Oriental. Servicio Geológico Colombiano, 54 p. Medellín.

Zapata, S., Cardona, A., Jaramillo, C., Valencia, V. & Vervoort, J. 2016b. U–Pb LA–ICP–MS geochronology and geochemistry of Jurassic volcanic and plutonic rocks from the Putumayo region (southern Colombia): Tectonic setting and regional

correlations. Boletín de Geología, 38(2): 1–38. https://doi.org/10.18273/revbol.v38n2-2016001

Zapata, G., Arango, M.I., Rodríguez, G. & Correa–Martínez, A.M. 2018. Catálogo de unidades litoestratigráficas de Colombia: Riolitas El Uvo, cordillera Oriental. Servicio Geológico Colombiano, 39 p. Medellín.

Zartman, R.E. & Doe, B.R. 1981. Plumbotectonics–the model. Tectonophysics, 75(1–2): 135–162. https://doi.org/10.1016/0040-1951(81)90213-4

Zhao, Z.F., Dai, L.Q. & Zheng, Y.F. 2013. Postcollisional mafic igneous rocks record crust–mantle interaction during continental deep subduction. Scientific Reports, 3(3413): 1–6. https://doi.org/10.1038/srep03413

Zhao, S.W., Lai, S.C., Pei, X.Z., Qin, J.F., Zhu, R.Z., Tao, N. & Gao, L. 2019. Compositional variations of granitic rocks in continental margin arc: Constraints from the petrogenesis of Eocene granitic rocks in the Tengchong Block, SW China. Lithos, 326–327: 125–143. https://doi.org/10.1016/j.lithos.2018.12.026

Zorpi, M.J., Coulon, C., Orsini, J.B. & Cocirta, C. 1989. Magma mingling, zoning and emplacement in calc–alkaline granitoid plutons. Tectonophysics, 157(4): 315–329. https://doi.org/10.1016/0040-1951(89)90147-9

Zuluaga, C.A. & López, J.A. 2019. Ordovician orogeny and Jurassic low–lying orogen in the Santander Massif, northern Andes (Colombia). In: Cediel, F. & Shaw, R.P. (editors), Geology and tectonics of northwestern South America: The Pacific–Caribbean–Andean junction. Frontiers in Earth Sciences. Springer Nature Switzerland, p. 195–250. https://doi.org/10.1007/978-3-319-76132-9_4

Zuluaga, C.A., Pinilla, A. & Mann, P. 2015. Jurassic silicic volcanism and associated continental–arc basin in northwestern Colombia (southern boundary of the Caribbean Plate). In: Bartolini, C. & Mann, P. (editors), Petroleum geology and potential of the Colombian Caribbean margin. American Association of Petroleum Geologists, Memoir 108, p. 137–160. https://doi.org/10.1306/13531934M1083640

Explanation of Acronyms, Abbreviations, and Symbols:

ASI	Aluminum saturation index
ca.	Circa, about
CA–ID–TIMS	Chemical abrasion isotope dilution thermal ionization mass spectrometry
CAP	Continental arc potassic
cf.	Confer, compare
GCDkit	Geochemical Data Toolkit
HREE	Heavy rare earth element
IOP	Initial oceanic arc potassic rocks
KDE	Kernel density estimates
LA–ICP–MS	Laser ablation inductively coupled plasma mass spectrometer
LA–MC–ICP–MS	Laser ablation multi–collector inductively coupled plasma mass spectrometer
LOI	Loss on ignition
LOP	Late oceanic arc potassic rocks
LREE	Light rare earth element
MALI	Modified alkali–lime index
MASH	Melting–assimilation–storage–homogenization
PAP	Postcollisional arc potassic
PDPs	Probability density plots
REE	Rare earth element
SHRIMP	Sensitive high–resolution ion

Authors' Biographical Notes

Julián Andrés LÓPEZ–ISAZA is a researcher at the Servicio Geológico Colombiano. He was a professor of petrology and structural geology at the Universidad Industrial de Santander. His work is concentrated in the northern Andes and applies to tectonic evolution and metallogenesis.

Carlos Augusto ZULUAGA is a full professor and researcher at the Departamento de Geociencias of the Universidad Nacional de Colombia. He works on petrology applied to crustal evolution, thermodynamic modeling, and the tectonic evolution of the northern Andes.